ABSTRACT

Title of Dissertation: AN ANALYSIS OF CONVECTIVE TRANSPORT, LIGHTNING NO_X PRODUCTION, AND CHEMISTRY IN MIDLATITUDE AND SUBTROPICAL THUNDERSTORMS

Lesley Elaine Ott, Doctor of Philosophy, 2006

Dissertation directed by: Research Professor Kenneth E. Pickering
Department of Atmospheric and Oceanic Science

The impact of lightning NO_x production and convective transport on tropospheric chemistry was studied in four thunderstorms observed during field projects using a 3-dimensional (3-D) cloud-scale chemical transport model (CSCTM). The dynamical evolution of each storm was simulated using a cloud-resolving model, and the output used to drive the off-line CSCTM which includes a parameterized source of lightning NO_x based on observed cloud-to-ground (CG) and intracloud (IC) flash rates. Simulated mixing ratios of tracer species were compared to anvil aircraft observations to evaluate convective transport in the model. The production of NO per CG flash (P_{CG}) was estimated based on mean observed peak current, and production per IC flash (P_{IC}) was scaled to P_{CG}. Different values of P_{IC}/P_{CG} were assumed and the results compared with in-cloud aircraft measurements to estimate the ratio most appropriate for each storm. The impact of lightning NO_x on ozone and other species was examined during the storm in

the CSCTM and following each storm in the convective plume using a chemistry-only version of the model which includes diffusion but without advection, and assumes clear-sky photolysis rates.

New lightning parameterizations were implemented in the CSCTM. One parameterization uses flash length data, rather than flash rates, as input, and production per meter of flash channel length is estimated. A second parameterization simulates indivdual lightning flashes rather than distributing lightning NO_x uniformly among a large number of gridcells to better reproduce the variability of observations.

The results suggest that P_{IC} is likely on the order of P_{CG} and not significantly less as has been assumed in many global modeling studies. Mean values of P_{CG}=500 moles NO and P_IC=425 moles NO have been estimated from these simulations of midlatitude and subtropical continental thunderstorms. Based on the estimates of production per flash, and an assumed ratio of the number of IC to CG flashes and global flash rate, a global annual lightning NO source of 8.6 Tg N yr^{-1} is estimated. Based on these simulations, vertical profiles of lightning NO_x mass for subtropical and midlatitude continental regimes have been computed for use in global and regional chemical transport models.

AN ANALYSIS OF CONVECTIVE TRANSPORT, LIGHTNING NO_X PRODUCTION, AND CHEMISTRY IN MIDLATITUDE AND SUBTROPICAL THUNDERSTORMS

by

Lesley Elaine Ott

Dissertation submitted to the Faculty of the Graduate School of the
University of Maryland, College Park in partial fulfillment
of the requirements for the degree of
Doctor of Philosophy
2006

Advisory Committee:

Professor Russell Dickerson, Chair
Research Professor Kenneth Pickering, Advisor
Professor Robert Hudson
Professor Da-Lin Zhang
Professor George Goldenbaum

Acknowledgements

I would like to express my gratitude to my advisor, Dr. Kenneth Pickering, for his support, guidance, and patience over the years. I would also like to thank Dr. Gera Stenchikov of Rutgers University and Dr. Alex DeCaria of Millersville University for their numerical modeling assistance. This research was supported by the NSF grant ATM-9912336 and by NASA grants NNG04GD32G, NAG511276, and NAG511956.

I would like to thank Dr. Mary Barth of NCAR for her help with the WRF model. I would also like to thank Dr. Donghai Wang of NASA Langley Space Flight Center, and Drs. Ruei-Fong Lin and Steve Lang of NASA Goddard Space Flight for providing model output which was used to drive the cloud-scale chemical transport model used in this dissertation. Observations are an important component of this work and I would also like to thank those who provided data from several field projects: Jimena Lopez and Max Loewenstein from NASA Ames Research Center; Eric Richard from NOAA Aeronomy Laboratory; Brian Ridley, Jim Dye, and Mary Barth from NCAR; Heidi Huntrieser, Hartmut Höller and Thorsten Fehr from Deutsches Zentrum für Luft- und Raumfahrt.

TABLE OF CONTENTS

LIST OF TABLES

LIST OF FIGURES

Chapter 1. Introduction

1.1 Motivation

Tropospheric NO_x ($NO+NO_2$) is of interest largely due to its influence on tropospheric ozone concentrations. NO_x from anthropogenic sources which originates at the surface requires transport processes to reach the free troposphere. Lightning is a particularly significant source of NO_x to the free troposphere because it produces NO_x directly in the middle and upper troposphere where it is longer lived and may have a greater impact on ozone mixing ratios in this region of the atmosphere as well as tropospheric column ozone. However, many aspects of the physics of lightning and of lightning NO_x production are still highly uncertain despite numerous attempts to investigate them. In large part, this is due to the difficulty of directly observing these phenomena or replicating them in a laboratory. This dissertation seeks to provide improved estimates of NO production by lightning through use of a cloud-resolving chemical model and airborne observations.

Results are presented from four case studies of thunderstorms observed during three field projects in different midlatitude and subtropical locations. Each storm has been simulated by a cloud-resolving model and the output used to drive a cloud-scale chemical transport model which employs a parameterization of lightning NO_x production. Estimates of lightning NO_x production were made by specifying different production scenarios and comparing the model results with in-cloud chemical observations.

A number of previous studies have attempted to extrapolate results from a single thunderstorm to obtain estimates of the global lightning NO_x source despite the large variability of lightning activity between storms. By using a number of different storms observed in three different regions, the goal is to produce a global source estimate which is more representative of global thunderstorm and lightning activity. In addition to a global source estimate, these cloud-scale simulations provide valuable insight into the vertical distribution of lightning NO_x for use in regional and global chemical transport models. Better understanding the magnitude of the global source as well as ts vertical distribution will aid in improving the representation of NO_x, O_3, and other chemical species in global chemical transport models and future studies of pollution transport and climate.

1.2 Tropospheric ozone

The importance of ozone in the atmosphere is well established. Stratospheric ozone acts to prevent UV radiation from reaching the surface, and to a great extent, prevents detrimental effects on human health including skin cancer and cataracts. Though ~90% ozone is found in the stratosphere, the presence of ozone in the troposphere is especially significant for a number of reasons. Boundary layer ozone directly affects human health by impairing respiratory function which has resulted in the classification of ozone as a criteria pollutant for air quality by the U.S. Environmental Protection Agency. High concentrations of low level ozone result in lower crop yields, causing significant economic loss annually. Besides these well known roles, ozone impacts the atmosphere in a number of other important ways. Ozone is an effective greenhouse gas in the lower stratosphere and the upper troposphere, affecting the thermal structure of the atmosphere as well as climate. In addition, ozone affects the abundance of the hydroxyl radical (OH), and as a result, the oxidizing capacity and chemistry of the atmosphere.

Ozone in the troposphere is the result of downward transport from the stratosphere as well as in-situ photochemical production. Much uncertainty still surrounds the relative contribution of each source. In order for ozone to be produced photochemically, ozone precursors must be present in sufficient quantities. Therefore, the importance of this source is likely to vary spatially and temporally.

1.3 Photochemical ozone production

In the stratosphere, where the majority of ozone resides, molecular oxygen is photolyzed by ultraviolet radiation to form two oxygen atoms. Ozone is then produced by the reaction of molecular and atomic oxygen. However, since most of the UV radiation incident on the Earth is absorbed in the stratosphere, photochemical production of ozone in the troposphere results from different processes. In the clean troposphere, ozone production and loss can be described by the following set of three reactions.

$$NO_2 + h\nu \rightarrow NO + O(^3P) \tag{1.1}$$

$$O(^3P) + O_2 + M \rightarrow O_3 + M \tag{1.2}$$

$$NO + O_3 \rightarrow NO_2 + O_2 \tag{1.3}$$

NO_2 is photolyzed by UV and visible radiation forming NO and atomic oxygen. Molecular and atomic ozone combine to form one ozone molecule, which is then destroyed through reaction with NO. This produces and destroys one ozone molecule, resulting in no net loss or gain of ozone. Ozone also undergoes photolysis (1.4) and the OH radical is produced from (1.5). The OH radical is important for the oxidation of CO and CH_4 in the clean tropopshere, producing HO_2 and CH_3O_2, respectively. CH_3O_2 is known as a peroxy radical (referred to as RO_2).

$$O_3 + h\nu \rightarrow O(^1D) + O_2 \tag{1.4}$$

$$O(^1D) + H_2O \rightarrow 2OH \tag{1.5}$$

In the polluted troposphere, greater quantities of HO_2 result from reactions which produce H or HCO. The oxidation of either biogenic or anthropogenic hydrocarbons produces more complex peroxy radicals. HO_2 and RO_2 react with NO through the following reactions.

$$HO_2 + NO \rightarrow OH + NO_2 \tag{1.6}$$

$$RO_2 + NO \rightarrow RO + NO_2 \tag{1.7}$$

Both reactions convert NO to NO_2 without the consumption of an ozone molecule. These reactions, combined with (1.1) and (1.2), demonstrate how ozone can accumulate in the troposphere when NO_x and hydrocarbons are present.

Ozone production efficiency, the net ozone production per NO_x molecule consumed, depends nonlinearly on the abundance of both NO_x and hydrocarbons. The degree of nonlinearity depends on the ratio of hydrocarbons to NO_x, as well as the types of hydrocarbon species present [Liu et al., 1987; Lin et al., 1988]. For large values of the hydrocarbon to NO_x ratio, ozone production is limited by the availability of NO_x. For small values of the ratio, ozone production is limited by the availability and reactivity of the hydrocarbon mixture. As a result, ozone production efficiency can vary greatly under different conditions.

Convective processes play an important role in the production and distribution of chemical species involved in ozone photochemistry. Dickerson et al. [1987] demonstrated that thunderstorms can transport boundary layer pollutants to the upper troposphere, increasing their lifetimes. Convective transport of ozone precursors such as NO_x and NMHC's has been shown to enhance ozone production efficiency [Pickering, et

Table 1.1. Sources of Tropospheric NO_x [Bradshaw et al., 2000]

	Recommended Value (Tg N yr^{-1})	Range (Tg N yr^{-1})
Fossil Fuel	23	16-30
Biomass Burning	8.5	4-16
Lightning	6.5	3.2-26
Soil	5.5	3-8
NH_3 Oxidation	0.6	0.3-3
Aircraft	0.51	0.5-0.6
Oceans	0.5	0-1
Stratosphere	0.12	0.08-1

al., 1990]. In addition, NO_x reservoir species such as HNO_3, PAN, and other nitrate species are transported during convection to the upper troposphere increasing their atmospheric residence time and the distance they may be transported.

1.4 Sources of tropospheric NO_x

In order to fully understand the budget and distribution of tropospheric ozone, it is necessary to understand the sources of NO_x in the troposphere. Bradshaw et al. [2000] reviewed the magnitudes of sources found in the literature and recommended the values found in Table 1.1. Fossil fuel combustion, biomass burning, lightning and soil emissions are the four major sources of NO_x in the troposphere.

While the two largest sources of tropospheric NO_x are emitted at the surface, lightning NO_x is produced largely in the middle to upper troposphere where its lifetime is longer and, consequently, its ability to produce ozone, greater. Of the main sources of tropospheric NO_x, lightning is also associated with the widest range of uncertainty, ranging almost an order of magnitude, though most recent estimates are confined to the lower half of this range. Reducing the uncertainty associated with lightning NO_x production is critical to improving the understanding of both tropospheric NO_x and ozone.

1.5 Lightning NO_x production

A typical lightning flash can heat the air in its immediate vicinity to temperatures of approximately 30,000 K, efficiently dissociating molecular oxygen and nitrogen. Chameides [1986] examined the relationship between equilibrium NO concentrations and temperature and found that equilibrium NO concentration peaked at nearly 10% at 4000 K, then decreased at higher temperatures. The formation of NO is governed by the Zeldovich mechanism which consists of the reactions 1.6-1.8 below. The extended Zeldovich mechanism includes a 4th reaction which may also contribute to thermal NO formation.

$$O_2 \leftrightarrow O + O \tag{1.6}$$

$$O + N_2 \leftrightarrow NO + N \tag{1.7}$$

$$N + O_2 \leftrightarrow NO + O \tag{1.8}$$

$$N + OH \leftrightarrow NO + H \tag{1.9}$$

While the chemical reactions which result in lightning NO production may be known, the physical processes governing production, as well as the magnitude of the production itself, remain a source of vigorous debate. Uncertainties in the amount of NO_x produced per Joule of energy and per flash, the amount of energy per flash, average flash length, and even the global flash rate make obtaining an accurate estimate of global lightning NO_x production extremely difficult as discussed in Price et al. [1997]. This has contributed to the wide range of estimates of lightning NO_x production found in the literature.

Complicating matters further is the uncertainty regarding the relative production of IC and CG flashes. On the basis of previous studies which suggested that IC flashes were less energetic than CG flashes [e.g. Holmes et al., 1971], many studies of lightning NO_x production have assumed that IC flashes were less efficient than CG flashes at producing NO. Price et al. [1997] assumed that production by an IC flash (P_{IC}) was one tenth of production by a CG flash (P_{CG}) in estimating the strength of the global lightning NO_x source. In estimating regional lightning NO_x production, Biazar and McNider [1995] used data from the National Lightning Detection Network (NLDN) which detects only CG flashes, neglecting production by IC flashes entirely. In contrast, Gallardo and Cooray [1996] suggested that IC flashes may dissipate nearly as much energy as CG flashes and therefore P_{IC} may be on the order of P_{CG}. Supporting the Gallardo and Cooray [1996] hypothesis, a two-dimensional (2-D) cloud-scale modeling study by DeCaria et al. [2000] suggested that the P_{IC}/P_{CG} ratio is likely between 0.5 and 1.0, and a three-dimensional (3-D) simulation of the same storm narrowed this range to between 0.75 and 1.0 [DeCaria et al., 2005].

A recent article by Zhang et al. [2003] used observational evidence and an analysis of the assumptions presented in Price et al. [1997] to conclude that, on average, an IC flash dissipates between 50-100% as much energy as a CG flash. Price et al. [1997] estimated the energy dissipated per IC and CG flash by multiplying the charge transferred per flash and the potential difference over which the charge is transferred. For IC flashes, Price et al. [1997] assumed that NO was produced only during processes associated with negative recoil strokes referred to as K-changes. The charge transferred per K-change was calculated based on data presented in Ogawa and Brook [1964] and multiplied by an estimate of potential difference to estimate the energy dissipated per IC flash. Zhang et al. [2003] argued that because the Ogawa and Brook [1964] observations show the most frequently occurring number of K-changes per IC flash was 6, the energy dissipated per IC flash should be calculated assuming that a typical IC flash has 6 K-changes rather than 1 as in Price et al. [1997]. In addition, Zhang et al. [2003] challenge the assumptions of electric potential used in Price et al. [1997]. Using estimates of electric potential calculated from electric field soundings in 10 thunderstorms by Marshall and Stolzenburg [2001] and the method of Price et al. [1997] for estimating the energy dissipated per flash, Zhang et al. [2003] found that the energy dissipated by IC flashes is likely to be on the order of the energy dissipated by CG flashes.

A number of early theoretical and laboratory studies of lightning NO_x production focused on estimating production per unit of energy dissipated [e.g. Chameides et al., 1977; Levine et al., 1981; Borucki and Chameides, 1984]. In order to estimate production per flash or to extrapolate to an estimate of global lightning NO_x production using this method, it is necessary to know the energy dissipated by a typical flash. As discussed in the review paper by Lawrence et al. [1995], the energy per flash is a quantity with a large degree of variability and uncertainty which makes determining a typical value difficult.

Estimates of NO_x production by lightning using laboratory experiments, theoretical assumptions regarding the physics of lightning flashes, data from field experiments, and global models were summarized in Zhang et al. [2003] and range from 8 to 5000 moles of NO per flash. A number of estimates of NO production per flash and per meter flash length have been obtained through the use of data from several recent field projects including STERAO (Stratosphere Troposphere Experiment: Radiation, Aerosol, Ozone) over northeastern Colorado in 1996, LINOX (Lightning-produced NO_x),

Table 1.2. Estimates of NO Production per Flash

Author(s)	Field Project	Method	NO production (moles NO per flash)
DeCaria et al. [2000]	STERAO	2-D cloud model, aircraft observations	230 – 460
DeCaria et al. [2005]	STERAO	3-D cloud model, aircraft observations	345 – 460
Fehr et al. [2004]	EULINOX	3-D cloud model, aircraft observations	330-462
Huntrieser et al. [1998]	LINOX	Aircraft observations	66 – 498
Skamarock et al. [2003]	STERAO	3-D cloud model, aircraft observations, lightning observations	43
Théry et al. [2000]	EULINOX	Lightning observations	500

in southern Germany in 1996, and EULINOX (The European Lightning Nitrogen Oxides Project) over central Europe in 1998. Unlike estimates of NO production per unit energy, these estimates do not require assumptions to be made regarding the typical energy per flash in order to obtain a global source estimate. Estimates of NO production per lightning flash are summarized in Table 1.2 while estimates of NO production per meter flash length are presented in Table 1.3. For the July 12 STERAO storm over Colorado, DeCaria et al. [2000] used a 2-D cloud-resolving model, and DeCaria et al. [2005] used a 3-D cloud-resolving model, anvil NO observations, and observed lightning flash rates calculated from interferometer and NLDN (National Lightning Detection Network) observations to estimate P_{CG} and the likely P_{IC}/P_{CG} ratio. Based on analysis of lightning interferometer and aircraft data, Skamarock et al. [2003] estimated NO_x production per

Table 1.3. Estimates of NO Production per meter Flash Channel Length

Author(s)	Field Project	Method	NO production (moles NO per m flash length)
Höller et al. [1999]	LINOX	Lightning observations	$1.7 – 6.6 \times 10^{-2}$
Huntrieser et al. [2002]	EULINOX	Aircraft observations	4.5×10^{-3}
Skamarock et al. [2003]	STERAO	3-D cloud model, aircraft observations, lightning observations	1.7×10^{-3}
Stith et al. [1999]	STERAO	Aicraft observations	$3.3 \times 10^{-4} – 1.7 \times 10^{-2}$

interferometer flash and per meter flash length produced by lightning in the July 10 STERAO storm. The interferometer flash data included many short duration flashes that likely would not be detected by other lightning detection systems. Whether or not these short duration flashes are productive of NO is an open question. If not, then the NO production per meter in the July 10 STERAO storm would be larger than computed by Skamarock et al. [2003]. Stith et al. [1999] estimated NO production per meter flash length based on an analysis of NO spikes measured by aircraft during the same storm, as well as other STERAO storms. Using a similar approach, Huntrieser et al. [2002] estimated NO production per meter flash length for the July 21 EULINOX storm over Germany. For the same storm, an average production of NO per flash was estimated by Théry et al. [2000] based on an average flash length of approximately 30 km calculated from interferometer data (mostly IC flashes). Through analysis of CG lightning peak current data for the July 21 EULINOX storm as recorded by BLIDS (Blitz Informationsdienst von Siemens), Fehr et al. [2004] estimated P_{CG} and a P_{IC}/P_{CG} ratio of

1.4 which was confirmed by a cloud-resolving model simulation that included a lightning parameterization, followed by comparison with anvil NO_x observations. Based on aircraft chemical measurements from LINOX, Huntrieser et al. [1998] estimated NO production per flash while Höller et al. [1999] estimated the amount of NO produced per meter flash length for the same project using lightning observations from LPATS (Lightning Position And Tracking System). All of the above estimates of NO production were based on aircraft NO_x measurements in storm anvils. In contrast, Langford et al. [2004] used remote sensing techniques to measure NO_2 column abundances in the core region of a thunderstorm over Boulder, Colorado, and estimated a larger value of 963 moles of NO produced per CG flash by assuming that all NO_x was NO_2 in the lower portion of the storm after dark. The wide range of values found using data from various field projects suggests that lightning NO_x production may vary greatly between storms and individual flashes, though all estimates of lightning NO_x production contain significant uncertainty because of the number of assumptions required in translating aircraft observations into NO production values. Further investigation is required to constrain the magnitude of NO production per flash in order to reduce uncertainty in the global source estimate. The representation of lightning NO_x in 3-D regional and global chemical transport models (CTMs) is critical to the model's representation of ozone and other species such as OH [e.g. Stockwell et al., 1999, Labrador et al., 2004]. Labrador et al. [2005] found that both the magnitude of the global lightning NO_x source and its vertical distribution can significantly affect tropospheric trace gas concentrations in a global CTM.

1.6 The Cloud-Scale Chemical Transport Model

Output from several different cloud-resolving models has been used to drive a 3-D Cloud-Scale Chemical Transport Model (CSCTM) developed at the University of Maryland and fully detailed in DeCaria [2000] and DeCaria et al. [2005]. Temperature, density, wind, hydrometeor (rain, snow, graupel, cloud water, and cloud ice), and diffusion coefficient fields from the cloud model simulation are read into the CSCTM every five or ten minutes in the simulation, and these fields are then interpolated to the model time step of 15 seconds. The transport of chemical tracers is calculated using a van Leer advection scheme. The CSCTM employs parameterizations of lightning NO_x production which use observed flash rates, avoiding the difficulty of explicit modeling of thunderstorm electrification. In the DeCaria et al. [2005] version of the lightning NO_x parameterization, lightning NO_x production is calculated using observed IC and CG flash rates and a specified scenario of P_{IC} and P_{CG} to calculate the mass of NO injected into the cloud at each time step. The NO produced by CG flashes is distributed unimodally in the vertical centered around the -15°C isotherm, while the NO produced by IC flashes is distributed bimodally (with the lower mode centered on the -15°C isotherm and the upper mode isotherm located between -30 and -60°C) based on the vertical distributions of very high frequency (VHF) sources of IC and CG flashes presented in MacGorman and Rust [1998]. The upper mode isotherm is selected in each storm based on the height of the observed storm and the altitude of the peak observed NO_x mixing ratios. At each model level, the lightning NO is distributed uniformly to all grid cells within the 20 dBZ contour computed from simulated hydrometeor fields.

A passive version of the CSCTM includes only the transport of tracer species and production of lightning NO_x without any chemical reactions. In the passive version, the IC- and CG- produced NO_x can be isolated from pre-existing NO_x which allows a number of different production scenarios to be evaluated quickly. To account for the effects of chemical reactions, a full version of the CSCTM combines tracer transport and lightning production with a chemical solver and photochemical mechanism, better simulating the chemical environment within the storm. Soluble species are removed from the gas phase by cloud and rain water, but multiphase reactions are not included. Photolysis rates are calculated as a function of time, and are perturbed by the cloud. A chemistry-only version of the CSCTM is used to estimate 24-hour ozone production in the convective outflow that is assumed to be translated downwind. In this version, chemical reactions and diffusion are included, while cloud-scale advection is turned off. Clear sky photolysis rates are assumed and photolysis rates are calculated as a function of time.

1.7 Methods and objectives

Figure 1.1 provides a brief synopsis of the methodology used in each case study presented. The dynamical and microphysical evolution of storms from the Cirrus Regional Study of Tropical Anvils and Cirrus Layers – Florida Area Cirrus Experiment (CRYSTAL-FACE; Ridley et al., 2004; Lopez et al., 2006), EULINOX [Huntrieser et al, 2002], and STERAO [Dye et al., 2000] field projects have been simulated using several different cloud-scale models. The simulation of each storm was compared with the observed storm development using radar and satellite observations to ensure that it adequately replicated observed storm features such as anvil size and cloud top height.

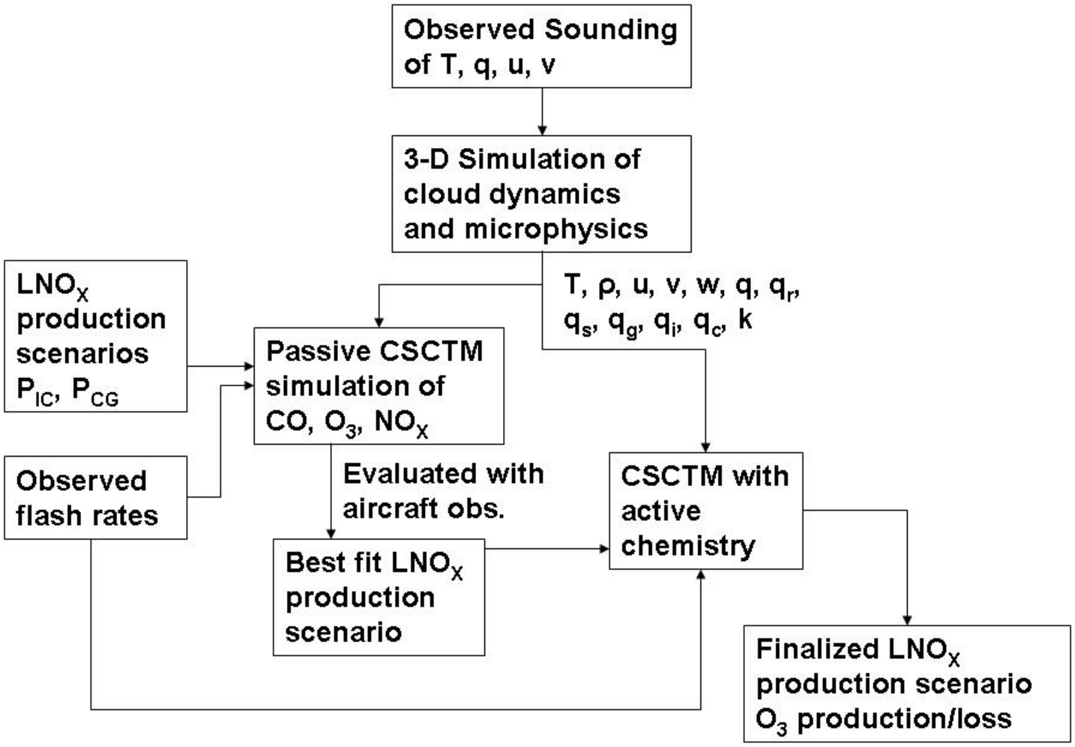

Figure 1.1. Method of estimating lightning NO_x production per IC and CG flash.

The temperature, wind, and hydrometeor fields from each storm simulation were used to drive the offline passive version of the CSCTM. Initial condition profiles of O_3, NO_x, and CO or CO_2 were constructed from out-of-cloud aircraft observations. Simulated in-cloud mixing ratios of O_3 and CO or CO_2 at anvil levels were compared with in-cloud aircraft observations of these species to determine whether of not the simulated convective transport was reasonable. If the transport of species such as O_3, CO, and CO_2 was reasonably simulated, the convective transport of NO_x should also be reasonable. Therefore, if this is the case, lightning NO_x production can be simulated by adding lightning NO_x to the convectively transported NO_x in the storm and a reasonable estimate of production per flash can be obtained. Observed IC and CG flash rates were read into the model and various production per flash scenarios of P_{IC} and P_{CG} were simulated in separate model runs. The results of these simulations were compared with in-cloud aircraft observations of NO_x to determine which production scenario resulted in the best comparison.

Once a best-fit production scenario was estimated using the passive transport version of the CSCTM, the full version of the CSCTM was run assuming this production scenario. The results from the CSCTM simulation including chemical reactions were again compared with aircraft measurements to ensure that the model results still compared favorably with observations when chemistry is included. The lightning NO_x scheme in the model was also turned off to produce a "no-lightning" simulation. The two simulations, one which included lightning NO_x and one which did not, were used to estimate the affect of lightning NO_x on ozone during the lifetime of the storm. Chemical fields at the end of the CSCTM simulations with chemistry were used to initialize the chemistry-only version of the model. By integrating both simulations forward for 24 hours and comparing the results, a rough estimate of ozone production per day due to the presence of lightning NO_x was obtained in the convective plume.

Production per flash has been estimated for all four case studies. An average production per IC and per CG flash was computed over all storms, and combined with assumptions of a global flash rate and global IC to CG ratio to estimate the global lightning NO_x source. In addition, at the end of each CSCTM simulation, the mass of N fixed by lightning was calculated at each model level, and the percentage of the total mass of lightning NO_x calculated for 1-km thick layers. These four simulated cases, along with a simulated squall line observed during PRE-STORM (Preliminary Regional Experiment for STORM; Rutledge and MacGorman, 1988) and the July 12 STERAO storm simulated by DeCaria et al. [2005] were divided into two meteorological regimes (midlatitude continental and subtropical) and average vertical profiles of lightning NO_x mass were calculated for each regime. These profiles can be used to specify the vertical distribution of the lightning NO_x source in global and regional CTMs.

The objectives of the research presented in this dissertation are:

a) To develop more realistic methods of representing lightning NO_x in cloud-scale models in order to facilitate estimates of NO production per flash and per unit flash channel length

b) To estimate production per IC and CG flash in a sample of storms representative of midlatitude and subtropical convection and to extrapolate these estimates of production per flash to obtain an estimate of the global lightning NO_x source

c) To examine the effect of lightning NO_x on atmospheric chemistry during the storm and in the 24 hours following the storm

d) To calculate the vertical distribution of lightning NO_x mass following convection for use in global and regional chemical transport models.

The work presented in this dissertation includes several important advancements in the study of lightning NO_x production and its effect on atmospheric chemistry. I developed a new lightning placement scheme which more realistically reproduces the variability of NO_x observations in the active lightning region than the DeCaria et al. [2005] scheme. In addition, I developed a second scheme which allows lightning NO_x production to be estimated per meter of flash channel length. The development of new 3-

D lightning mapping systems will provide more information on the length of IC and CG flashes in the near future and this scheme will allow for further estimates of NO production per meter flash length to be made. In addition to improvements in the representation of lightning NO_x in the CSCTM, this dissertation also details the implementation of the DeCaria et al. [2005] lightning scheme in a version of the Weather Research and Forecasting model which simulates both gas and aqueous phase chemistry (WRF-Aqchem). Chemistry in WRF-Aqchem is calculated online meaning that hydrometeor, temperature, and velocity fields do not need to be interpolated to a smaller time step as is necessary when using the offline CSCTM driven by cloud-resolving model fields saved every 5 or 10 minutes. The inclusion of lightning NO_x in WRF-Aqchem allows the effects of lightning NO_x on soluble species to be investigated.

Chapter 2 describes simulations of the July 21 EULINOX storm which will also be published in the *Journal of Geophysical Research*. In Chapter 3, simulations of the July 10 storm observed during the STERAO field project are presented. Chapter 4 details the simulations of the July 16 and July 29 storms observed over South Florida during the CRYSTAL-FACE campaign. In Chapter 5, an average lightning NO_x production scenario is calculated based on the simulations presented in Chapters 2-4 and the DeCaria et al. [2005] work. A brief discussion of lightning NO_x production using the average scenario in the June 10-11 PRE-STORM event is also included in Chapter 5, as is an estimate of the global lightning NO_x source and average vertical profiles of lightning NO_x following convection. These results are also included in a manuscript which will soon be submitted for publication. The final chapter presents a brief summary of the work presented in this dissertation.

Chapter 2. Simulations of the July 21 EULINOX storm

2.1 The EULINOX project

The EULINOX [Huntrieser et al., 2002] field campaign was conducted in central Europe during June and July 1998 with the goal of better understanding lightning NO_x production. During the project, airborne measurements were collected by the Deutsches Zentrum für Luft- und Raumfahrt (DLR) Falcon and the Do228 research aircraft. Both measured NO_x, O_3, CO and CO_2, as well as meteorological parameters in and around thunderstorms in the region of the experiment. The Do228 flew primarily in the boundary layer and lower troposphere below 4 km, while the Falcon investigated the upper troposphere and performed a number of anvil penetrations through monitored thunderstorms. CG lightning occurrences were recorded by an LPATS system known as BLIDS. In addition, total 3-D lightning activity (IC+CG) within the 100 km area surrounding the EULINOX operation center was mapped by a VHF (very high frequency) interferometer from the French Office Nationale d'Etudes et de Recherches Aerospatiales (ONERA). Both radar and satellite observations were used to monitor the development of thunderstorms in the region.

2.2 Observed storm evolution

On the evening of July 21, 1998 the evolution of a severe thunderstorm west of Munich, Germany was documented and is shown in figure 2.1. After an initial period of intensification, the storm split into two distinct cells evident on the radar image at 1852 LST (1652 UTC). The northernmost cell became multicellular in structure and was observed to decay soon after the cell-splitting event, while the southern cell strengthened

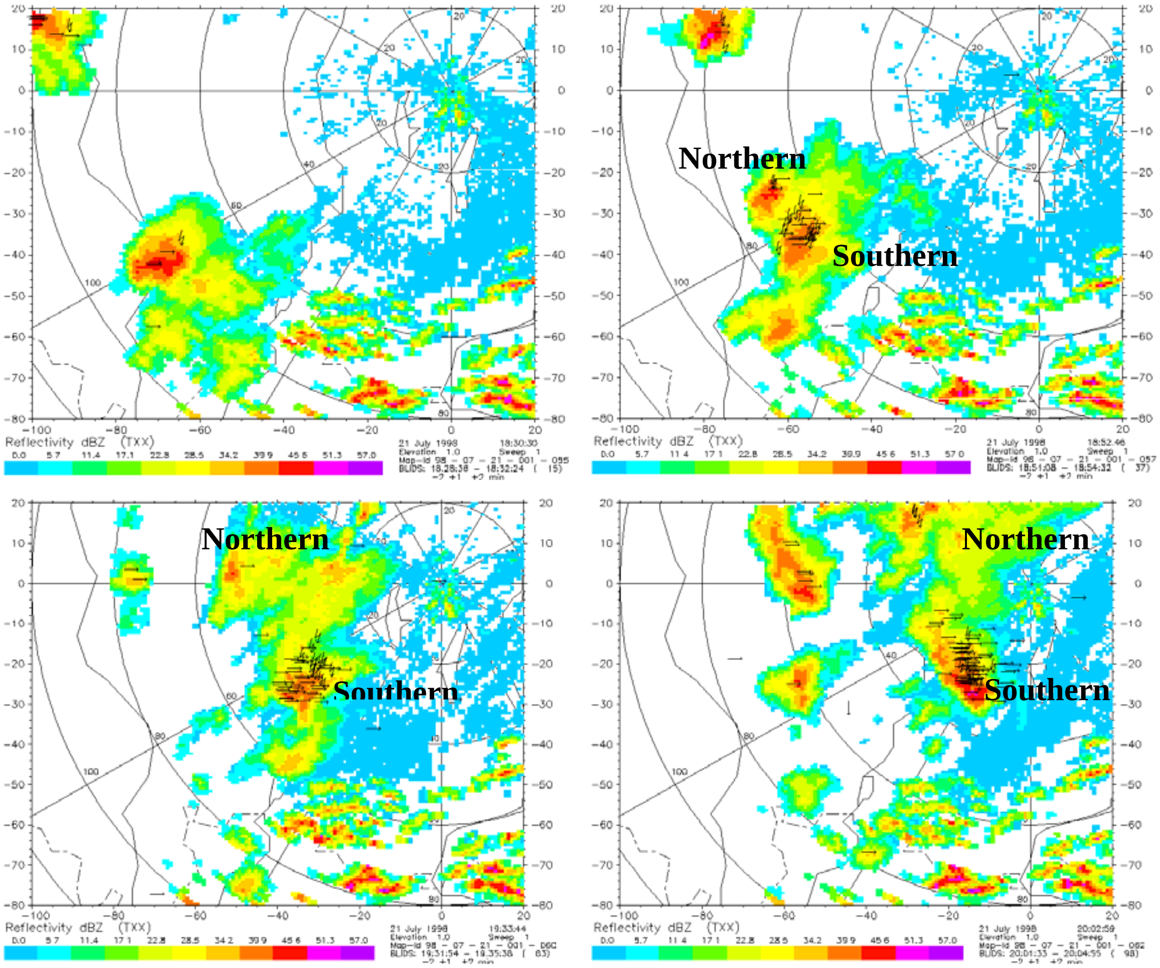

Figure 2.1. 1° elevation scans from the POLDIRAD at 1640, 1652, 1733, and 1802 UTC on July 21, 1998 with BLIDS CG flashes recorded during the 2 minutes before and after each radar scan overlaid. Horizontal arrows denote positive flashes and jagged arrows indicate negative flashes. Distances are km from POLDIRAD [Höller et al., 2000].

and developed supercell characteristics including a distinct hook echo (see radar image observed at 1933 LT; Höller et al., 2000). From 1400 to 2200 UTC total lightning activity within the entire storm was monitored by the ONERA interferometer, and cloud-to-ground lightning activity was recorded by BLIDS. Théry [2000] compared flashes recorded by BLIDS and the ONERA interferometer and found that many low amplitude positive flashes recorded by BLIDS were IC rather than CG. This was also true for flashes with weak negative peak current, but to a lesser degree. Flashes with peak current between -5 and +15 kA were removed [Höller et al., 2000] and the remaining BLIDS flashes counted to obtain CG flashrates, which were subtracted from counts of interferometer flashes to yield IC flashrates. By comparing plots of the locations of interferometer and BLIDS flashes with plots of radar reflectivity, flashes belonging to the northern and southern cells were identified. Figure 2.2 shows that the southern cell contained the majority of lightning activity with IC flashes dominating the total lightning activity after 1710 UTC. In the period shown, 360 CG flashes and 2565 IC flashes were recorded in the southern cell (mean IC/CG ratio = 7.1) while in the northern cell there were 289 CG flashes and 815 IC flashes (mean IC/CG ratio = 2.8). The storm was penetrated seven times during the period from 1735 to 1842 UTC by the Falcon while flying between 6.3 and 9.2 km AGL near the active convective cells and in the lower anvil. Figure 2.3 [Huntrieser et al., 2002] shows the Falcon flight track

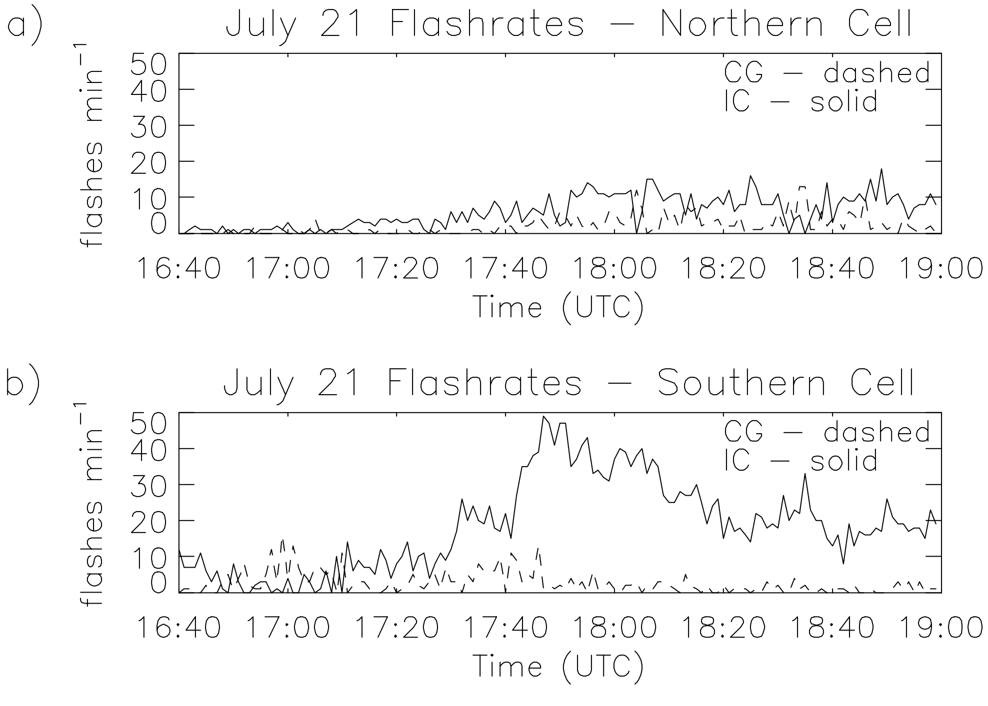

Figure 2.2. Time series of IC and CG flash rates for the (a) northern and (b) southern cells in the July 21 EULINOX storm.

superimposed on a map of VHF signals recorded by the interferometer from 1740 to 1810 UTC. During this period, nearly 400 IC and CG flashes were recorded. The Falcon flew between 8 and 9 km AGL in the vicinity of the maximum lightning activity where the majority of freshly produced NO would be observed. NO mixing ratios up to 25 ppbv were observed during this period [Huntrieser et al., 2002].

Fehr et al. [2004] simulated the EULINOX storm of July 21, 1998 using a modified, cloud-resolving version of the PennState/NCAR Mesoscale Model 5 (MM5) with a 1 km horizontal resolution which included a parameterized lightning NO_x source with emissions represented by a Lagrangian particle model. Lightning NO_x particles were distributed within a vertical flash channel with the vertical distance between particles depending on atmospheric pressure. Flash rates were parameterized using the

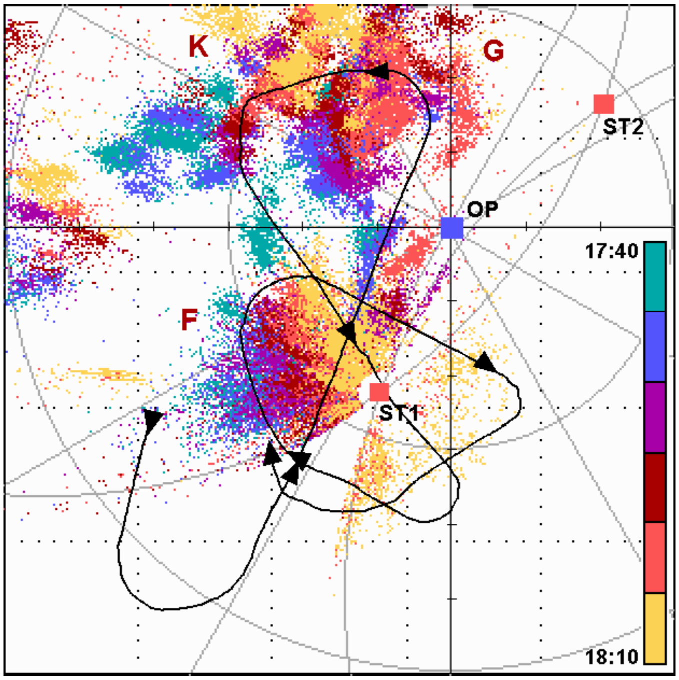

Figure 2.3. Locations of VHF sources recorded by interferometer at stations ST1 and ST2 between 1740 and 1810 UTC on July 21, 1998 overlaid with the Falcon’s trajectory during the same time period. Red letters indicate the location of electrified cells [Huntrieser et al., 2002].

methods of Price and Rind [1992, 1993] and Pickering et al. [1998] and compared with observed flash rates. The parameterization overestimated total lightning activity considerably, so observed flashrates were used to estimate lightning NO_x production by comparing model results with NO measurements taken during three of the seven Falcon anvil penetrations. A production scenario in which a CG flash produces approximately 330 moles of NO per flash and an IC flash is 1.4 times more productive of NO than a CG flash compared favorably with the observations used. An estimated 50-80% of the lightning produced NO_x was transported to the anvil region, with 97% of anvil NO_x resulting from IC flashes.

2.3 Simulated storm evolution

The July 21 EULINOX storm was simulated by Dr. Georgiy Stenchikov from Rutgers University using the 3-D Goddard Cumulus Ensemble (GCE) model (Tao and Simpson, 1993; Tao et al., 2001). The model was initialized with a single sounding provided by Dr. Thorsten Fehr, formerly of DLR, that included data from a German Weather Service radiosonde, the ascent of the DLR Falcon aircraft, and a dropsonde released during the Falcon's flight, all of which were no more than 90 minutes ahead of the storm. CAPE for this sounding was 1590 J/kg [Fehr et al., 2004]. The sounding also showed winds veering at low levels which is conducive to splitting. Convection was initiated with a single warm thermal perturbation and a flat orography was assumed. The horizontal resolution was 2 km and there were 50 vertical levels, with a resolution of 0.5 km. The model was run for 5 hours.

The GCE simulation successfully reproduced a number of features of the observed storm. A single cell first appeared 20 minutes into the simulation. At 70 minutes, the cell splitting has begun. Because the early stages of the cell splitting was observed on radar at ~ 1650 UTC (Figure 2.1), 70 minutes in the simulation was chosen to correspond to this time for the purposes of comparison with aircraft observations and the use of observed flash rates in the lightning NO_x calculation. Thus, the beginning of the simulation was assumed to correspond to 1540 UTC. In Figure 2.4, a single cell is visible 30 minutes into the simulation. The cell has completely split in two at 100 minutes in the model simulation. The southern cell has developed a supercell circulation and an apparent hook echo at this time. At 150 minutes, a third cell has developed between the original two cells. The southern cell has begun to decay at 180 minutes, and the northern cell becomes dominant.

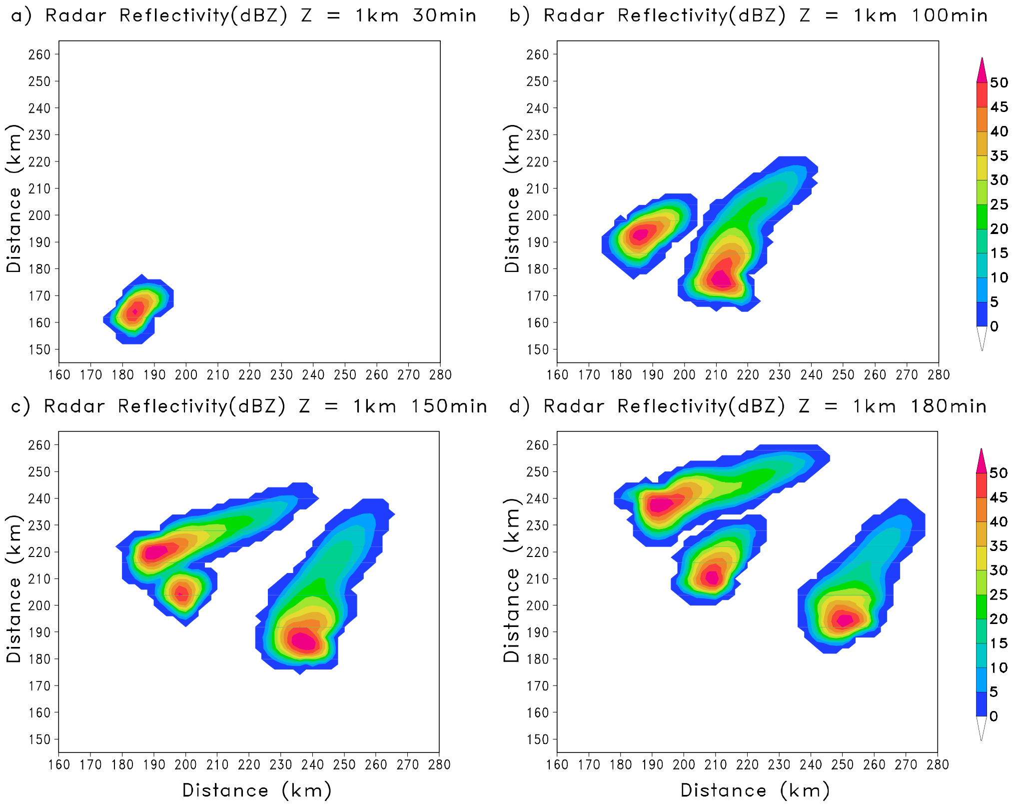

Figure 2.4. Radar reflectivity at 1 km elevation computed from GCE hydrometeor fields at (a) 30, (b) 100, (c) 150, and (d) 180 minutes in the simulation of the July 21 EULINOX storm.

Some simulated storm features were similar to observations and some differed. The model correctly predicted the splitting of the initial cell. However, in the observed system the northern cell weakened rapidly after the cell splitting event and the southern cell became the dominant feature, evolving into a supercell. The simulated southern cell, while demonstrating supercell characteristics and dominating for a period of time, did not persist as long as observed. Cloud top heights reached 14 km which compared favorably with observations [Höller et al., 2000] and the MM5 simulation presented by Fehr et al. [2004]. Discrepancies between the simulated storm and observations may be because the nonuniformity of terrain and initial conditions [Stenchikov et al., 2005] were not accounted for in the GCE simulation. Boundary conditions may also have contributed to these differences. However, comparison with observations showed that the simulated storm evolution was fairly reasonable for the period of 180 minutes that was chosen for the chemistry-transport calculations in this study.

At 1657 UTC, just after the cell splitting event, the southern cell was observed by dual-Doppler radar and the 3-D wind field reconstructed. At this time, a maximum updraft speed of 24 m s^{-1} was observed while the strongest downdraft was 9 m s^{-1} [Höller et al., 2000]. At the corresponding time in the simulation (80 minutes), the maximum updraft velocity was 34 m s^{-1} while the maximum downdraft was 7 m s^{-1}. Due to the location of the storm with respect to the radar, dual-Doppler analysis was not possible at other times. Maximum updraft velocities were approximately 36 m s^{-1} between 90 and 130 minutes in the GCE simulation, and then decreased. This is lower than the maximum updraft of 49 m s^{-1} reported in the Fehr et al. [2004] simulation. Downdraft velocities were also less than those presented in Fehr et al. [2004] in which a maximum of 25 m s^{-1}

was recorded. Throughout the GCE simulation, downdraft velocities were typically less than 10 m s^{-1}. Low level inflow to the simulated storm occurred between 0.5 and 3 km while outflow from the anvil was greatest between 9 and 11 km.

2.4 Tracer transport and lightning NO_x production

The passive version of the CSCTM was used to calculate the transport of CO_2, NO_x, and O_3. CO, which in polluted regions has a stronger vertical gradient than CO_2 and would be preferable to CO_2 as a tracer of upward transport, was not measured on this day. An initial profile of CO_2 was constructed using data from the Falcon ascent and a value of 355 ppbv above the tropopause taken from Strahan et al. [1998]. An initial profile of O_3 was constructed using data from the Falcon ascent, the DO-228 boundary layer data for the day, and a climatological average ozone profile for the latitude of Munich above 9 km. The NO_x profile was composed of data taken from the Falcon ascent in the free troposphere and from a profile one standard deviation greater than the average NO_x boundary layer profile during the EULINOX project [Huntrieser et al., 2002]. A profile with values larger than the project mean in the boundary layer was assumed because no actual measurements were available and high measured boundary layer values of CO_2 and O_3 suggested polluted NO_x conditions on this day. Sensitivity calculations were also performed using the EULINOX boundary layer average and the boundary layer average plus two standard deviations in order to assess the effects of this uncertainty on the lightning NO production results. The initial condition profiles for CO_2, NO_x, and O_3 are shown in Figure 2.5. IC and CG flash rates for the northern and southern cells (as shown in Figure 2.2) were read into the model at 3-minute intervals beginning 21 minutes into the simulation to correspond to the time when lightning was

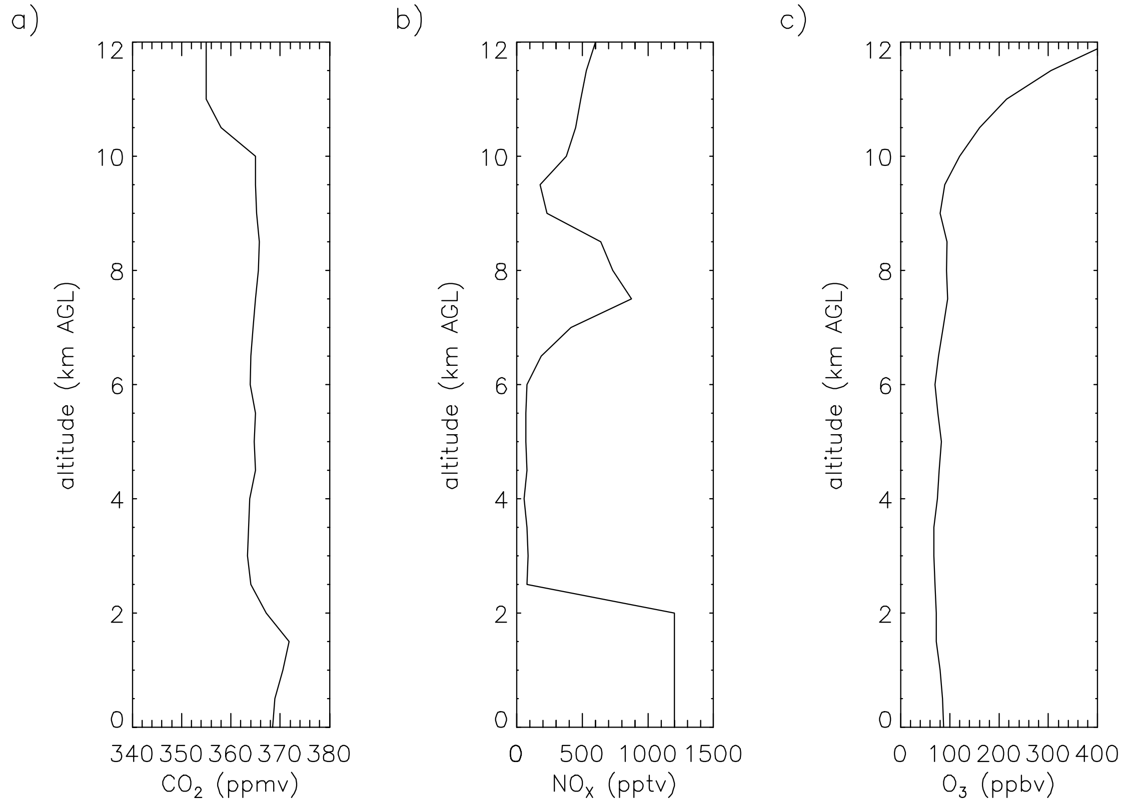

Figure 2.5. Initial condition profiles of (a) CO_2, (b) NO_x, and (c) O_3 prior to the July 21 EULINOX storm.

first observed, and the amount of lightning NO_x produced in each time interval was calculated.

2.4.1. CO_2 and O_3 transport

Figure 2.6 shows a vertical cross section of CO_2 through the southern cell at 150 minutes when the cell was at maximum strength, oriented 65 degrees counterclockwise from due east. Air containing the maximum CO_2 mixing ratios exceeding 370 ppmv initially in the 1-2 km region has been transported to over 12 km in the core updraft region, and as high as 10 km in the anvil, indicating strong upward motion at this time. Both the core and the downwind anvil regions of the storm are largely comprised of air that resided in the boundary layer prior to convection, while there is little evidence of entrainment of environmental air with lower CO_2 mixing ratios. The model also suggests downward transport of smaller mixing ratios of CO_2 in the 8-11 km altitude region behind the storm and from 0.5 to 3.5 km.

In order to compare simulated tracer transport with mixing ratios observed during the series of seven anvil penetrations, data collected by the Falcon aircraft were averaged over approximately 11-second intervals to yield a spatial resolution equivalent to the model, and then binned into 0.5 km thick layers. Unfortunately, in-cloud observations were only available for three 0.5 km thick layers centered at 8, 8.5 and 9 km AGL. Therefore, the comparison with model results includes only a 1.5-km thick layer. The

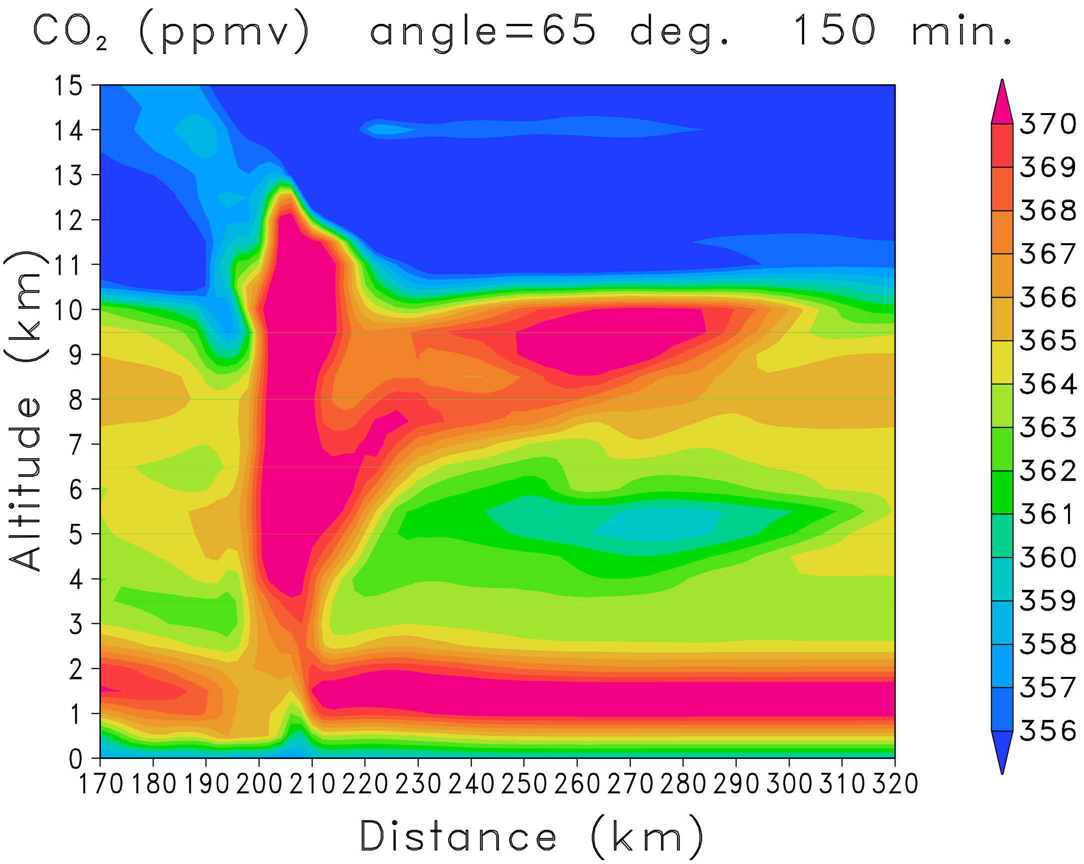

Figure 2.6. Cross section of CO_2 mixing ratios in the southern cell from the CSCTM simulation of the July 21 EULINOX storm at 150 minutes at an angle of 65° counterclockwise from east along the axis of the southern cell.

analysis would have benefited from observations at a wide range of altitudes as were available for the July 12 STERAO-A storm simulated by DeCaria et al. [2005] in which the research aircraft executed a spiral ascent through the storm anvil, measuring NO from 7 to 11 km MSL. The area covered during each penetration was calculated from flight position data. The average distance covered during 6 of the 7 anvil penetrations was determined to be approximately 24 km in the x-direction and 36 km in the y-direction. A box of this size was placed around the core of the southern cell where radar observations and flight data show that the Falcon was primarily sampling. The grid cells within this box were sampled at times in the simulation corresponding to the times of the aircraft sampling at each level, and cumulative probability distribution functions (pdfs) calculated for each level. In addition, the mean, mode and standard deviation of observed and simulated NO_x, O_3 and CO_2 mixing ratios at 9 km were calculated and are shown in Table 2.1. The model does an excellent job in estimating the mean values at this altitude. However, it appears that the distribution of observed O_3 mixing ratios at this level is substantially broader than that simulated.

Table 2.1. Statistics of Observed and Simulated Tracer Mixing Ratios at 9 km in the July 21 EULINOX storm

	Mean	Mode	Standard Deviation
Obseved CO_2 (ppmv)	367.0	366.4	1.5
Simulated CO_2 (ppmv)	367.8	371.8	3.4
Observed O_3 (ppbv)	90.0	84.8	15.8
Simulated O_3 (ppbv)	89.1	84.1	5.6
Observed NO_x (ppbv)	2.4	1.3	1.7
Simulated NO_x (ppbv)	2.6	0.3	2.1

* Statistics are computed over the sampling box shown in Figure 2.12a.

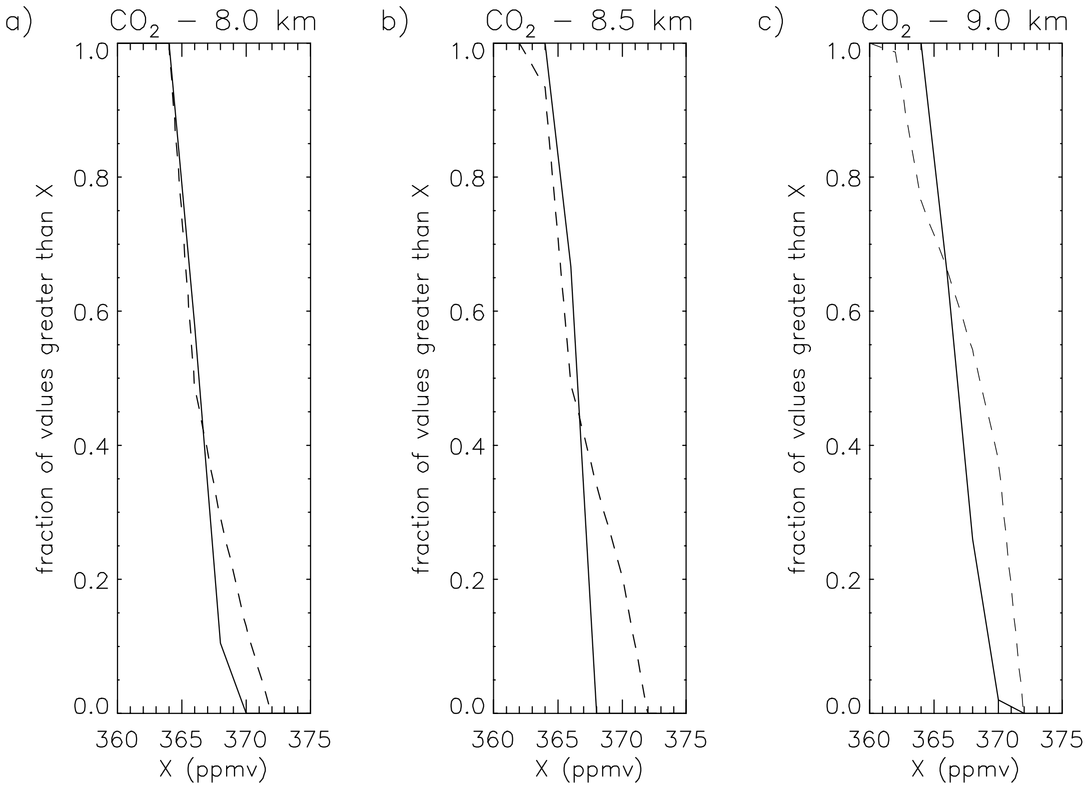

Figure 2.7. Pdfs of observed (solid) and simulated (dashed) CO_2 mixing ratios at (a) 8, (b) 8.5, and (c) 9 km in the July 21 EULINOX storm.

Figure 2.7 shows that at 8, 8.5 and 9 km AGL, the distribution of simulated CO_2 matches the observed distribution well with a slight overestimation of the maximum values. At 9 km, the model also underestimates the minimum values, suggesting that the downward transport at the rear of the storm may not have been as pronounced as seen in the model. Figure 2.8 shows pdfs of observed and simulated O_3 at 8 and 9 km, the only two levels for which a sufficient number of observations were available to calculate pdfs. At both levels, the simulations underestimate the maximum values and overestimate the minimum values. The overestimation of minimum values is due in part to the initial condition profiles used. Though ozone as low as 63 ppbv was observed in the storm, the lowest value in the initial condition profile was 67 ppbv at 3.5 km because there was no observational evidence outside the storm to suggest that values lower than this would be appropriate. When chemical reactions were included in the model (see Section 3.3.) a small loss of ozone occurred at 8 km, slightly improving the comparison between the simulated and observed minimum values though overestimation of the minimum values is still noticeable, particularly at 9 km. The underestimation of the maximum values suggests the model may be underrepresenting downward transport, although this is not supported by analysis of the CO_2 distributions. This contradiction may be the result of a lack of sufficient observations of CO_2 and O_3 near the tropopause to well define the vertical gradients in this region that were used in the initial condition profiles.

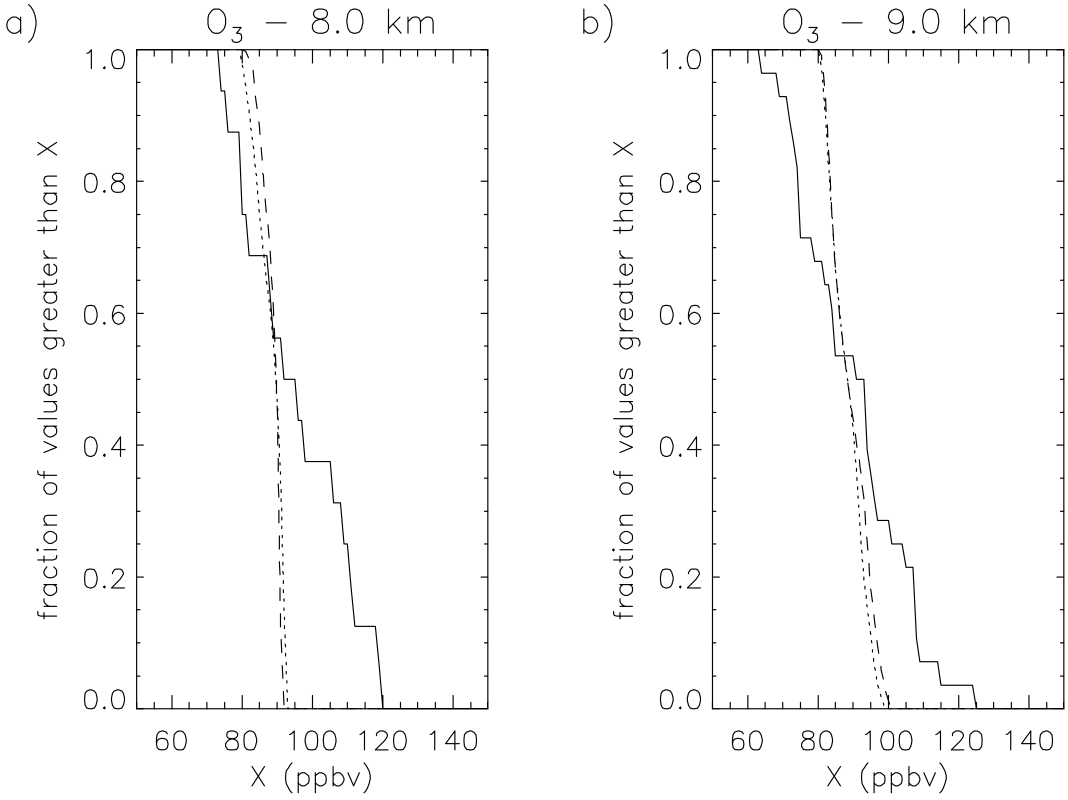

Figure 2.8. Pdfs of observed (solid) and simulated (without chemical reactions – dashed, with chemical reactions - dotted) O_3 mixing ratios at (a) 8 and (b) 9 km in the July 21 EULINOX storm.

Additionally, the observed discrepancy could have been caused by time interpolation of the driving field and approximation errors. If downward transport was slightly underrepresented by the model, it is unlikely to significantly affect the estimates of lightning NO_x production because NO_x mixing ratios immediately above the tropopause were similar to the enhanced mixing ratios of NO_x between 7 and 9.5 km in the initial condition profile.

2.4.2 Lightning NO_x production

Two different schemes were used in the model to estimate the production of lightning NO_x. These schemes differ from the lightning NO_x parameterization used in DeCaria et al. [2005] in which lightning NO_x was distributed bimodally in the vertical and uniformly to all grid cells within the 20 dBZ contour of the cloud at each level as if the NO_x was instantly diffused throughout this region of the cloud. The DeCaria et al. [2005] model results were compared to the general profile shape and integrated column mass of observed NO_x. This approach performed well for the July 12 STERAO storm in which the anvil observations were located relatively distant from the convective cores. In that case, the aircraft measured the integrated effects of many flashes on NO_x mixing ratios. However, in the EULINOX storm, the aircraft flew in a much more electrically active part of the storm, necessitating a different approach. These new schemes (developed as part of the dissertation research) attempt to replicate more realistically actual flashes and the range of NO_x mixing ratios observed by putting lightning NO_x from individual flashes into smaller subsets of grid cells within the simulated cloud.

The first scheme allows an estimate to be made of NO production per flash and the second allows an estimate of production per meter flash length. In the first scheme, observed flash rates for the northern and southern cells are input along with a scenario of IC and CG production specified in terms of moles of NO produced per flash. The average horizontal extent of a flash was calculated from interferometer data and is input for each 3-minute lightning time step, as is the total number of IC and CG flashes in each cell of the storm. The areas in which lightning occurred in the northern and southern cells were estimated from plots of observed IC and CG flashes. Areas of approximately this size were centered 10 km downwind of the maximum updraft of the northern and southern cells in the model because Höller et al. [2000] noted that in this storm, based on an analysis of interferometer and radar observations, flashes tended to occur downwind of the updraft. The distance of 10 km was chosen based on visual inspection of plots of radar reflectivity overlaid with flash locations presented in Höller et al. [2000].

The vertical distribution of IC flash channel segments is derived from two Gaussian distributions, one centered at -30° C and the other at -15° C, which are summed, while the vertical distribution of CG flash channel segments consists of a single Gaussian distribution centered at -15° C [DeCaria et al., 2005]. These distributions, f(z), determine the number of grid cells in the horizontal to be included in an IC or CG flash at each model level as shown in Figure 2.9a. The vertical distribution of the number of grid cells included in a CG flash results in no grid cells in the lowest two layers of the model receiving direct placement of lightning NO. To a first approximation, this configuration is supported by data from 3-D lightning mapping systems which record a nearly negligible amount of flash channels near the surface compared with that which occurs aloft. At the top of the cloud, as determined by the uppermost nonzero value of f(z), an initiation point is selected at random within the designated area downwind of the the updraft. After this point is selected, the flash is constrained to an area equaling the average horizontal flash extent. At each level, the locations of a number of grid cells given by f(z) are selected at random, such that tortuosity of the flash is simulated. NO is distributed to all grid cells along each flash with a dependence on pressure as described in DeCaria et al. [2000] because of laboratory experiments showing a linear relationship between pressure and NO production [Wang et al., 1998]. Figure 2.9b shows a schematic diagram of lightning NO placement in the southern cell. The dashed line represents the

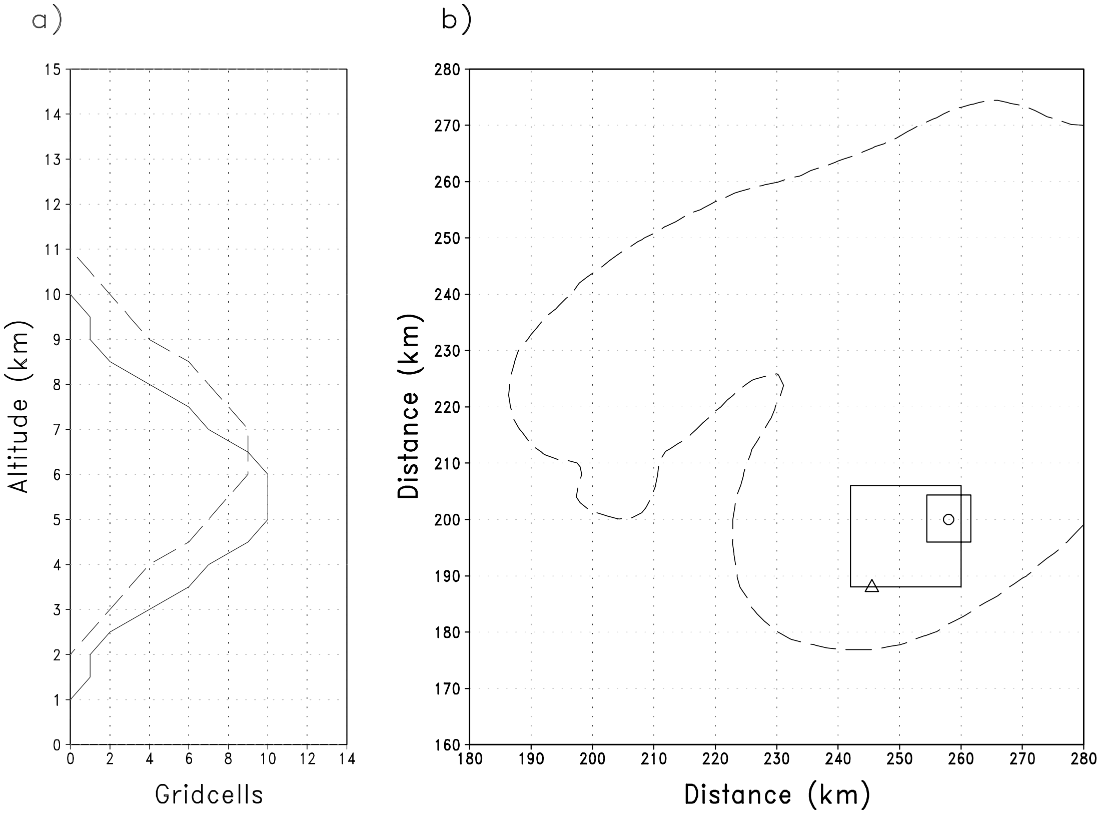

Figure 2.9. (a) Vertical distribution of the number of grid cells in the horizontal included at each model level in a CG flash (solid line) and in an IC flash (dotted line). (b) Schematic diagram of lightning NO_x placement in the July 21 EULINOX storm. Dashed line represents computed 20 dBZ radar reflectivity contour at 9 km 150 minutes into the simulation. Triangle shows the location of the maximum updraft and the larger box is the area from which an initiation point for the lightning is selected. The circle marks the initiation point, and the smaller box shows the area in which the flash is constrained.

20 dBZ contour at 9 km 150 minutes into the simulation. The maximum updraft velocity location is identified by the triangle. The larger box centered downstream of the updraft velocity maximum designates the area from which an initiation point for the flash, marked with an open circle, is selected. The smaller box centered about the initiation point is the area determined by the average horizontal flash extent. Various NO_x production scenarios were simulated to determine which most closely matched observed NO_x mixing ratios in the electrically active region of the storm.

The second scheme is similar to the first, except that the specified production is per meter of flash channel length and production per flash is calculated by the model using the average hourly length per flash as given in Théry et al. [2000]. Lightning flashes are constructed in the same manner as in the first parameterization, and the most appropriate production per meter flash length is estimated by comparing results from various production scenarios with aircraft observations.

To calculate lightning NO_x production, P_{CG} was estimated to be approximately 360 moles of NO per flash based on observed peak current and a relationship between peak current and energy dissipated from Price et al. [1997]. The upper mode of the vertical distribution of IC NO_x was assumed to be at the height of the -30° C isotherm, while the lower mode was assumed to be at the height of the -15° C isotherm. Several different values of the P_{IC}/P_{CG} ratio were simulated and the results compared with observations. The common assumption that P_{IC} is one tenth P_{CG} from Price et al. [1997] was simulated and the pdf of observed and simulated NO_x at 9 km is shown in Figure 2.10a. The assumption that IC flashes are significantly less productive of NO than CG flashes clearly underestimates NO_x at all levels. Fehr et al. [2004] found a P_{IC}/P_{CG} ratio of 1.4 most appropriate for a simulation of the same storm. Figure 2.10b shows the 9 km pdf with NO_x production based on this assumption. At this level, where the majority of NO_x observations were taken, assuming a P_{IC}/P_{CG} ratio of 1.4 results in an overestimation of the lightning NO_x source. At 8 and 8.5 km, fewer observations were available, but the maximum observed mixing ratios exceeding 15 and 20 ppbv were reasonably simulated at these levels using the ratio of 1.4. Therefore the comparison of the $P_{IC}/P_{CG} = 1.4$ scenario with observations at these two levels was better than at 9 km.

A scenario in which P_{IC} is equal to P_{CG} was also simulated and the pdfs for 8, 8.5, and 9 km are shown in Figure 2.11. At 9 km, the comparison between the observed and

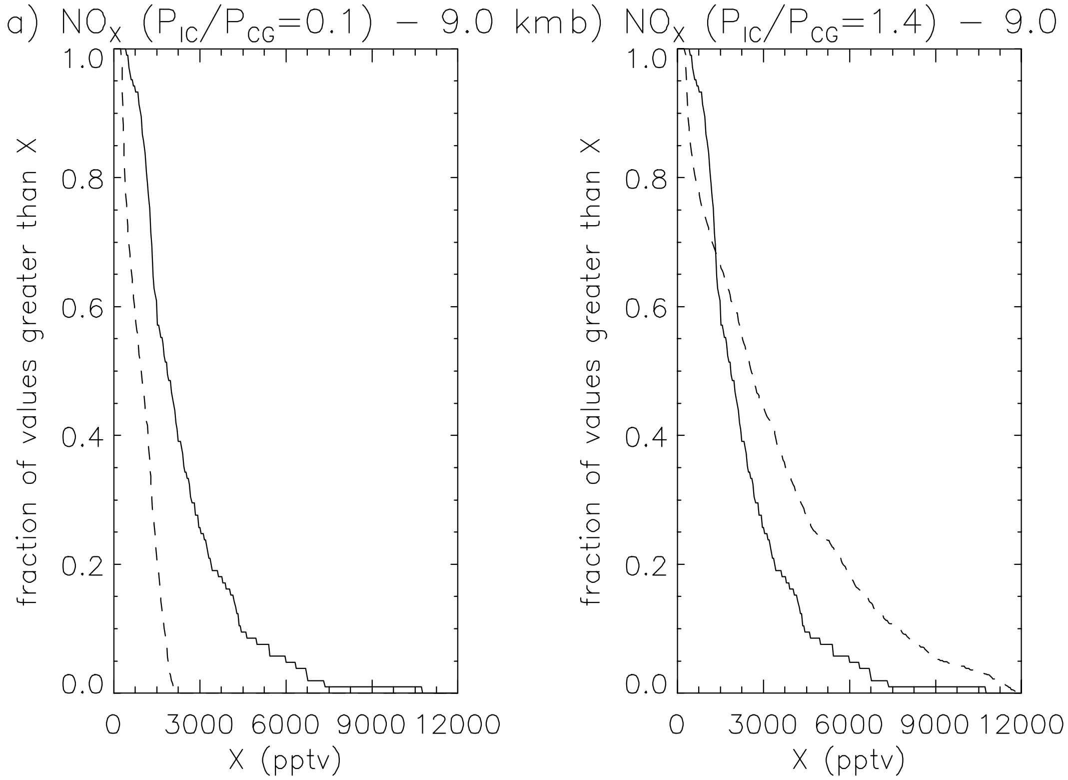

Figure 2.10. Pdfs of observed (solid) and simulated (dashed) NO_x mixing ratios at 9 km in the July 21 EULINOX storm assuming (a) $P_{IC}/P_{CG} = 0.1$, and (b) $P_{IC}/P_{CG} = 1.4$.

simulated distributions is much better than in the P_{IC}/P_{CG} of 0.1 and 1.4 scenarios shown in Figure 2.10. At 8 and 8.5 km, the model is able to reproduce the distribution below 6 ppbv fairly well, but fails to produce the large NO_x mixing ratios observed. Figure 2.12a shows a plot of NO_x at 9 km 180 minutes into the $P_{IC}=P_{CG}$ simulation with the box used for sampling model output. NO_x mixing ratios exceeding 9 ppbv are evident in the core of the southern cell and mixing ratios over 2 ppbv extend outward in the anvil a distance of over 70 km.

To determine which production scenario was the most appropriate, the mass of N in NO_x in the column between 7.75 and 9.25 km AGL was also calculated by averaging

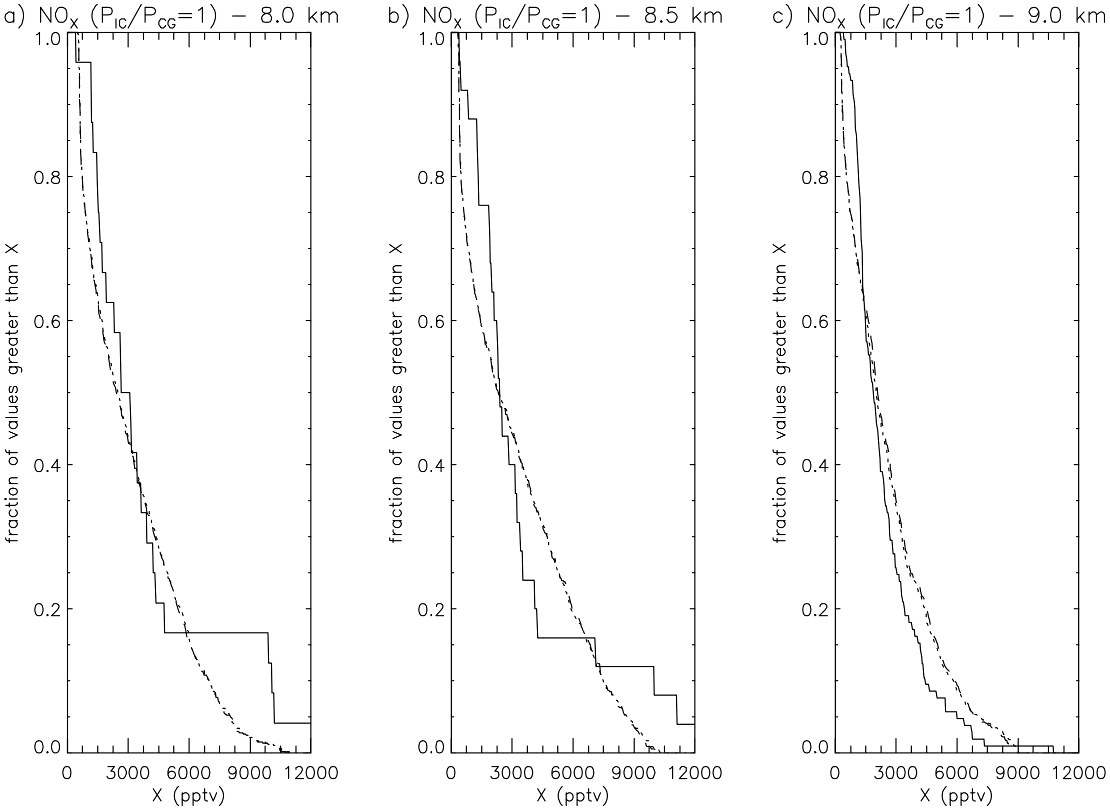

Figure 2.11. Pdfs of observed (solid) and simulated (assuming $P_{IC}=P_{CG}$=360 moles NO – dashed, assuming P=1.25x10-2 moles NO per meter flash channel length - dotted) NO_x mixing ratios at (a) 8, (b) 8.5, and (c) 9 km in the July 21 EULINOX storm assuming P_{IC}/P_{CG} = 1.0.

observations and model results in each of the three 0.5 km layers. The observations yield a column mass of 1.1 x 10^{-3} g N m^{-2}. The accuracy of the NO and NO_2 instruments are 5 and 10% respectively [Huntrieser et al., 2002]. Therefore, in terms of measurement error in the column mass estimate, 10% would be an upper limit. However, there is additional uncertainty because it is impossible to know how well the aircraft observations represent a particular area within the storm. Assuming a production scenario in which an IC flash produces only one tenth as much NO as a CG flash greatly underestimated column mass, producing 3.4 x 10^{-4} g N m^{-2}. The assumption from Fehr et al. [2004] that an IC flash produces 1.4 times as much NO as a CG flash led to a column mass of 1.4 x 10^{-3} g N m^{-2}, an overestimation of approximately 27%. Of the three scenarios presented, assuming an IC flash produces as much NO as a CG flash provided the best comparison with observations with a column mass of 1.1 x 10^{-3} g N m^{-2}. The inclusion of chemical reactions in the model tends to decrease NO_x which caused an underestimation of the observed column mass of approximately 10% (see Section 2.5). Based on the comparison of the pdfs and column mass of the observed and simulated storms, this scenario was selected as the most appropriate of the three for this storm. An increase or decrease of one standard deviation in the boundary layer NO_x resulted in a change of only 3% in the calculated column mass of N in NO_x. The assumption that boundary layer NO_x mixing ratio has little impact on our ability to deduce the appropriate lightning NO_x production scenario is thus supported.

The second scheme was used to estimate NO production per meter flash channel length. In this scheme, various values of production per meter were specified, and

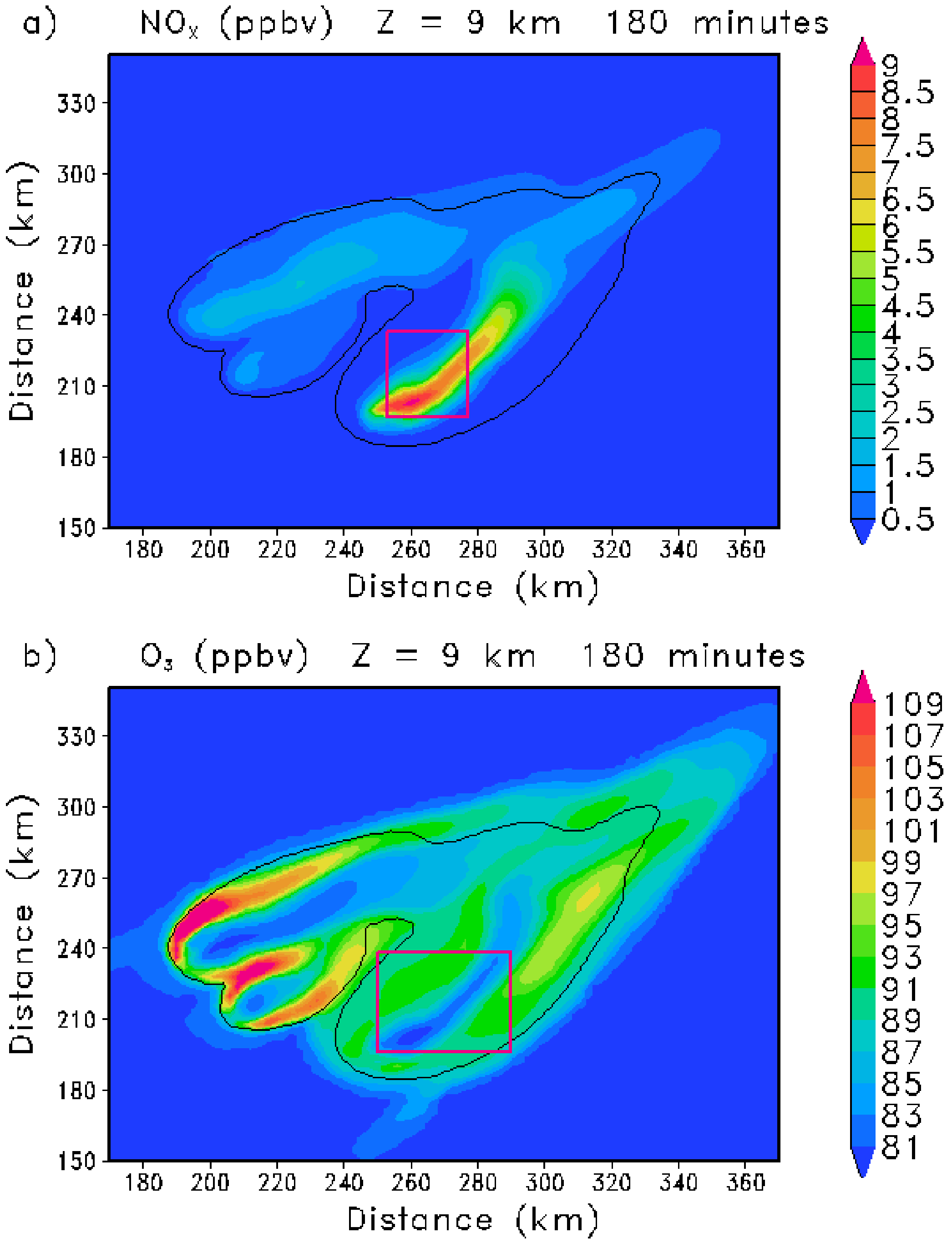

Figure 2.12. (a) NOx mixing ratios at 9 km elevation assuming P_{IC}=P_{CG}=360 moles NO/flash at 180 minutes in the passive CSCTM simulation of the July 21 EULINOX storm. The red box indicates the grid cells sampled for calculation of column mass and pdfs and the black line indicates the 20 dBZ contour of computed radar reflectivity. (b) O_3 mixing ratios at 9 km at 180 minutes in the CSCTM simulation of the July 21 EULINOX storm including chemical reactions. The black line indicates the 20 dBZ contour of computed radar reflectivity. The red box indicates the area for computing average O_3 profiles.

production per IC and CG flash was calculated using hourly average interferometer-observed flash lengths of 21.5, 27.9, and 31.4 km from Théry et al. [2000] for the hours beginning at 16, 17 and 18 UTC, respectively. By calculating pdfs (Figure 2.11) and column mass, a production of 1.25 x 10^{-2} moles NO per meter of flash channel length was found to yield results comparable to the P_{IC}=P_{CG}=360 moles NO per flash scenario. Note that the pdfs are nearly identical to those from the first scheme.

The average hourly flash lengths of Théry et al. [2000] did not differentiate between IC and CG flashes. Dotzek et al. [2000] attempted to estimate typical flash lengths for IC and CG flashes separately based on the heights of the main charge layers in the storm and the diameter of the storm with radar reflectivity greater than 30 dBZ. Using this method, they found typical lengths of 43 km for an IC flash, 26.5 km for a negative CG flash, and 29.5 km for a positive CG flash. It should be noted that because these estimates are based not on calculated lengths of IC and CG flashes, but on other parameters, there is a high degree of uncertainty. If these numbers are used in the model instead of the average hourly flash lengths from Théry et al. [2000], then a production scenario in which an IC flash produces 8.34 x10^{-3} moles NO per meter of flash channel length and a CG flash produces 1.35 x 10^{-2} moles of NO per meter of flash channel length would be needed to produce a favorable comparison with observations.

2.5. Simulation of the chemical environment of the storm

To investigate the impact of chemistry on the concentrations of species of interest such as NO_x and ozone, a CSCTM run including chemical reactions was performed. The same chemistry reaction scheme as used by DeCaria et al. [2005] was employed here, except that reaction schemes for isoprene and propene were added (see Appendix A).

Profiles of C_2H_6, C_2H_4, C_3H_6, C_3H_8, CH_3OOH, CO, H_2O_2, HCHO, HNO_3, isoprene, and PAN were taken from a July mean profile for the appropriate latitude and longitude of the EULINOX storm provided by Dr. Rokjin Park of Harvard University from the University of Maryland 3-D global Chemical Transport Model (UMD-CTM) [Park et al., 2004]. The NO to NO_2 ratio at each CSCTM model level was based on the ratios from the UMD-CTM, but the initial NO_x was equivalent to the values used in the passive version of the model. Profiles of hydrocarbons were scaled with the aid of airborne hydrocarbon measurements collected during the 1999 Konvektiver Transport von Spurengasen (KONVEX) campaign to ensure they represented values typical of the relatively polluted German atmosphere. Boundary layer concentrations of isoprene were held constant (e.g. at 1 ppbv in the bottommost layer of the model) during daylight hours to reflect a balance between the emissions and reactive losses of these compounds. At the conclusion of the 180-minute simulation, isoprene mixing ratios were approximately 6 pptv in the core updraft region of the storm, and were typically less than 1 pptv in the anvil region. A 15-minute "spin-up" simulation was performed using a column model which included the same chemical reactions as the full version of the 3-D CSCTM in order to allow the species to come into equilibrium. The CSCTM was run with the flash rate parameterization using the lightning NO_x production scenario P_{IC}=P_{CG}=360 moles NO/flash. Column mass and pdfs were computed from the model output using the same methods as for the passive version of the model. The use of global model output along with observed NO_x resulted in a small decrease in NO_x in the initial conditions during spin-up, such that the column mass for the flash rate and flash length scenarios simulated was 1.0 x 10^{-3} g N m^{-2}, a difference of 10% from the observations. In order to match the observed column mass of 1.1 x 10^{-3} g N m^{-2}, the P_{IC}/P_{CG} must be increased to 1.15 and the production per meter flash channel length increased to 1.42 x 10^{-2} moles NO. A case in which no lightning NO_x was included was also simulated to determine the lightning NO_x effects on in-cloud chemistry.

Figure 2.12b shows ozone concentrations 180 minutes into the simulation assuming a P_{IC}/P_{CG} ratio of 1.15 at the 9 km level. Lower ozone air has been transported upwards in the convective cores and is present in the outflow of the storms. There is significant downward transport of ozone surrounding the cores of the cells, increasing ozone mixing ratios above those of the environmental air (outside the cloud) in the anvil region. At the end of the 180 minute simulation, lightning NO_x resulted in additional O_3 production of less than 0.1 ppbv in regions outside of the cloud at 9 km. At 8 and 9 km, the inclusion of chemical reactions in the model continued to result in the underestimation of maximum ozone mixing ratios (see Figure 2.9), suggesting that downward transport may be underrepresented in the model.

In order to identify the effect of lightning NO_x on O_3 production during the storm, O_3 concentrations were averaged at 180 minutes in the simulation within the 40 km by 40 km sampling box shown in Figure 2.12b at each model level for both the lightning and no-lightning cases. The values from the simulation without lightning NO_x were subtracted from the values from the simulation which included a lightning NO_x source. Figure 2.13 shows that during the lifetime of the storm, the injection of lightning NO_x results in a net loss of ozone averaging less than 3 ppbv at all levels. The maximum net loss during this 3 hour period exceeds 9 ppbv at 5.5 km. This is due to the large quantities of NO_x (up to 9 ppbv) being introduced into the model. Large NO mixing ratios from lightning rapidly destroy ozone through the NO + O_3 reaction as described by Wang and Prinn [2000]. The ozone destruction resulting from including lightning NO_x in the model is likely short-lived. After the cloud dissipates, much of the NO_2 produced by the NO + O_3 reaction will be photolyzed to produce NO and $O(^3P)$, resulting in O_3 production (see following section).

2.6. Simulation of chemistry in the convective plume

The chemistry-only version of the CSCTM was used to estimate downstream ozone production in the 24 hours following the storm. Three-dimensional chemical fields at 180 minutes in the CSCTM simulation were used to initialize the chemistry-only

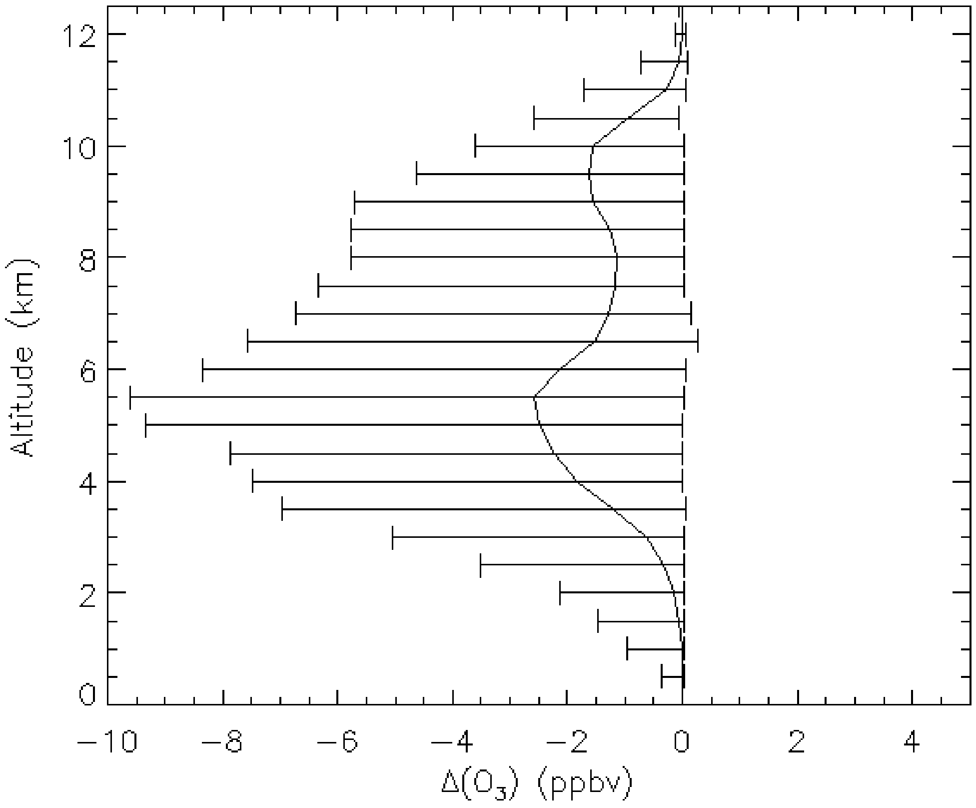

Figure 2.13. Change in O_3 mixing ratios due to lightning NO_x during the July 21 EULINOX storm. Solid line is the average (over the sampling box) and brackets indicate minimum and maximum change.

version. For these calculations, the storm is assumed to have dissipated and clear-sky photolysis rates are used. The same 40 x 40 km sampling box shown in Figure 2.12b was used to analyze the results at the end of the 24 hour simulations. Table 2.2 gives the average mixing ratios within the sampling box at 10 km AGL for a number of species at the beginning and end of the chemistry-only simulation that included lightning NO_x. Ozone production averaged 10.3 ppbv day^{-1} in the storm core at this altitude, while substantial NO_x conversion to HNO_3 took place. Decreases in HCHO and CH_3OOH were caused by photolysis.

The impact of lightning NO_x on ozone was examined by averaging the change in ozone mixing ratios within the box for the lightning and no-lightning cases. Figure 2.14 shows that, on average with lightning, there is additional net O_3 production maximizing at approximately 5 ppbv day^{-1} at 5.5 km in the 24 hours following the storm. The injection of lightning NO_x causes a small decrease in net ozone production averaging less than 1 ppbv day^{-1} between 8 and 10 km. There is a maximum decrease in net O_3 production exceeding 6 ppbv day^{-1} at 9 km, and maximum additional net production of nearly 16 ppbv day^{-1} at 5 km due to lightning . Figure 2.15 shows a scatter plot of lightning NO_x versus the 24-hour change in net O_3 production resulting from the inclusion of lightning NO in the model for the grid cells contained in the sampling box shown in Figure 12.2b at 10 km. The general shape of the plot shows the change in net ozone production maximizing with lightning NO_x mixing ratios less than 1 ppbv, then becoming less positive as lightning NO_x increases. After lightning NO_x mixing ratios exceed approximately 3 ppbv, lightning NO_x causes decreased net ozone production in the model.

Table 2.2. Average Species Concentrations at 10 km at the Beginning and End of the Chemistry-Only Simulation of the July 21 EULINOX storm

Species	Average Mixing Ratio Immediately Following Convection (ppbv)	Average Mixing Ratio 24 hours after Convection (ppbv)
NO_x	3.51	1.42
O_3	95.6	105.9
HNO_3	0.184	1.92
HCHO	0.744	7.57×10^{-2}
H_2O_2	0.769	0.411
CH_3OOH	0.251	6.50×10^{-2}
$CH_3CO_3NO_2$	0.605	0.644
OH	2.82×10^{-5}	1.88×10^{-5}
HO_2	1.51×10^{-4}	3.62×10^{-4}
RO_2	3.12×10^{-5}	1.13×10^{-5}

* Averages are computed over the anvil averaging box shown in Figure 2.12b.

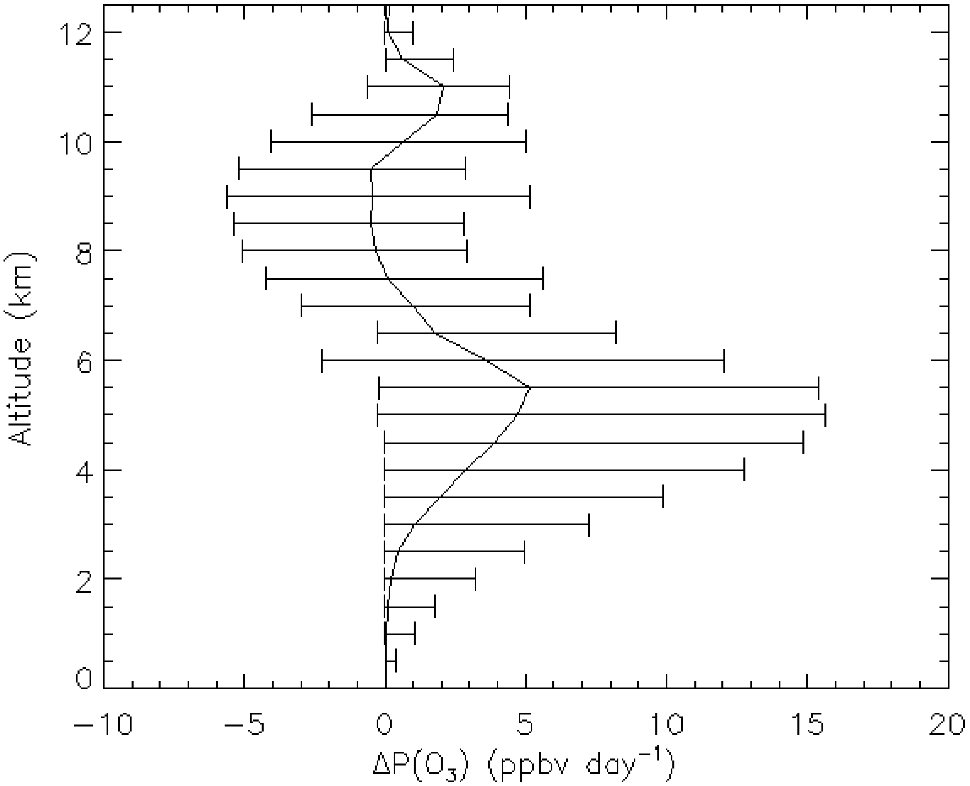

Figure 2.14. Change in net O_3 production due to lightning NO_x in the 24 hours following the July 21 EULINOX storm. Solid line is the average (over the sampling box) and brackets indicate minimum and maximum change.

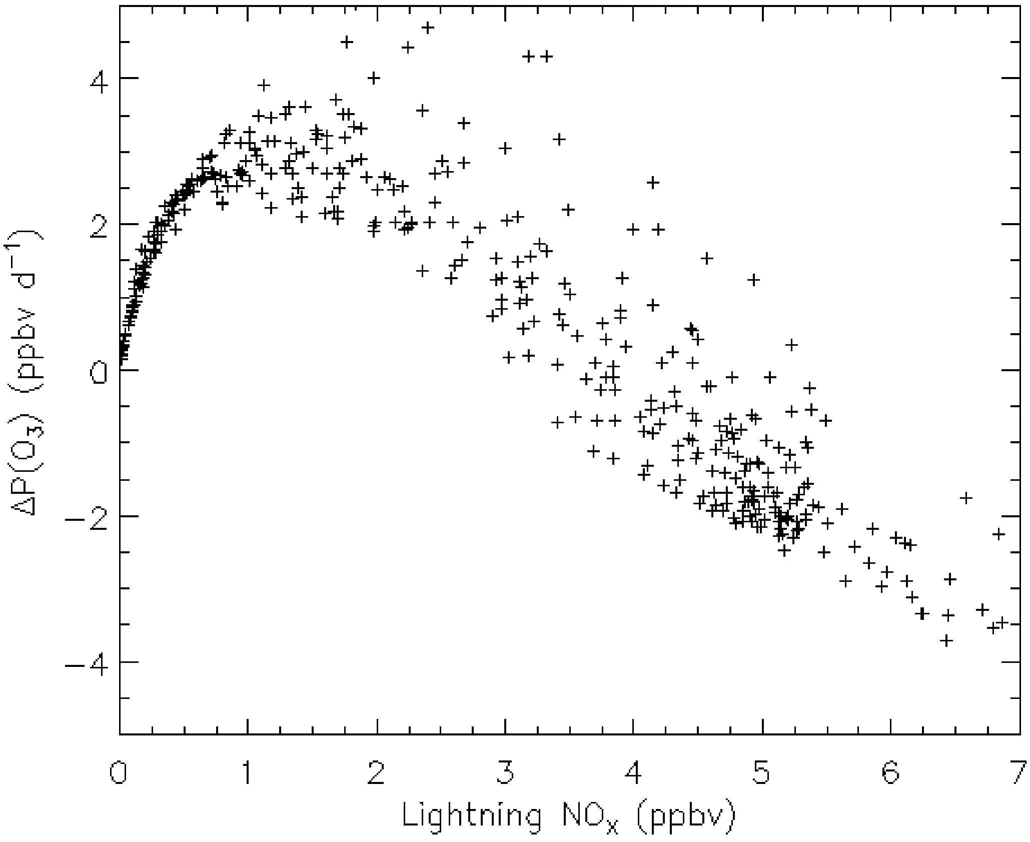

Figure 2.15. Change in net O_3 production due to lightning NO_x in the 24 hours following the July 21 EULINOX storm versus lightning NO_x at 10 km for grid cells contained in the sampling box.

Chapter 3. Simulations of the July 10 STERAO storm

3.1 The STERAO Project

The STERAO-A (Stratospheric-Tropospheric Experiment: Radiation, Aerosols, and Ozone – Deep Convection and the Composition of the Upper Troposphere and Lower Stratosphere; Dye et al. [2000]) field campaign was conducted in June and July of 1996. One of the chief objectives of the project was to investigate the impact of thunderstorms on the distribution of chemical species in the upper troposphere/lower stratosphere (UT/LS) region including the production of NO_x by lightning. The field project included two research aircraft. The NOAA WP-3D flew below 8 km in order to characterize the chemical environment in which thunderstorms developed while the University of North Dakota Citation sampled the meteorological and chemical properties of thunderstorm anvils. Throughout the project, the dynamical evolution of thunderstorms in the project area was observed by the Colorado State University CHILL Doppler radar. The location, peak current, and time of occurrence of CG lightning flashes were recorded by the NLDN. In addition, total lightning activity (IC + CG) in thunderstorms observed during the field project was mapped by the ONERA interferometer. Because of the availability of detailed lightning observations and anvil measurements of chemical species, the STERAO project provides a rich dataset for investigating lightning NO_x production and convective transport.

3.2 Observed storm evolution

At approximately 2100 UTC on July 10, 1996, a multicellular thunderstorm organized in a NW-SE line developed near the Wyoming-Nebraska border and was observed as part of the STERAO field project. The storm anvil was investigated by the Citation aircraft from 2237 to 0105 UTC including a spiraling ascent from 0024 to 0050 UTC. Figure 3.1 shows images from the CHILL Doppler radar at 7.5 km MSL from 0006 and 0024 UTC with segments of the Citation's flight track overlaid. After 0115 UTC, the storm became unicellular with supercell characteristics [Dye et al., 2000].

CG flashrates were calculated by counting the number of flashes recorded by the NLDN per 1 minute period. IC flashrates were obtained by counting the number of interferometer flashes with duration greater than 100 ms per 1 minute period and subtracting the number of CG flashes. The first lightning flash occurred at 2152 UTC. Figure 3.2 shows that for the duration of the storm, IC lightning activity was dominant. From 2200 to 0200, only 80 CG flashes were recorded by the NLDN, while 3265 IC flashes were recorded by the interferometer. The interferometer maps lightning flashes in three dimensions allowing flash lengths to be calculated for each flash. Dr. Eric Defer of ONERA provided estimates of the length of each IC and CG flash from 2152 to 0231 UTC (personal communication). Table 3.1 shows the number of IC and CG flashes per hour from 2200 – 0200 UTC as well as average IC and CG flash lengths. During each of the four hour-long periods, the average length of a CG flash was greater than the average length of an IC flash. In addition, during the first two hours shown, IC flashes had much shorter lengths (9.39 and 12.39 km) than in the last two hours (28.84 and 32.67 km). The strongest lightning activity occurred after the storm transitioned from a multicellular to unicellular structure at approximately 0115 UTC.

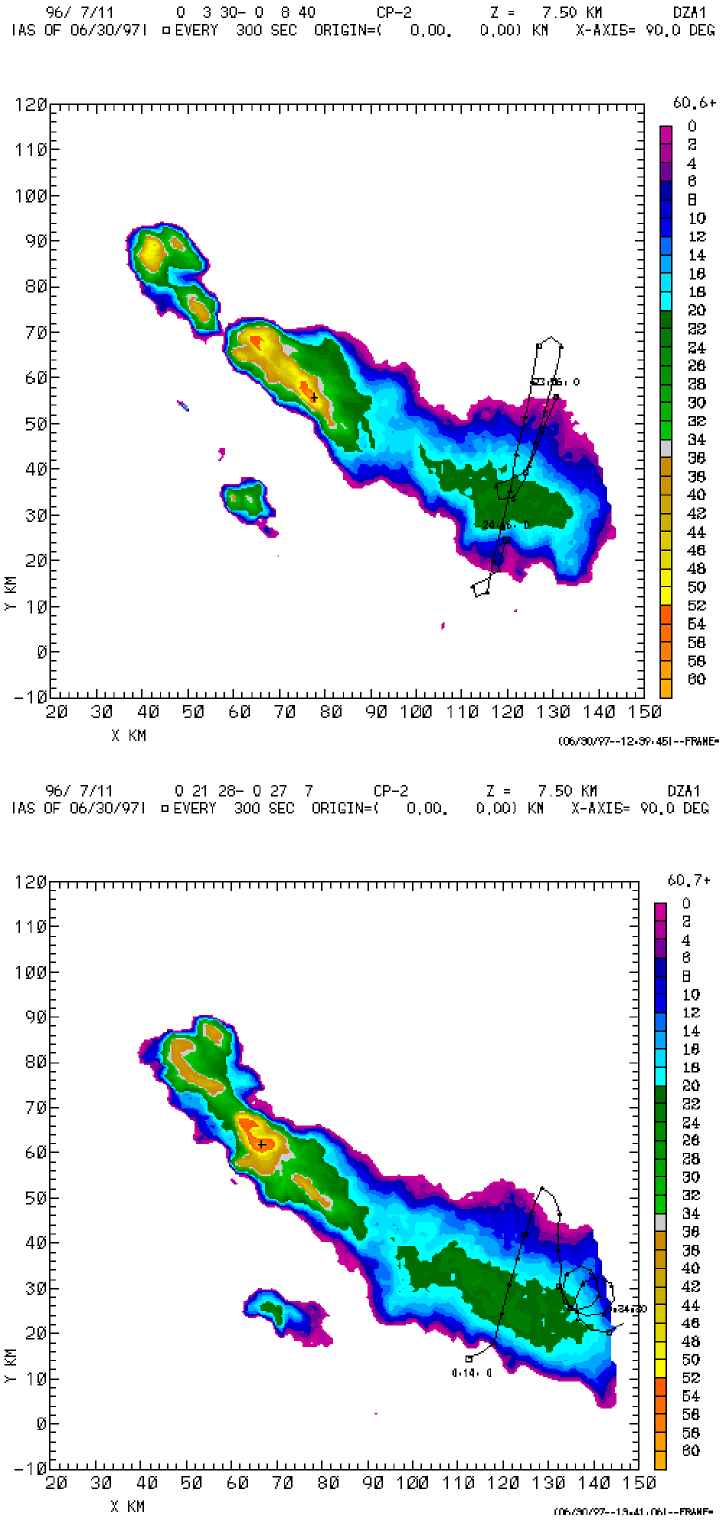

Figure 3.1. Radar reflectivity from the CHILL Doppler radar at 7.5 km MSL from 0006 UTC and 0024 UTC on July 10, 1996. The black line indicates the relevant portion of the Citation flight track.

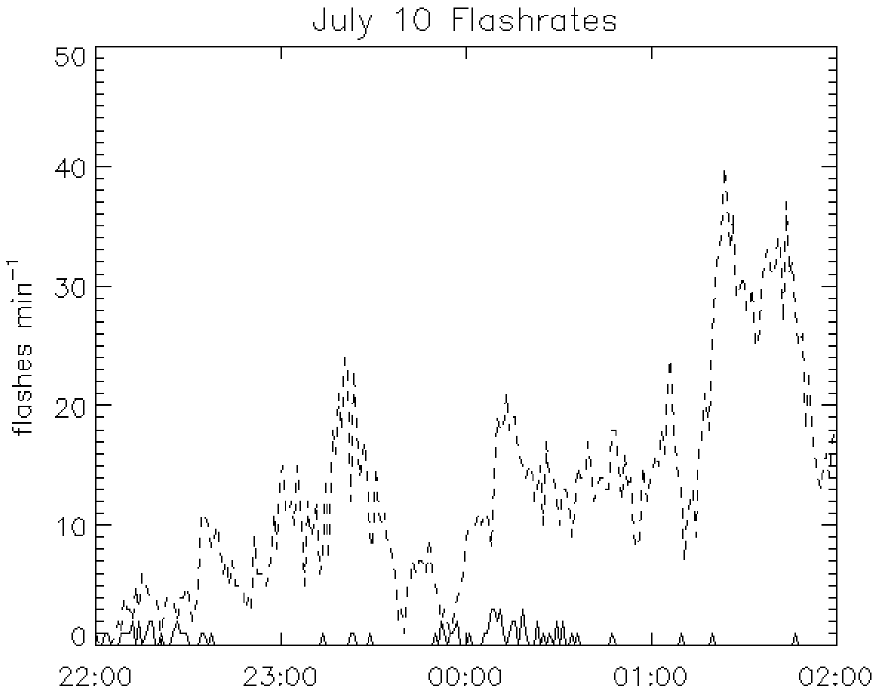

Figure 3.2. Observed CG flash rates (solid) calculated from NLDN data and observed IC flash rates (dashed) calculated from interferometer and NLDN data for the July 10 STERAO storm.

Table 3.1. Number of IC and CG flashes per hour and average flash lengths in the July 10 STERAO storm

Hour (UTC)	Number IC flashes	Number CG flashes	Average IC length (km)	Average CG length (km)
2200	275	24	9.39	57.72
2300	620	12	12.39	50.09
0000	838	38	28.84	65.63
0100	1532	6	32.67	45.39
All	3265	80	25.88	59.41

3.3 Simulated storm evolution

The July 10 STERAO storm was simulated by Dr. Georgiy Stenchikov from Rutgers University using the 3-D GCE model with a horizontal resolution of 2 km and a vertical resolution of 0.5 km. The simulation was initialized with a single composite

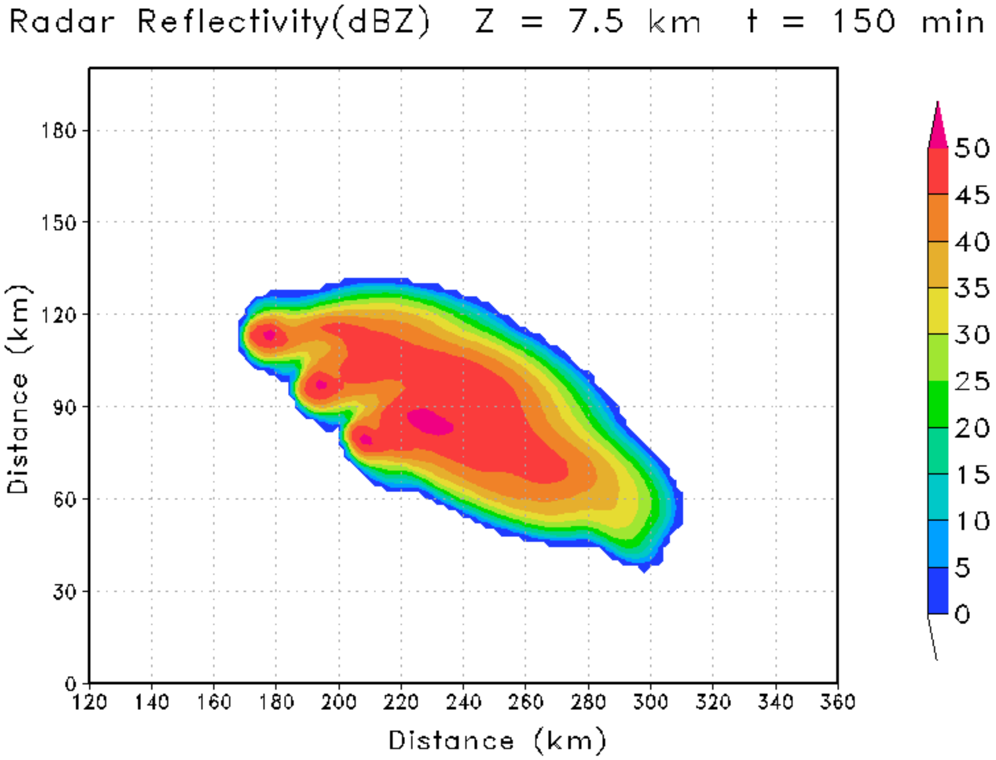

Figure 3.3. Radar reflectivity computed from GCE hydrometeor fields at 7.5 km MSL 150 minutes into the simulation of the July 10 STERAO storm.

sounding which was comprised of the 2050 UTC Fort Morgan Airport sounding and meteorological data from the Citation and WP3D aircraft [Skamarock et al., 2000]. Convection was initialized with three warm thermal perturbations organized in a NW-SE line. Three distinct cells were visible 30 minutes into the simulation. Figure 3.3 shows radar reflectivity computed using hydrometeor fields from the GCE at 7.5 km MSL 150 minutes into the simulation. The spacing of the cells compares favorably with observations, but the simulation creates a larger anvil than observed by radar. The simulated speed of the storm also matched the observed storm speed well. In the mature phase of the simulated storm, precipitation top heights were typically 16 km MSL. Vertical cross sections of radar reflectivity from Dye et al. [2000] showed the precipitation top height slightly exceeding 16.5 km MSL at 2312 UTC. At 2209, 0005, and 0128 UTC, precipitation top heights exceeded 14 km MSL but did not reach the 16 km level typical of the simulated storm. While the 3-hour GCE simulation reproduced a number of observed storm features, it did not capture the transition of the storm from multicellular to unicellular which occurred after 0100 UTC.

Maximum vertical velocities of 37 m s^{-1} occurred near the end of the 180 minute GCE simulation. This is greater than the maximum vertical velocity of 30 m s^{-1} reported by Skamarock et al. [2000] in their 180-minute simulation of the July 10 STERAO storm using the COMMAS (Collaborative Model for Multiscale Atmospheric Simulation). Vertical velocity in the July 10 storm was also estimated by Dye et al. [2000] by vertically integrating the mass continuity equation with horizontal velocities derived from Doppler radar observations. At 2310, approximately 130 minutes after the beginning of convection, maximum vertical velocities of 18 m s^{-1} were calculated by Dye et al. [2000]. Maximum downdraft velocities at this time were estimated to be 8 m s^{-1} at anvil levels, and 15 m s^{-1} near the base of the cloud [Dye et al., 2000]. Because vertical velocities at other times were not presented, it is difficult to judge how representative velocities at this time are. In the GCE simulation 130 minutes after the beginning of convection, maximum vertical velocities exceeded 35 m s^{-1} while the greatest downdraft speed was only 6 m s^{-1}. At the end of the 180-minute simulation, the updrafts in the two northernmost cells have begun to weaken, while the updraft in the southern cell has strengthened. Though the observed transition from multi- to unicellular structure was not reproduced by the 3 hour GCE simulation of the storm, the weakening of the northern cells and the strengthening of the southern cell suggests that a longer simulation may succeed in capturing this feature.

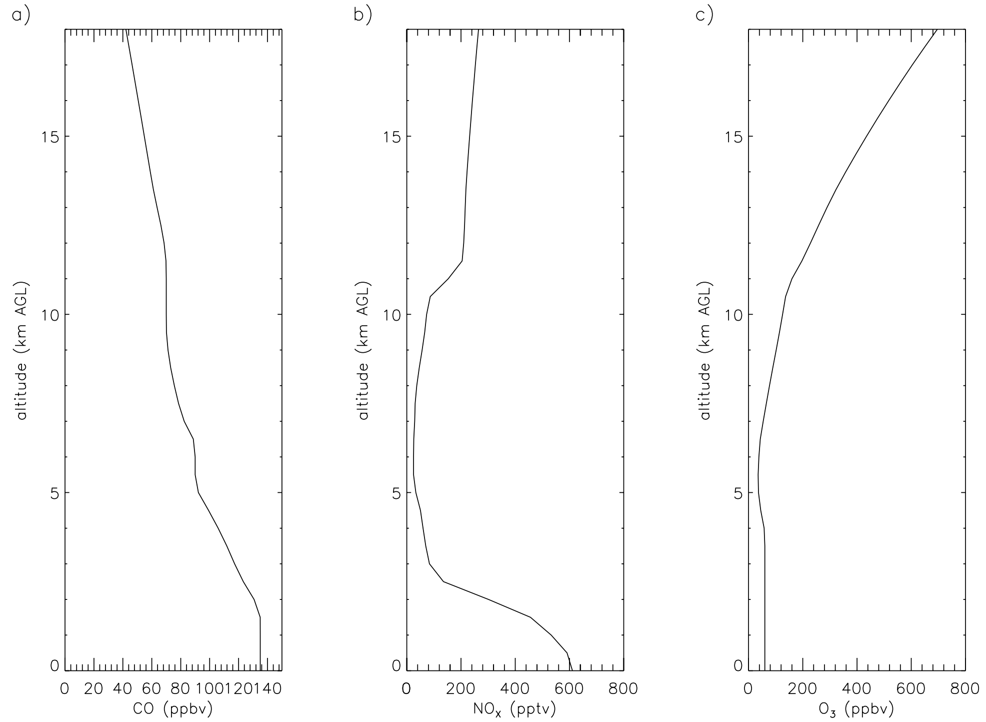

Figure 3.4. Initial condition profiles of (a) CO, (b) NO_x, and (c) O_3 prior to the July 10 STERAO storm.

3.4 Tracer transport and lightning NO_x production

The passive version of the CSCTM was used to analyze the transport of NO_x, O_3, and CO in the storm and to estimate lightning NO_x production. Initial condition profiles were constructed using WP3D and Citation observations outside of the cloud and taken from Skamarock et al. [2000] (see Figure 3.4).

In order to compare observations with model results, data collected from the Citation during anvil penetrations from 2237 to 0105 UTC were averaged over 10 second intervals and binned into 0.5 km thick layers from 7.75 to 12.75 km. Model output was sampled from 60 to 180 minutes in the simulation and included all gridcells with computed radar reflectivity between 0 and 30 dBZ because in-cloud portions of the flight, (shown in Figure 3.1) occurred in the anvil where reflectivity was typically less than 30 dBZ.

3.4.1 CO and O_3 transport

Figure 3.5 shows the pdfs of CO at 8, 10, and 12 km MSL. Below 11 km, the model consistently underestimates CO, suggesting, that at these levels, upward transport and detrainment into the anvil in the simulation are too weak. At 11 and 11.5 km, the simulation predicts the observed distribution of CO mixing ratios fairly well. At 12 and 12.5 km, the model slightly overestimates the distribution of CO, suggesting that upward transport and detrainment may be slightly overrepresented at these levels. Figure 3.6 shows the pdfs of simulated and observed O_3 at 8, 10, and 12 km MSL. At all levels

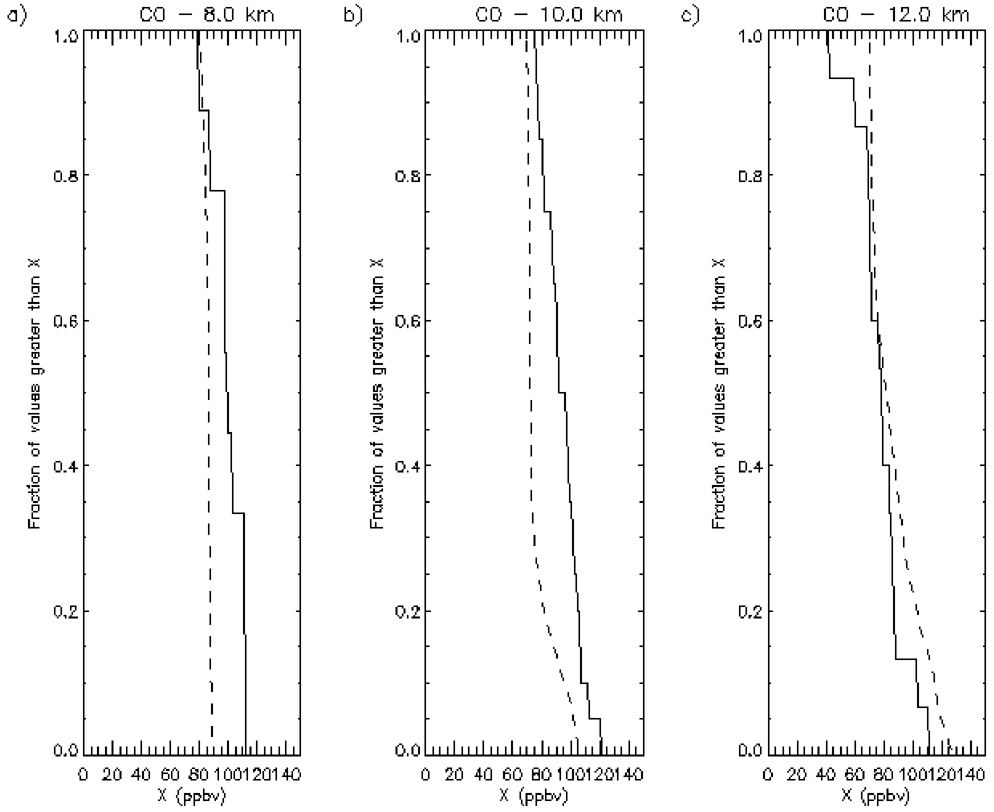

Figure 3.5. Pdfs of simulated (dashed) and observed (solid) CO at (a) 8, (b) 10, and (c) 12 km MSL in the July 10 STERAO storm.

except 10 km, the model tends to underestimate the distribution of O_3 observed by the Citation, suggesting that at most anvil levels, downward transport from the upper troposphere may be too small or upward transport of lower O_3 air may be overestimated..

Figure 3.7 shows horizontal cross sections of simulated CO and O_3 mixing ratios at 10 km MSL as well as vertical cross sections of CO and O_3 through the core and anvil of the southernmost cell. At 10 km MSL, CO mixing ratios exceeding 130 ppbv are found in the storm cores. The vertical cross section of CO shows that the highest CO mixing ratios are found in the core updraft region. Entrainment of environmental air with lower CO concentrations results in more dilute mixing ratios in the anvil outflow region.

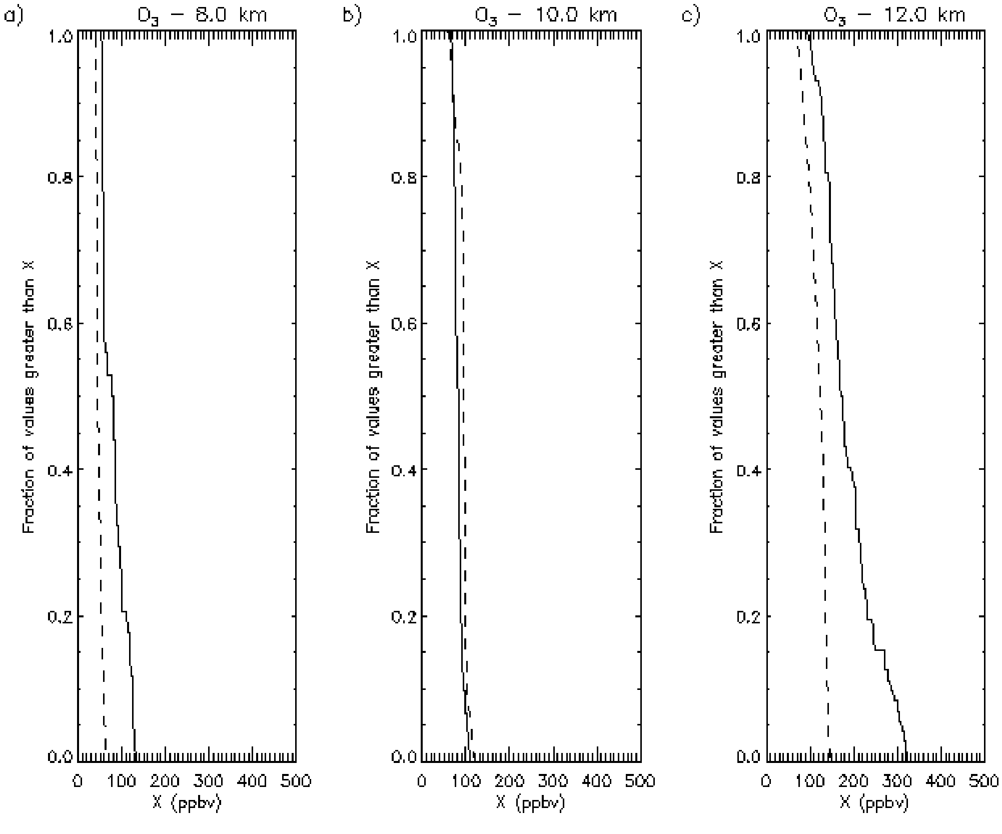

Figure 3.6. Pdfs of simulated (dashed) and observed (solid) O_3 at (a) 8, (b) 10 and (c) 12 km MSL in the July 10 STERAO storm.

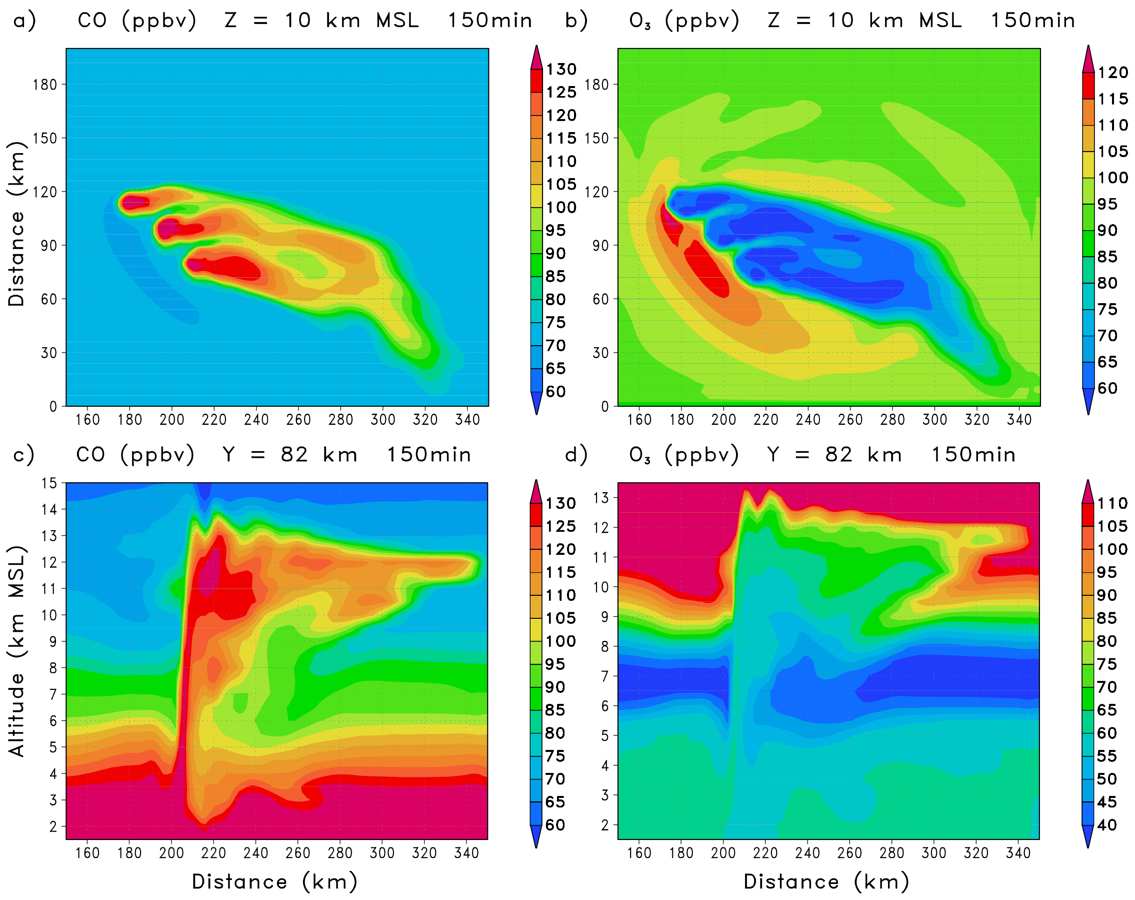

Figure 3.7. Horizontal distributions at 10 km MSL of simulated (a) CO and (b) O_3, and vertical cross sections of (c) CO and (d) O_3 through the core of the southernmost cell of the July 10 STERAO storm.

O_3 minima are found in the storm cores and anvil at 10 km MSL as lower O_3 air from the lower troposphere has been transported upward. A maximum in O_3 is found to the rear of the cell cores where higher O_3 air has been transported downward.

3.4.2 Lightning NO_x production

The presence of an interferometer during the STERAO campaign allowed for the observation of IC flash rates and information on the locations of both IC and CG flashes. For these reasons, and due to concerns that the simulated anvil was larger than observed, the modified version of the lightning scheme used in the simulation of the July 21 EULINOX storm was used in the simulation of lightning NO_x production in the July 10

STERAO storm. Because lightning NO_x is placed into a smaller area of the cloud as opposed to being distributed throughout the interior of the 20 dBZ contour, the size difference between the simulated and observed anvils will not result in excessive dilution of lightning NO_x.

Plots of radar reflectivity overlaid with VHF sources recorded by the interferometer from Dye et al. [2000] showed the majority of lightning occurred slightly downwind of the maximum reflectivity cores of the cells. The locations of IC and CG flashes were plotted and the average size of the area containing lightning was estimated at times throughout the storm. Three boxes of approximately this size were placed 10 km downwind of the maximum updraft location in each of the three storm cores. The observed storm of July 10 was organized into a NW-SE line of cells that grew and decayed. The simulated storm of three cells was a simplification of the more complicated evolution of the observed storm. Therefore it was not possible to identify individual flashes as being associated with any one of the three simulated cells as was done in the July 21 EULINOX simulation. Instead, when a flash was to be simulated, a random number was selected to determine which of three simulated cells the flash should be associated with, and then the lightning NO_x from the flash was placed into the corresponding box. The average horizontal flash extent was not calculated for this storm as in the EULINOX storm because the raw interferometer files were not available. Instead, an average value of horizontal flash extent from the EULINOX data of 12 km in the x direction by 12 km in the y direction was assumed throughout the simulation. A schematic of this version of the lightning NO_x placement scheme is shown in Figure 3.8. The location of the maximum updraft in each cell is marked with an x, and a box for selecting the flash initiation point is centered 10 km downwind. The flash initiation point is selected at random from this area and the flash is then confined to the smaller area of the horizontal flash extent. The vertical and horizontal distribution of lightning NO_x followed the same scheme as in the July 21 EULINOX simulation.

Lightning NO_x production was estimated by calculating the mean peak current of CG flashes observed by the NLDN. Using the relationship between peak current and energy dissipated from Price et al. [1997], P_{CG} was estimated to be approximately 390 moles NO. The upper mode of the vertical distribution of IC NO_x was assumed to be at the height of the -50° C isotherm, while the lower mode was assumed to be at the height

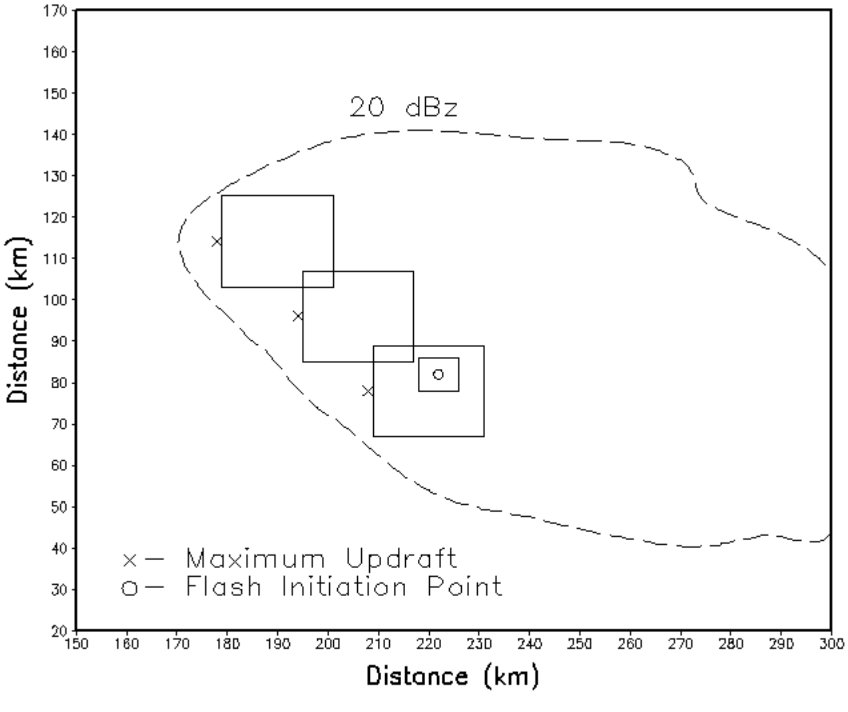

Figure 3.8. Schematic diagram of the lightning placement in the July 10 STERAO storm. Dashed line represents computed 20 dBZ radar reflectivity contour at 10 km 150 minutes into the simulation. X shows the location of the maximum updrafts and the larger boxes are the area from which an initiation point is selected. The circle marks the initiation point, and the smaller box shows the are in which the flash is constrained.

of the -15° C isotherm. Various values of the P_{IC}/P_{CG} ratio were simulated and the results compared with observations. Due to uncertainty in the accuracy of the NO_2 instrument aboard the Citation, NO_2 was estimated using observed NO and O_3 and the photostationary state assumption. Clear sky photolysis rates were assumed, and these rates were also multiplied by a factor of 2 based on the work of Madronich [1987] which showed that actinic flux can be increased within clouds, in order to bracket the NO_2 estimate. The observed column mass of N in NO_x was calculated for the 5 km thick layer extending from 7.75 to 12.75 km MSL by binning observations into 0.5 km thick layers and computing layer mean mixing ratios of NO and NO_2. Assuming that photolysis rates were enhanced by the anvil cloud by a factor of 2 produces a column mass of 2.4×10^{-4} g N m^{-2}, while assuming photolysis rates were unaffected by the cloud yields a column mass of 2.8×10^{-4} g N m^{-2}. Table 3.2 shows estimates of column mass computed by assuming different production scenarios. The scenario in which a P_{IC}/P_{CG} ratio of 0.5 was assumed overestimated column mass but compared more favorably with observations at some levels in terms of pdfs and mean vertical profiles than the scenario in which a P_{IC}/P_{CG} ratio of 0.3 was assumed. Figure 3.9 shows the pdfs of observed and simulated NO_x assuming both a P_{IC}/P_{CG} ratio of 0.3 and a P_{IC}/P_{CG} ratio of 0.5. At 8 and 10 km MSL, the model matched the observed NO_x mixing ratios fairly well when a P_{IC}/P_{CG} ratio of 0.5 was assumed, though at 10 km MSL, the model tended to slightly underestimate NO_x. At these levels, the assumption of a P_{IC}/P_{CG} ratio of 0.3 resulted in an underestimation of the observations. At 12 km, the model overestimated NO_x compared to observations when the P_{IC}/P_{CG} ratio of 0.5 was assumed, but compared well with the observations when a P_{IC}/P_{CG} ratio of 0.3 was assumed. The pdfs of NO_x and CO suggest that the below 11 km, upward transport and detrainment in the model may have been slightly weaker than observed which resulted in too little lightning and boundary layer NO_x reaching these altitudes. At 12 and 12.5 km, the pdfs of simulated and observed CO suggested that upward transport and detrainment may have been slightly

Table 3.2. Calculated column mass of N in NO_x in the July 10 STERAO storm

P_{CG} (moles NO per flash)	P_{IC}/P_{CG}	Column Mass (g N m^{-2})
390	0.1	1.7×10^{-4}
390	0.3	2.5×10^{-4}
390	0.5	3.3×10^{-4}
390	0.75	4.3×10^{-4}
390	1.0	5.3×10^{-4}

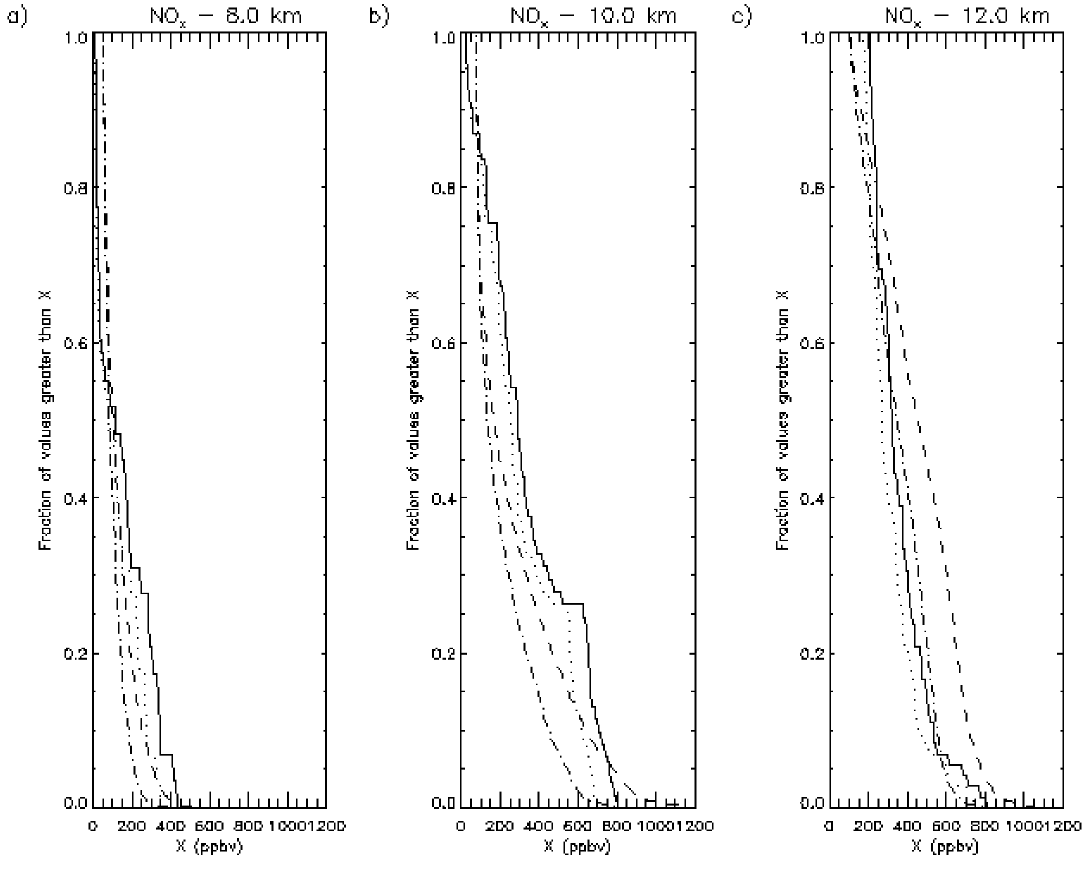

Figure 3.9. Pdfs of observed (NO_2 estimated assuming cloud-enhanced photolysis rates – dotted, NO_2 estimated assuming clear sky photolysis rates – solid) and simulated (assuming P_{IC}=195, P_{CG}=390 moles NO – dashed, assuming P_{IC}=117, P_{CG}=390 moles NO – dash dot) NO_x at (a) 8, (b) 10, and (c) 12 km in the July 10 STERAO storm.

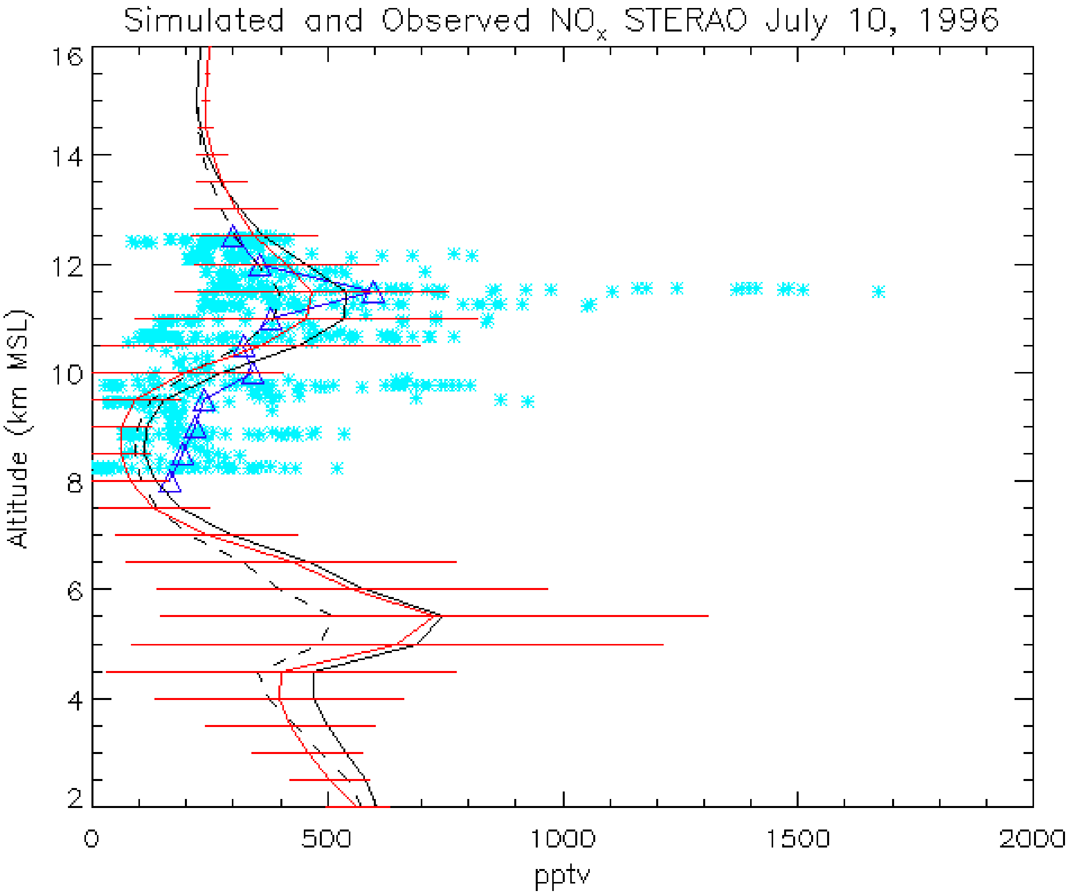

Figure 3.10. Observed in-cloud NO_x averaged over 10-second intervals (asterisks, with observed layer means indicated by triangles), overlaid with mean simulated in-cloud NO_x (without chemistry) assuming P_{CG}=390 moles NO and P_{IC}/P_{CG}=0.5 (solid black) and P_{IC}/P_{CG}=0.3 (dashed) for the July 10 STERAO storm. The red line shows the mean in-cloud NO_x from a simulation in which chemical reactions are included and P_{IC}/P_{CG}=0.6 Red bars indicate the standard deviation of in-cloud model output.

overestimated in the model. This would result in too much lightning NO_x reaching these levels which is consistent with the pdfs of NO_x when a P_{IC}/P_{CG} ratio of 0.5 was assumed.

Figure 3.10 shows observed NO_x averaged over 10-seconds intervals assuming that photolysis rates are not enhanced by the presence of the cloud as well as mean simulated in-cloud NO_x assuming P_{IC}/P_{CG} ratios of 0.3 and 0.5. The assumption of a P_{IC}/P_{CG} ratio of 0.3 matches the bulk of observations fairly well from 10 to 13 km MSL though the peak observed values are underestimated. Assuming a P_{IC}/P_{CG} ratio of 0.5

leads to an overestimation of the majority of observations between 10 and 13 km MSL but results in a more favorable comparison with observations between 8 and 10 km then assuming a P_{IC}/P_{CG} ratio of 0.3.

The July 10 STERAO storm was also simulated using a modified version of the lightning scheme described above which allowed NO production per meter flash channel length to be estimated. In addition to the observed IC and CG flashrates, the average flash length per 3 minute period was read into the model and the production per flash was calculated by multiplying the average flash length by an estimate of production. Various values of production were assumed and the results compared with observations to determine which was the most appropriate. Table 3.3 gives the estimated column mass of N in NO_x for a number of estimates of NO production per meter flash channel length. Assuming a production of 1.25 x 10^{-2} mol NO per meter flash channel length yields a more favorable comparison with observed column mass than other production estimates found in the literature or in simulations of the July 21 EULINOX storm (see Chapter 2).

Table 3.3. Calculated column mass of N in NO_x in the July 10 STERAO storm

Lightning NO_x Production Scenario	Column Mass (g N m^{-2})
P=1.7-6.6 x 10^{-2} mol NO per m flash channel length [Höller et al., 1999]	3.2 – 8.7 x 10^{-4}
P=4.5 x 10^{-3} mol NO per m flash channel length [Huntrieser et al., 2002]	1.8 x 10^{-4}
P=1.7 x 10^{-3} mol NO per m flash channel length [Skamarock et al., 2003]	1.5 x 10^{-4}
P=3.3 x 10^{-4} – 1.7 x 10^{-2} mol NO per m flash channel length [Stith et al.,1999]	1.4 – 3.2 x 10^{-4}
P=1.42 x 10^{-2} mol NO per m flash channel (July 21 EULINOX storm)	2.9 x 10^{-4}
P=1.25 x 10^{-2} mol NO per m flash channel	2.7 x 10^{-4}

3.5 Simulation of the chemical environment of the storm

The CSCTM was also run including chemical reactions. The reaction scheme was the same as described in DeCaria et al. [2005] with 35 active chemical species, 76 gas phase chemical reactions, and 18 photolytic reactions included. Initial condition profiles of CH_3OOH, HCHO, HNO_3, and H_2O_2 were provided by Dr. Mary Barth of NCAR. In addition, initial condition profiles of PAN, C_2H_4, C_2H_6, C_3H_8, and C_4H_{10} were taken from profiles calculated using observations from the July 12 STERAO storm by DeCaria et al. [2005]. The single column "spin-up" version of the CSCTM was run for 15 minutes to allow the chemical concentrations to come into equilibrium before starting the simulation of the storm.

The CSCTM with chemistry was run assuming a production scenario in which P_{CG} was 390 moles NO and P_{IC} was 195 moles NO. In the passive version of the model, this scenario resulted in an overestimation of the column mass of N in NO_x. However, when chemical reactions were included, NO_x mixing ratios were reduced and the column mass was only 2.3×10^{-4} g N m^{-2}, an underestimation of the column mass of $2.4\text{-}2.8 \times 10^{-4}$ g N m^{-2} calculated from observations. In order to match the observed column mass, the P_{IC}/P_{CG} ratio was increased to 0.6. In addition, the estimate of production per meter flash length was increased from 1.25×10^{-2} to 2.1×10^{-2} mol NO per m flash length. Assuming either of these production scenarios produces a column mass of 2.6×10^{-4} g N m^{-2}. The decrease in NO_x when chemical reactions were simulated occurred mainly through conversion to HNO_3. The initial condition profile of O_3 from Skamarock et al. [2000], shown in Figure 3.4, was considerably larger in the region between 9 and 16 km AGL than the pre-convection profile of O_3 used in the simulation of the July 12 storm by

DeCaria et al. [2005] as well as the climatological O_3 profile for Boulder, Colorado from Logan et al. [1999]. Elevated O_3 mixing ratios increased HO_x in the cloud, resulting in a greater degree of conversion of NO_x to HNO_3 than noted in the DeCaria et al. [2005] simulation of the July 12 STERAO storm.

It is also interesting to note that the final estimate of the P_{IC}/P_{CG} ratio for this storm was 0.6, while the ratio of average IC to CG flash lengths (see Table 3.1) was 0.44. This result suggests that production per meter flash channel length may be greater for IC flashes than for CG flashes in the July 10 STERAO storm, though the lightning scheme which estimates production per meter length was not configured to test this hypothesis. Figure 3.11 shows the NO_x mixing ratios at 10 km MSL at the end of the 180-minute simulation assuming a P_{IC}/P_{CG} ratio of 0.6. The greatest NO_x mixing ratios of over 2.2 ppbv reside in the core region of the southernmost cell. The area of NO_x enhancement resulting from lightning NO_x production and convective transport extends over 150 km.

The CSCTM with chemical reactions included was also run without lightning NO_x production in order to isolate the influence of lightning NO_x on O_3 mixing ratios during the lifetime of the storm. This was done by averaging O_3 mixing ratios in the lightning and “no-lightning” simulations over the 40 km by 40 km area positioned in the storm core shown in Figure 3.11 and subtracting the average from the “no-lightning” case from the lightning case average. Figure 3.12 shows the mean change in O_3 mixing ratios over the course of the 3-hour simulation which results from including lightning NO_x in the model. The largest average increase in O_3 of only 0.1 ppbv occurs at 9.5 km. At most altitudes, the introduction of lightning NO_x results in a small loss of ozone averaging less than 0.5 ppbv. Over all grid cells sampled, the maximum O_3 loss is less

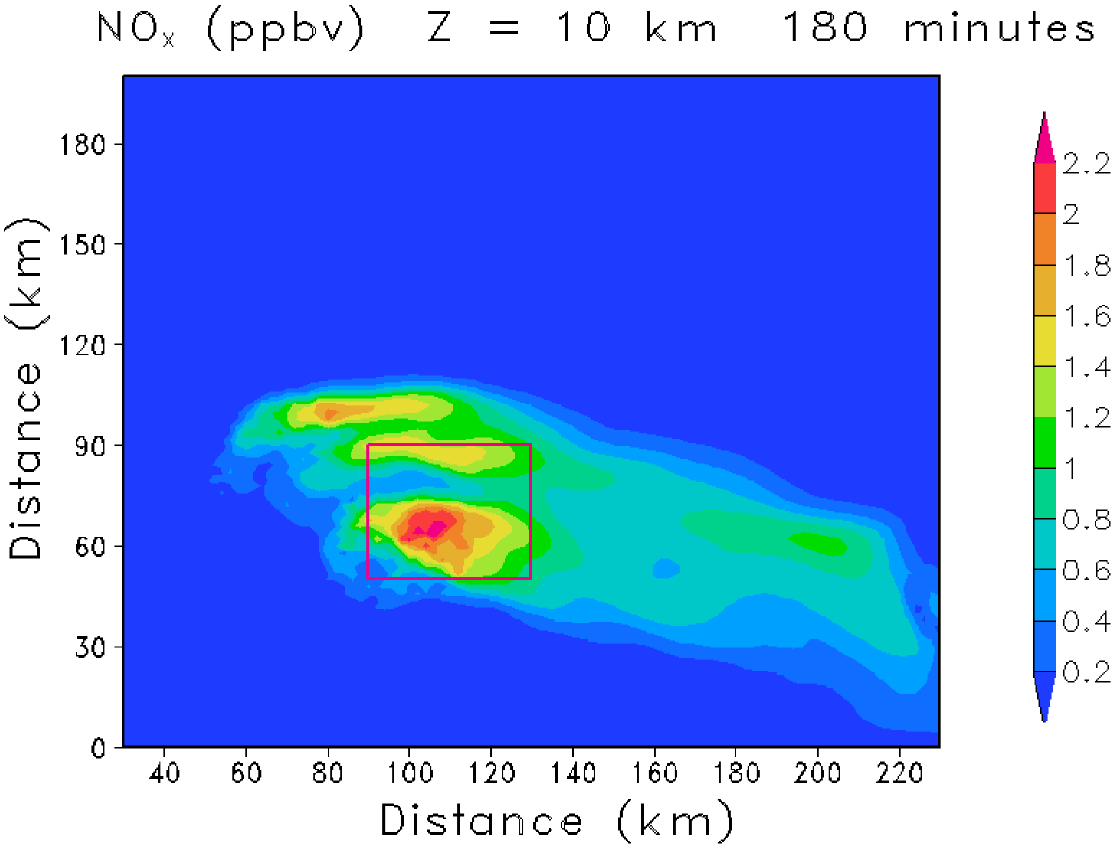

Figure 3.11. Simulated NO$_x$ assuming P_{IC}=234 moles NO and P_{CG}=390 moles NO 180 minutes into the simulation at 10 km MSL in the July 10 STERAO storm. The box indicates the grid cells sampled for calculation of average O$_3$ mixing ratios.

than 2 ppbv during the lifetime of the storm.

3.6 Simulation of chemistry in the convective plume

Chemical fields at the end of the lightning and "no-lightning" simulations were used to initialize the chemistry-only version of the CSCTM. These simulations were integrated forward for 24 hours to estimate the change in net O$_3$ production following the storm as a result of lightning NO$_x$. Figure 3.13 shows the mean change in net ozone production resulting from lightning calculated by averaging the 24-hour change in O$_3$ over the averaging box shown in Figure 3.11 for the lightning and "no-lightning" cases

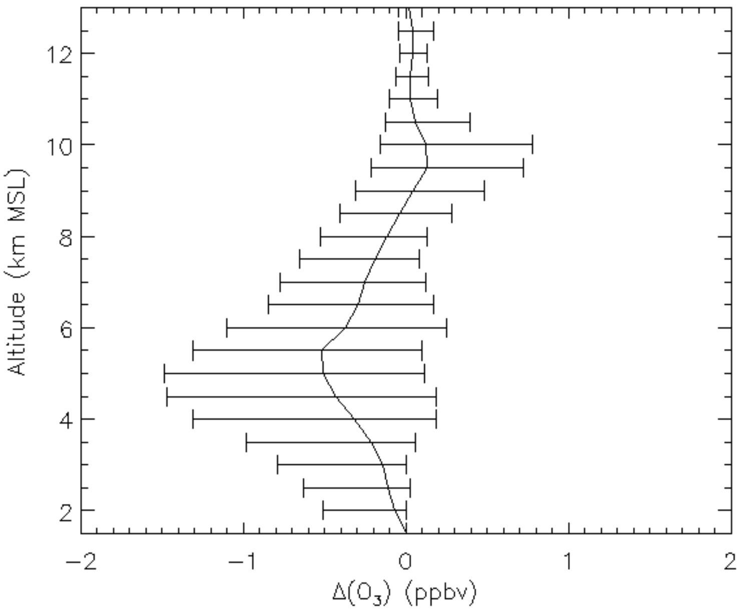

Figure 3.12. Change in O_3 mixing ratios due to lightning NO_x during the July 10 STERAO storm. Solid line is the average and brackets indicate minimum and maximum change (over the sampling box).

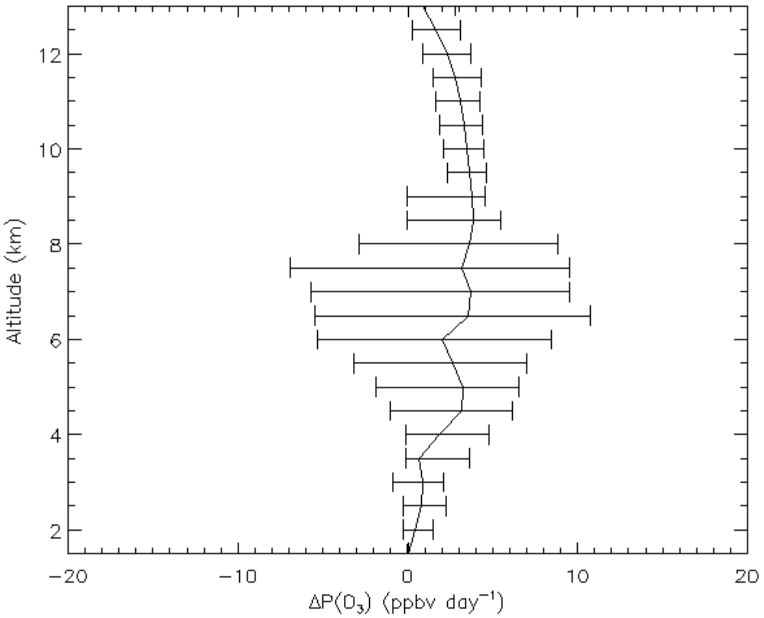

Figure 3.13. Change in net O_3 production due to lightning NO_x in the 24 hours following the July 10 STERAO storm. Solid line is the average and brackets indicate minimum and maximum change (over the sampling box).

Table 3.4. Average Species Concentrations at 10 km AGL at the Beginning and End of the Chemistry-Only Simulation of the July 10 STERAO storm.

Species	Average Mixing Ratio Immediately Following Convection (ppbv)	Average Mixing Ratio 24 hours after Convection (ppbv)
NO_x	1.01	0.475
O_3	70.0	78.5
HNO_3	5.21×10^{-2}	0.481
HCHO	0.553	5.20×10^{-2}
H_2O_2	1.42	0.683
CH_3OOH	0.286	6.80×10^{-2}
$CH_3CO_3NO_2$	0.300	0.300
OH	1.11×10^{-3}	1.08×10^{-4}
HO_2	4.95×10^{-3}	9.18×10^{-4}
RO_2	1.61×10^{-4}	3.16×10^{-5}

* Averages are computed over the sampling box shown in Figure 3.11.

subtracting the “no-lightning” average from the lightning case average. The mean increase in net ozone production maximizes at approximately 3 ppbv day^{-1}. Table 3.4 gives the average mixing ratios (over the sampling box shown in Figure 3.11) at 10 km AGL (11.5 MSL) of a number of species from the beginning and end of the 24-hour simulation (over the sampling box). In the 24 hours following the storm, ozone has increased by 8.5 ppbv. Figure 3.13 shows that only 2.8 ppbv of this increase resulted from lightning NO_x, while the other 5.7 ppbv was the result of convective redistribution of O_3 prescursors including NO_x and NMHCs. The CSCTM is not suitable for studying ozone production more than 24 hours after convection because the effects of the larger scale flow can not be simulated and the rate at which the convective plume is diluted, not known. If the plume was not diluted by environmental winds, the chemistry-only version of the model suggests that ozone production would decrease to a negligibly small rate after ~10 days when maximum the ratio of NO to O_3 mixing ratios is approximately 1.6×10^{-3} at 10 km AGL. Because environmental winds will increase the rate of dilution in the convective plume, ozone production should cease sooner than 10 days, though the persistence of the convective plume depends on weather patterns.

The column mass of ozone in the troposphere was calculated by averaging O_3 mixing ratios from the lightning and "no-lightning" cases over the box shown in Figure 3.11. The mass of ozone was then integrated from the surface to the tropopause height of 14.5 km AGL. Table 3.5 gives the calculated O_3 tropospheric column masses at the beginning and end of both simulations. The initial condition profile shown in Figure 3.4 corresponds to a column mass of 1.288 g O_3 per m^{-2}. Immediately following the 3-hour simulation of the storm, the tropospheric column mass of ozone has decreased by approximately 6% for both the lightning and "no-lightning" cases due to convective mixing which brings lower ozone air to the mid- and upper troposphere and higher ozone air to lower levels where ozone is more rapidly destroyed. At the conclusion of the 24-hour chemistry-only simulations, O_3 column masses in the troposphere have rebounded in both cases. Lightning NO_x results in a 2% increase in the tropospheric column mass of O_3 in the day following the convective event. In the 24-hour simulation with lightning, the tropospheric column mass of O_3 has nearly returned to its preconvective level.

Table 3.5. Column Mass of Tropospheric Ozone from Chemistry and Chemistry-Only Simulations of the July 10 STERAO storm

	O_3 column mass after 3-hr. chemistry simulation (g O_3 m^{-2})	O_3 column mass after 24-hr. chemistry-only simulation (g O_3 m^{-2})
Without lightning NO_x	1.211	1.253
With lightning NO_x	1.209	1.281

3.7 WRF simulations of the July 10 STERAO storm

The July 10 STERAO storm has also been simulated by scientists at NCAR using the WRF model. A version of WRF which calculates gas and aqueous phase chemistry online (WRF-Aqchem) has been developed by Dr. Mary Barth of NCAR and used to simulate the chemical environment of the storm and to investigate the fate of soluble species. The version of WRF used in these studies is a 3-D non-hydrostatic compressible model containing the Advanced Research WRF (ARW) dynamical core and includes a Runga Kutta scheme for tracer transport [Barth et al., 2006]. The July 10 STERAO storm was simulated using a horizontal grid of 161 by 161 with a resolution of 1 km and 50 vertical layers with resolution decreasing with altitude to the model top of 19.5 km. WRF-Aqchem includes 16 chemical species, 28 gas phase reactions, and 15 aqueous phase reactions.

3.7.1 The WRF simulation of the July 10 STERAO storm

The WRF simulation of the dynamical evolution of the July 10 STERAO storm was initialized in the same manner as the GCE simulation with a single sounding used to initialize the domain and three warm thermal perturbations used to initiate convection. Convection first developed 20 minutes into the simulation as three small cells. The northernmost two cells began to decay an hour into the simulation. Figure 3.14 shows the radar reflectivity computed from WRF hydrometeors at 7.5 km MSL, 80 minutes into the simulation. At this time, the two northern cells are still visible, though noticeably weaker and smaller in size than the southern cell. After this time, the simulated storm transitioned to a single cell structure which persisted until the end of the 180-minute

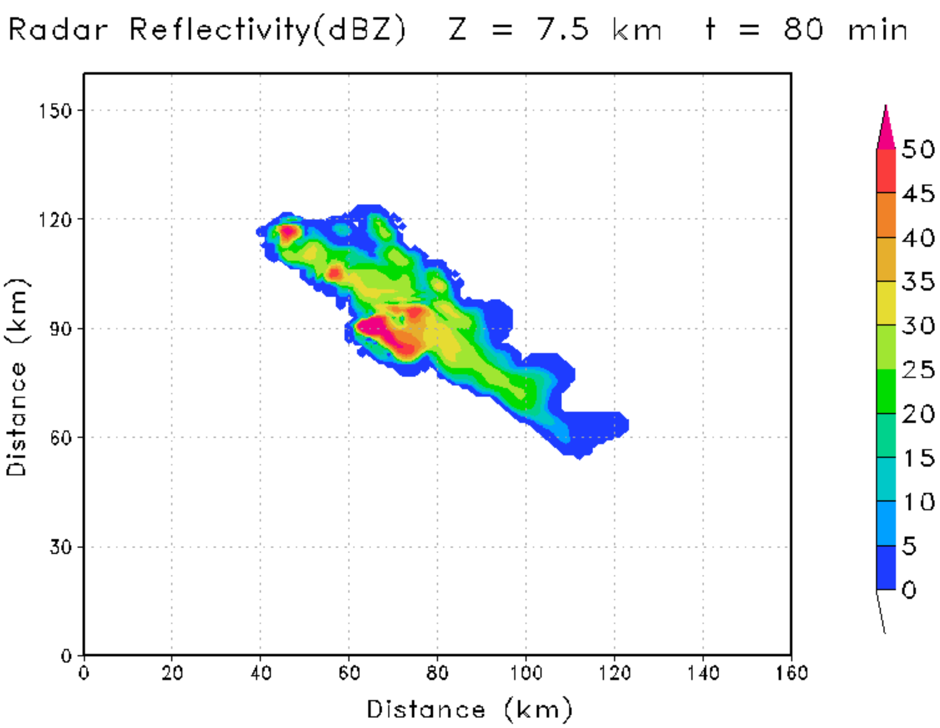

Figure 3.14. Radar reflectivity computed from WRF simulated hydrometeors at 7.5 km MSL 80 minutes into the simulation of the July 10 STERAO storm.

simulation. The WRF simulation succeeded in capturing the transition of the observed storm from multicellular to unicellular, although the multicell phase did not persist as long as observed. Radar observations showed this transition occurring at approximately 0115 UTC, nearly 210 minutes after the first lightning flash, while the simulation produced a multicell storm for only an hour. Precipitation top heights were typically 15.5 to 16.5 km MSL, with a maximum of 17 km MSL 110 minutes into the simulation which agreed well with the GCE simulation but slightly exceeded observations.

3.7.2. Lightning NO_x production in the WRF model

WRF-Aqchem did not originally include a lightning NO_x source. I collaborated with Mary Barth to incorporate the parameterization of lightning NO_x production from DeCaria et al. [2005] into the WRF model so that the impact of lightning NO_x on aqueous phase chemistry could be investigated. Translating the lightning scheme from the CSCTM to the WRF model framework presented a number of challenges. Radar reflectivity is used in the DeCaria et al. [2005] scheme to determine lightning NO_x placement. This was not calculated online in the original version of WRF-Aqchem. Instead a post-processing program was used to calculate radar reflectivity from the simulated hydrometeor fields. I incorporated code to calculate radar reflectivity into the model so that it could be calculated every time step in which lightning occurs and lightning NO_x production is calculated. Both the lightning and radar modules are called from WRF's "mediation layer". In terms of WRF's architecture, the "mediation layer" is the middle layer of code, in between the "driver layer" at the top, and the "model layer" at the bottom. The lightning and radar schemes belong to the "model layer" of WRF.

Because the dynamical and chemical calculations are extremely costly, it is highly desirable to run the WRF-Aqchem model on multiple processors. On a single processor, a 3-hour simulation takes nearly a week to complete while on two processors, the same simulation could be completed in only 3 days. In order to run on multiple processors, the model domain is divided into patches and the calculations for all the grid cells contained in each patch are computed by a single processor. The model is typically divided into patches horizontally rather than vertically. For example, the 161 by 161 grid might be divided into two patches such that the calculations for cells with an x coordinate less than 80 would be performed by one processor and the calculations for cells with an x coordinate greater than 80 would be performed by a second processor. The splitting of the domain did pose a problem for the lightning parameterization because the scheme requires that the number of grid cells with radar reflectivity greater than 20 dBZ be calculated. The amount of lightning NO_x distributed to each grid cell is then found by dividing the total amount of lightning NO_x at each level by the total number of cells within the 20 dBZ contour at that level. When run on multiple processors, the different processors must communicate with each other in order to calculate the total number of grid cells at each level which receive lightning NO_x. This can be done with intrinsic functions built into WRF, but only from the "mediation layer" of the code.

It is also imperative that the domain uses the same vertical distributions for IC and CG NO_x placement. If vertical distributions are calculated separately for each patch, the fraction of the domain on one processor may have a cloud top height which is higher than the fraction of the domain on the other processor depending on how the domain is divided into patches. Similarly, the height of the lower and upper mode isotherms could differ if calculated on separate patches. In order to allow the lightning NO_x code to run properly on multiple processors, it was necessary to modify the structure of the original code. The radar reflectivity module is called and it supplies the "mediation layer" with the 3-D array of computed reflectivity, as well as the number of grid cells within the 20 dBZ contour at each level, cloud top and base heights, and the levels of the upper and lower mode isotherms. The "mediation layer" then sums the number of grid cells with radar reflectivity greater than 20 dBZ over all patches, takes the minimum of the cloud base levels and maximum of the cloud top heights over all patches, as well as the maximum of upper and lower mode isotherm levels over all patches. These variables are then passed to the lightning NO_x module which is called from the mediation layer. Vertical distributions of lightning NO_x and the change in NO_x mixing ratios due to lightning were calculated in both the CSCTM and WRF-Aqchem simulations to ensure that the code in the WRF-Aqchem was working properly.

The main objective of including lightning NO_x in the WRF-Aqchem model was to investigate the impact of lightning NO_x on soluble species and to provide a platform for future studies of tracer transport and lightning NO_x production. Therefore, an extensive testing of a number of lightning NO_x production scenarios was not performed because this had already been done using the CSCTM driven by GCE output. A production scenario in which P_{IC} equals 195 moles NO and P_{CG} equals 390 moles NO was assumed for the WRF simulation and the results compared with observations in order to ensure that this production scenario compared reasonably with observations when used in the WRF model. Aircraft observations were sampled as described in section 3.4 to obtain layer mean averages and model output was sampled by averaging all grid cells from 60 to 180 minutes with computed radar reflectivity between 0 and 30 dBZ. Figure 3.15 shows the mean in-cloud observed and simulated NO_x. The simulation slightly underestimates the peak in mean NO_x observations found at 11.5 km MSL. However, the simulation reproduces the mean profile from 9 to 11 km MSL fairly well. Above 11.5 km and below minute simulation. The majority of NO_x remains at levels near the upper and lower modes of the vertical distribution of IC NO_x where it originated, although it has been advected downwind as far as 80 km. The maximum NO_x mixing ratios of over 3 ppbv are found in the 5.5 km MSL region. Dr. Mary Barth has used the version of WRF-Aqchem which included the DeCaria et al. [2005] lightning NO_x scheme to examine the effects of lightning NO_x on CH_3OOH, HCOOH, H_2O_2, and HCHO. The results,

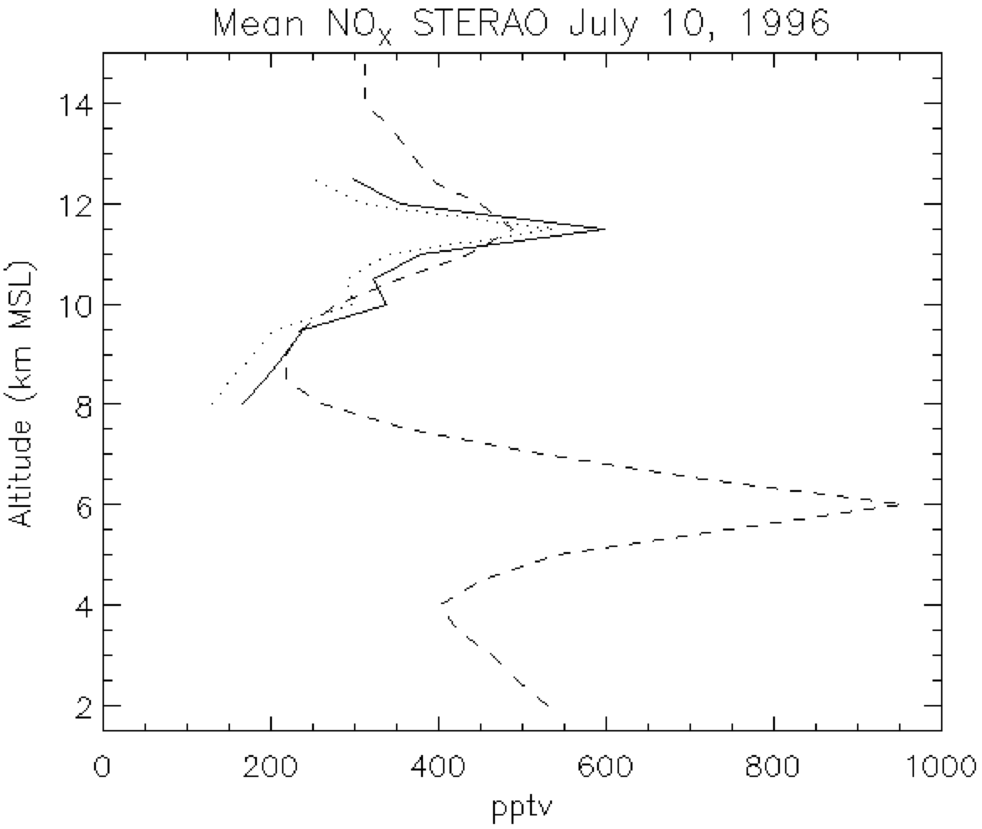

Figure 3.15. Mean in-cloud NO$_x$ mixing ratios calculated from observations (NO$_2$ estimated assuming cloud-enhanced photolysis rates – dotted, NO$_2$ estimated assuming clear sky photolysis rates – solid) and WRF-Aqchem model output (assuming P_{IC}=195 moles NO, P_{CG}=390 moles NO – dashed).

presented in Barth et al. [2006], show that lightning NO$_x$ has very little impact on these species during the lifetime of the storm, though the impact of lightning NO$_x$ in the convective plume was not examined.

3.8 Cloud model intercomparison

The WRF-Aqchem and the GCE and CSCTM were used in an intercomparison study of cloud–scale chemical transport models organized by Mary Barth of NCAR. A total of seven models simulated the July 10 STERAO storm using the same meteorological and chemical initial conditions. The goal of the study was to better

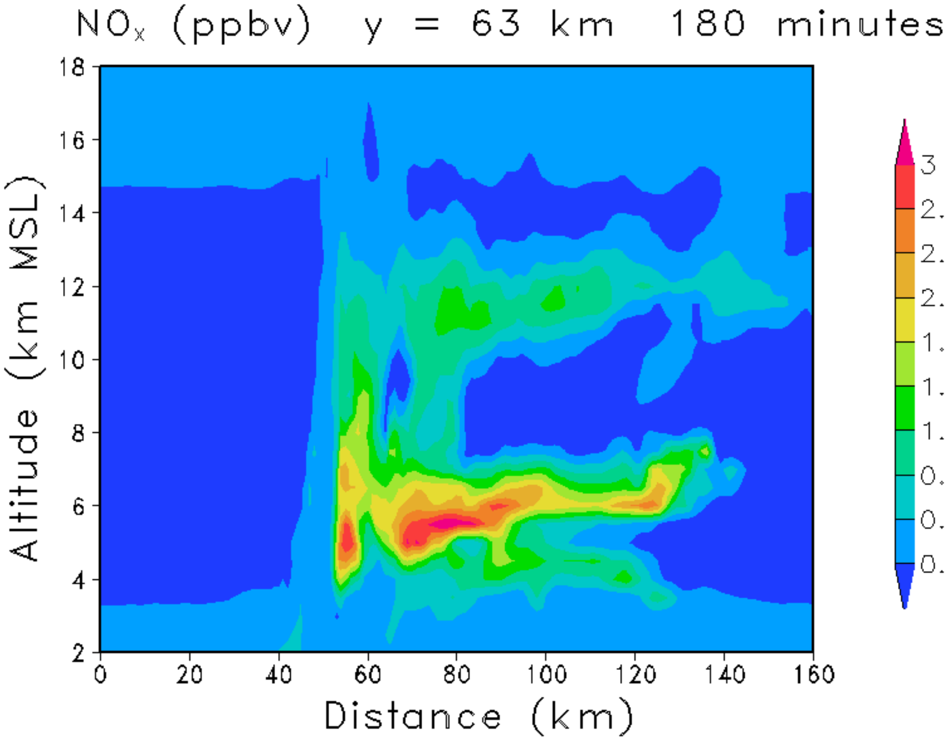

Figure 3.16. Vertical cross section of simulated NO_x mixing ratios (assuming P_{IC}=195 moles NO, P_{CG}=390 moles NO) from the WRF-Aqchem model at the end of the 180 minute simulation of the July 10 STERAO storm.

understand the variability found between different models. The WRF-Aqchem simulation did not include lightning NO_x production while the CSCTM simulation included the DeCaria et al. [2005] lightning NO_x scheme.

A comparison of the magnitude and level of maximum updrafts between output from the seven models and observations showed that all the models were able to reproduce these features well. WRF-Aqchem was the only model which captured the transition from multicellular to unicellular structure 150 minutes into the storm simulation, though most of the other models did show a weakening of some of the three cells. The GCE did not produce a weakening of the northern two cells until the end of the 3-hour simulation. It should also be noted that the GCE used a 2 km horizontal resolution, while the other cloud-models all used a 1 km resolution which may have caused some of the difference between the storm structure produced by the GCE and other models.

In addition to the observed storm features, in-cloud observations of CO, NO_x and O_3 were also compared to output from the seven models. Observations included were from two transects of the storm anvil and the models were sampled at an equivalent time and distance from the storm cores. All of the models, including the CSCTM and WRF-Aqchem, showed a good agreement in their representation of CO and O_3 and compared reasonably with observations. The CSCTM simulation was one of only three models which included schemes to represent lightning NO_x. To compare with observations during the first anvil transect, the models were sampled at 60 minutes. All models significantly underestimated observed NO_x mixing ratios with the models including a lightning NO_x source performing only slightly better than the models which did not include lightning. Model output was also sampled at 90 minutes to compare with data from a second transect. In this comparison, the 3 models including lightning NO_x compared much more favorably with observations than the other models. Only models including lightning NO_x were able to adequately reproduce the large NO_x mixing ratios observed in the storm anvil, underscoring the importance of representing lightning NO_x in models of all spatial scales.

Chapter 4. Simulations of the July 16 and July 29 CRYSTAL-FACE storms

4.1 The CRYSTAL-FACE Project

The NASA CRYSTAL-FACE project was designed to study the chemical and radiative properties of cirrus anvils. The CRYSTAL-FACE (Ridley et al., 2004; Lopez et al., 2006) field campaign was conducted in July, 2002 over South Florida. Six research aircraft were involved in the project, including the NASA WB-57 which measured microphysical, chemical (including CO, CO_2, O_3, and NO), and meteorological properties of tropical cirrus anvils in the vicinity of the tropopause. A variety of observations, including radar, lidar, and rawinsonde, were provided by land-based stations. Information on CG lightning during the campaign was collected by the NLDN.

I provided gridded maps of CG flash density (calculated from NLDN data) daily to the field during the campaign which could be used in flight evaluation and data interpretation. I also collaborated on the Ridley et al. [2004] paper on lightning NO_x during CRYSTAL-FACE by computing hourly flash rates for all storms observed during CRYSTAL-FACE and providing detailed information on lightning in the July 16 and July 29 storms. I also provided the aggregated (gridded) lightning data used in the analysis of the MOZART lightning scheme over south Florida during CRYSTAL-FACE presented in Ridley et al. [2004]. The comparison with observed flash rates led to the discovery of an error in the use of the Price and Rind [2002] flash rate scheme in the MOZART model. Once corrected, the total number of flashes predicted by the flash rate parameterization agreed well with NLDN observations.

Because the CRYSTAL-FACE project was not specifically designed to study processes related to lightning, observations of total (IC + CG) lightning activity, which were an integral part of both the STERAO and EULINOX projects, were not available during the CRYSTAL-FACE campaign. Though observed IC flash rates are an important component in estimating lightning NO_x production, aircraft observations from CRYSTAL-FACE provide a rare opportunity to investigate lightning NO_x production in the subtropics where a large percentage of the world's lightning occurs. For this reason, two storms from the CRYSTAL-FACE campaign were simulated and IC flash rates estimated for both.

4.2 The July 16 CRYSTAL-FACE storm

4.2.1 Observed storm evolution

On July 16, an isolated convective system developed northwest of Miami at approximately 1845 UTC. Figure 4.1 shows the CAPPI (Constant Altitude Plan Position Indicator) radar reflectivity at 1 km from the NPOL radar at 2011 UTC during the mature phase of the thunderstorm. Images from the EDOP cloud radar aboard the ER-2 aircraft show precipitation top heights were typically 14 km AGL. The cirrus anvil moved west across the Florida peninsula and was extensively sampled by the WB57 aircraft from 1936 to 2306 UTC. Figure 4.2 shows the visible image from the GOES-8 satellite taken at 2045 UTC with the flight track of the WB57 overlaid.

Figure 4.3 shows the number of CG flashes per minute recorded by the NLDN from 1900 to 2300 UTC. The storm was a relatively weak lightning producer with only 301 CG flashes recorded during this period and a maximum CG flash rate of 9 flashes per minute. Since the NLDN only recorded the occurrence of CG flashes during CRYSTAL-

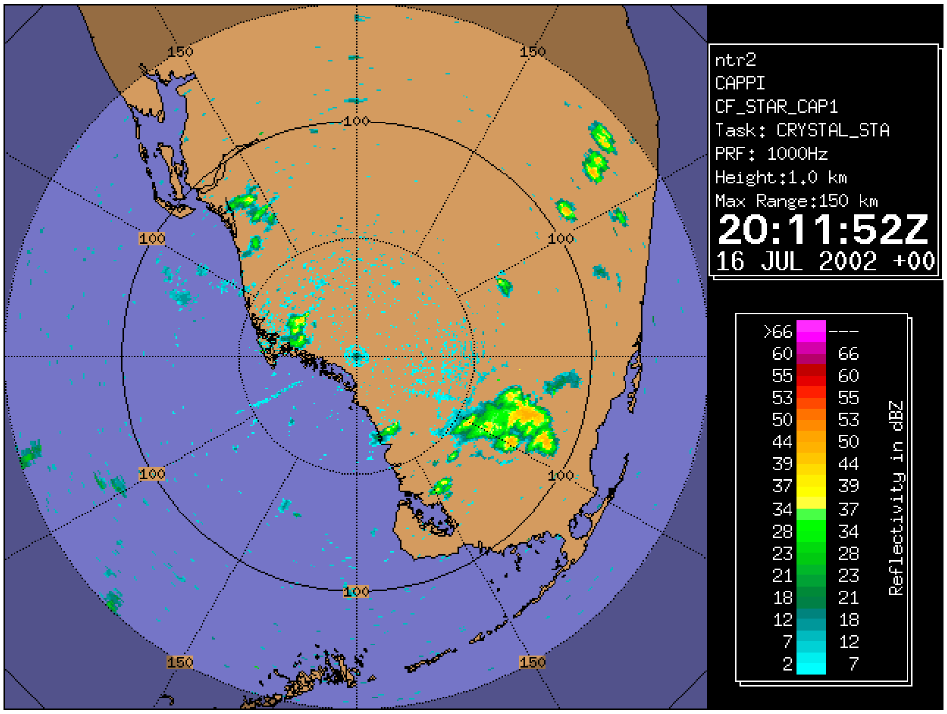

Figure 4.1. CAPPI reflectivty image from 2011 UTC on July 16, 2002 at 1 km elevation

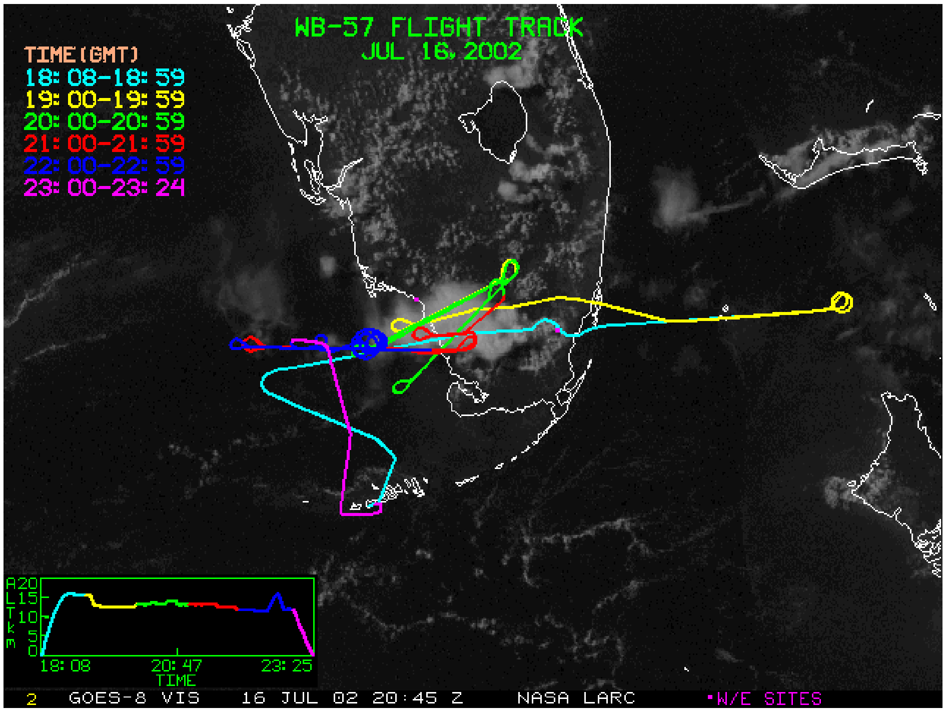

Figure 4.2. GOES-8 visible image at 2045 UTC on July 16, 2002 overlaid with the WB57 flight track.

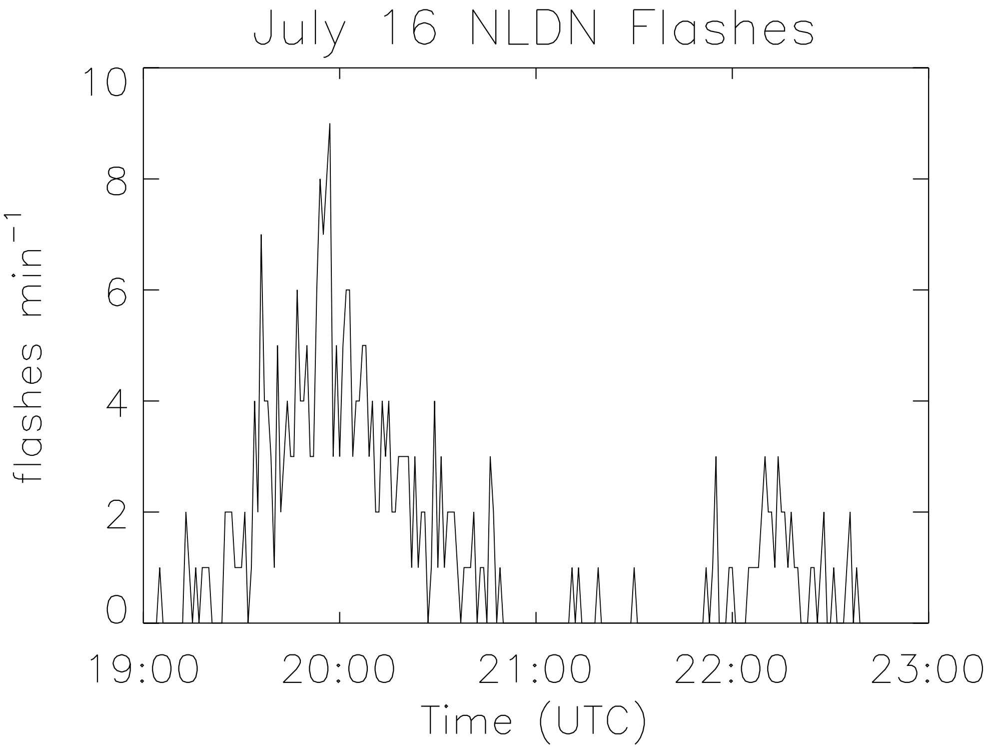

Figure 4.3. Observed CG flash rates in the July 16 CRYSTAL-FACE storm.

FACE, IC flash rates were estimated from the observed CG flash rates assuming the climatological IC to CG ratio of 2 for south Florida from Boccippio et al. [2001]. CG flash rates were estimated by removing weak positive flashes and adjusting for the network's detection efficiency as shown in Cummins et al. [1998].

4.2.2 Simulated storm evolution

The storm was simulated by Dr. Donghai Wang from NASA Langley Research Center using the Advanced Regional Prediction System (ARPS) described in Xue et al. [2000] and Xue et al. [2001] with a horizontal resolution of 2 km and vertical resolution varying from 25 m near the surface to 0.5 km near the top of the model domain at approximately 25 km. A number of observation types were assimilated into the model every hour. The convective system of interest which was sampled by the WB57 developed approximately an hour later in the model (2000 UTC) than observed. Figure 4.4 shows computed radar reflectivity at 2110 UTC in the simulation, about 70 minutes after the start of convection, at 1 km AGL. By comparing to Figure 4.1, which is also approximately 70 minutes after the beginning of convection, the simulated system covers a larger area than the observed at this time.

Differences between the observed and simulated storm features are in part due to the data assimilation which occurs every hour. Horizontal distributions of radar reflectivity like the one given in Figure 4.4 show that the storm increased in size and intensity immediately following the assimilation of observations, and then slowly decreased in size until the next assimilation of observations when the process was repeated. This effect of the assimilation also impacted the height of the cloud top and the top of the 20 dBZ contour in the simulation. Figure 4.5 shows the altitude of the top of

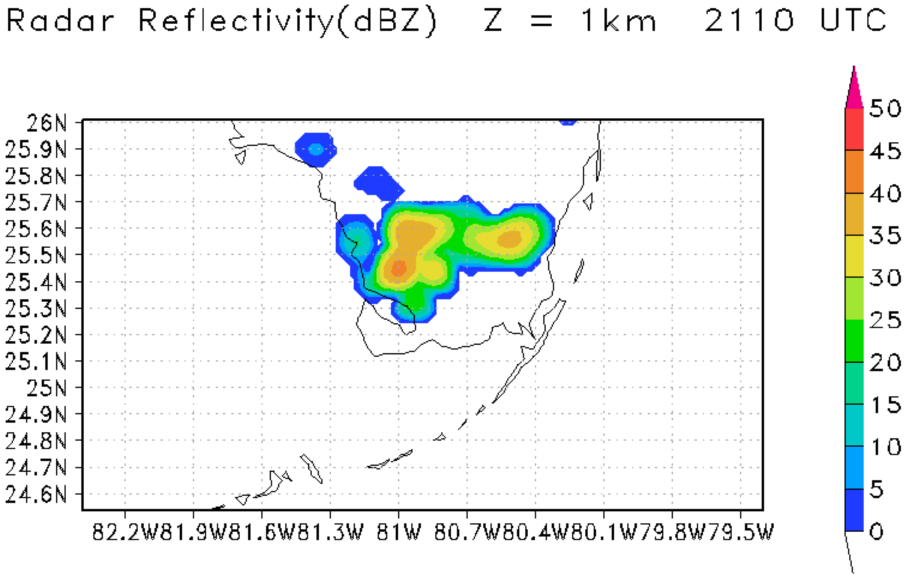

Figure 4.4. Radar reflectivity at 1 km calculated from ARPS simulated hydrometeor fields at 2110 UTC during the July 16 CRYSTAL-FACE storm.

the 20 dBZ contour versus time in the simulation. Observed precipitation top heights were typically ~ 14 km AGL but as a result of the assimilation, the height of the 20 dBZ contour repeatedly increases to over 15 km then decreases, dropping below the 14 km height observed until the next assimilation.

4.2.3 Tracer transport

I used the passive version of the CSCTM to analyze the transport of tracer species in the storm. Initial condition profiles of CO, NO_x, and O_3 were constructed using data from portions of the WB57's ascent and descent which were outside of cloud (see Figure 4.6). In order to verify the model results, observations were averaged over 14 second intervals to reproduce the 2-km spatial resolution of the model. Observations from the Cloud, Aerosol, Precipitation Spectrometer (CAPS) aboard the WB57 were used in conjunction with satellite images overlaid with portions of the WB57 flight track to determine which portions of the flight were in-cloud. In-cloud aircraft observations were

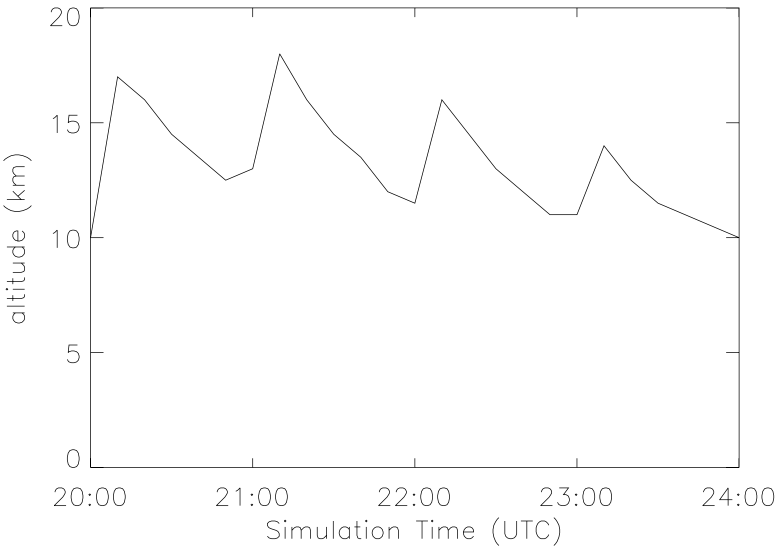

Figure 4.5. Maximum height of the 20 dBZ contour of radar reflectivity computed from ARPS hydrometeor fields in the July 16 CRYSTAL-FACE storm.

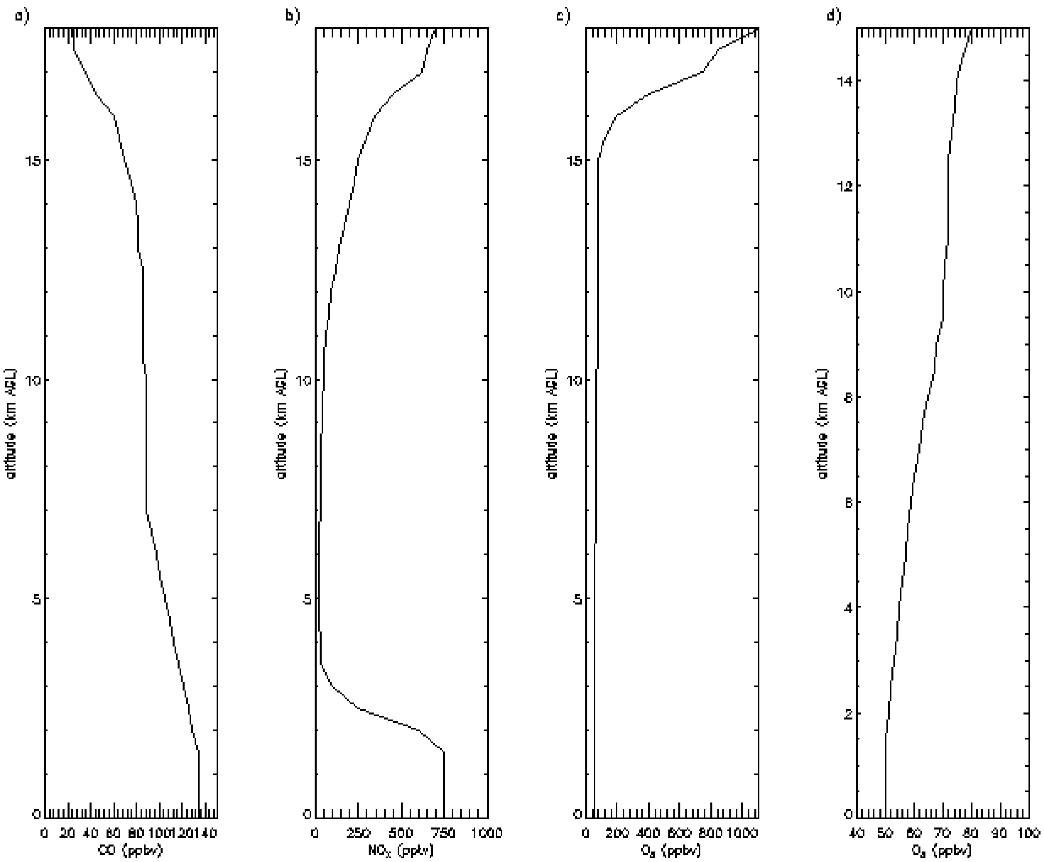

Figure 4.6. Initial condition profiles of (a) CO, (b) NO_x, (c) O_3, and (d) tropospheric O_3 for the July 16 CRYSTAL-FACE storm.

then binned into 0.5 km thick layers from 11.5 to 14 km and mean values and pdfs were calculated in each layer for each tracer species. The model output was sampled from 2040 to 2340 UTC, though an analysis of aircraft flight data was used to determine more specifically which times to include in the computed means and pdfs for each layer. Only grid cells with calculated radar reflectivity between 0 and 30 dBZ were used because the WB57 was flying primarily in the lower reflectivity anvil rather than the core of the storm.

Figure 4.7 shows the computed pdfs of simulated and observed CO at 11.5, 12.5, and 13.5 km AGL. At 11.5 km, the model overestimates the distribution of CO for nearly

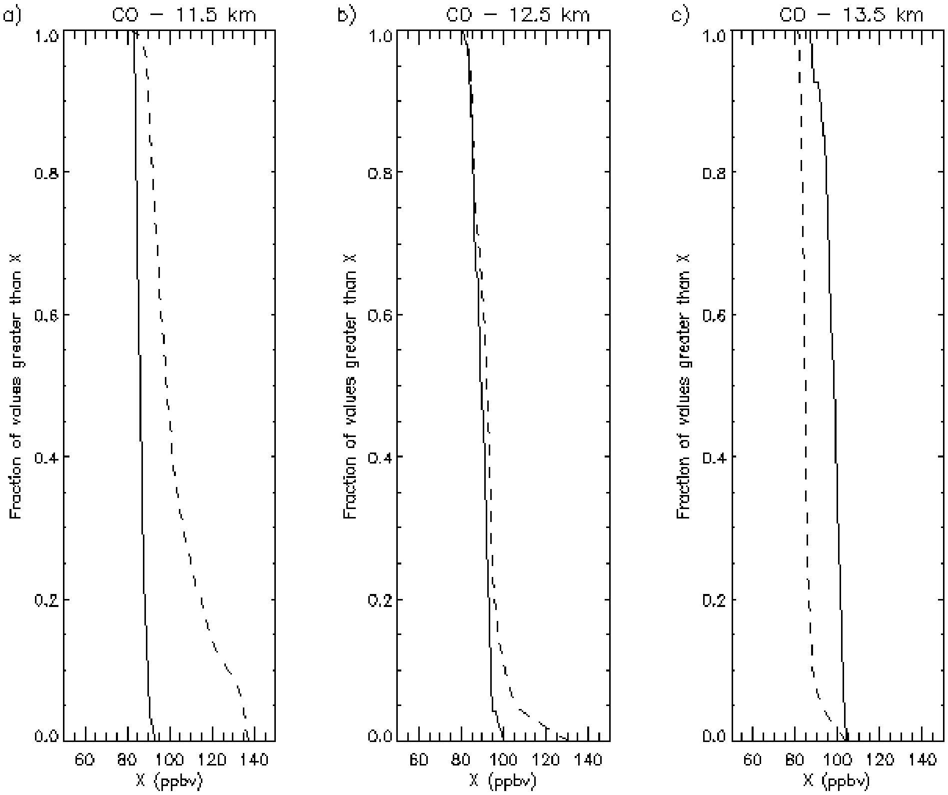

Figure 4.7. Pdfs of simulated (dashed) and observed (solid) CO at (a) 11.5, (b) 12.5, and (c) 13.5 km in the July 16 CRYSTAL-FACE storm.

all CO mixing ratios, though the greatest degree of overestimation occurs at high values of CO. The comparison at 12.5 km is more favorable, with the simulation reproducing the observed distribution well for approximately 80% of values and only overestimating the maximum CO mixing ratios. The simulation uniformly underestimates the distribution of CO observations at 13.5 km. Figure 4.8 shows a similar plot of computed pdfs of O_3 at the same levels. In general, the comparison of simulated O_3 with observations is better than CO. The simulation does overestimate the maximum O_3 mixing ratios at 11.5 and 12.5 km while reproducing well the distribution below 80 ppbv. The overestimation of the maximum CO and O_3 mixing ratios at 11.5 and 12.5 km suggests that both upward and downward transport in the model may be in excess of

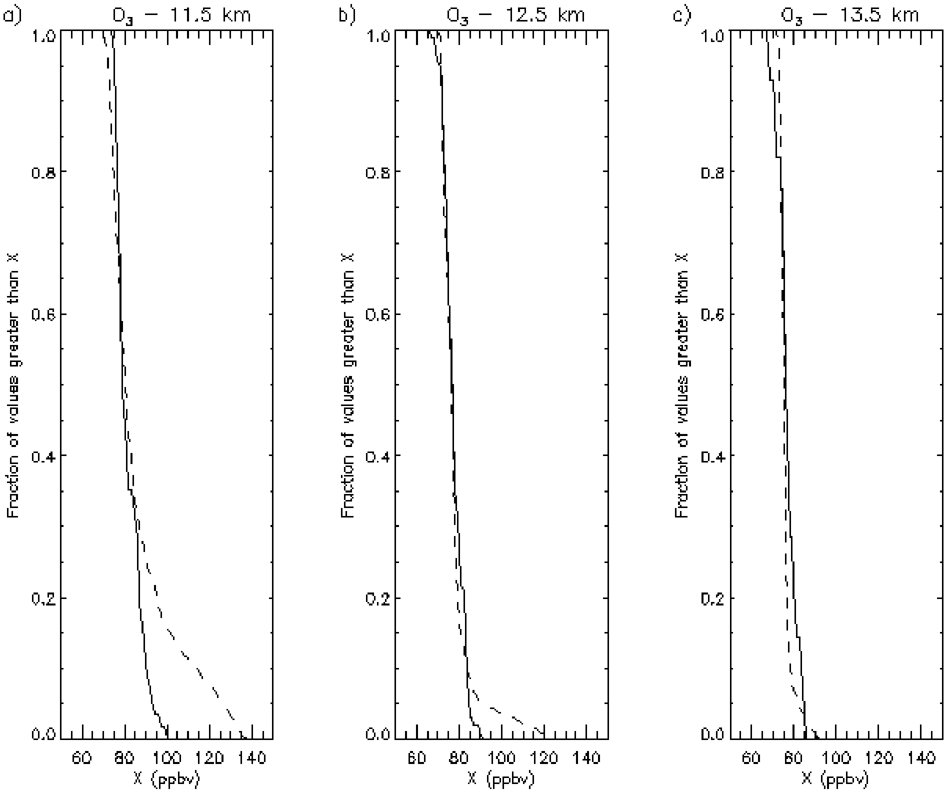

Figure 4.8. Pdfs of simulated (dashed) and observed (solid) O_3 at (a) 11.5, (b) 12.5, and (c) 13.5 km in the July 16 CRYSTAL-FACE storm.

transport in the observed storm. At 13.5 km, the simulation's underestimation of CO indicates that too little CO is being transported upward to this level. This is likely due in part to the changes in cloud top height discussed in section 4.2.2. When cloud top height decreases below 13.5 km, less CO would be transported to this level than if the cloud top height remained at approximately 14 km as was observed.

4.2.4 Lightning NO_x production

In addition to affecting the transport of tracer species, changes in cloud top height throughout the simulation profoundly affect the way the original lightning parameterization distributed lightning NO_x. In distributing NO_x produced by IC flashes, the model determines whether the top of the cloud is higher than the height of the upper mode isotherm. If so, NO_x produced by IC flashes is distributed bimodally in the vertical. However, if the cloud top is below the height of the upper mode isotherm, NO_x produced by IC flashes is distributed according to a unimodal distribution. Unaltered, the lightning parameterization distributed a large portion of the NO_x produced by IC flashes unimodally which caused most of the IC NO_x to be placed near the altitude of the lower mode isotherm. However, observations showed a mean NO_x mixing ratio in-cloud of 2 ppbv at 14 km. It was therefore necessary to modify the DeCaria et al. [2005] lightning scheme to place some NO_x above the top of the simulated cloud during the oscillations shown in Figure 4.5 when cloud height dropped below the upper mode isotherm. In the modified scheme, when the computed top of the 20 dBZ reflectivity contour is less than the height of the upper mode isotherm by less than 1.5 km, the top of the cloud is effectively raised by 1.5 km for the purpose of distributing IC NO_x. At the levels above the top of the simulated cloud, lightning NO_x is placed into grid cells with radar reflectivity greater than 20 dBZ at the uppermost cloud level.

Lightning NO_x production was first estimated by calculating the mean peak current of CG flashes observed by the NLDN. Using a relationship between peak current and energy dissipated from Price et al. [1997], P_{CG} was estimated to be 700 moles NO per flash. The upper mode of the vertical distribution of IC NO_x was assumed to be at the height of the -60° C isotherm, while the lower mode was assumed to be at the height of the -15° C isotherm. Various values of the P_{IC}/P_{CG} ratio were simulated and the results compared with aircraft observations. Because NO_2 was not measured during CRYSTAL, NO_2 was estimated using NO and O_3 observations and the photostationary state assumption. The observed column mass of N in NO_x was calculated for the 3 km thick

Table 4.1. Calculated column mass of N in NO_x in the July 16 CRYSTAL-FACE storm

P_{CG} (moles NO per flash)	P_{IC}/P_{CG}	Column Mass (g N m^{-2})
700	0.1	1.8×10^{-4}
700	0.5	3.6×10^{-4}
700	0.75	5.1×10^{-4}
700	1.0	6.4×10^{-4}

layer extending from 11.25 to 14.25 km by binning observations into 0.5 km thick layers and computing layer mean NO_x mixing ratios. Assuming that photolysis rates were enhanced by the cloud by a factor of 2 yielded a column mass of 5.0×10^{-4} g N m^{-2}, while assuming photolysis rates were not enhanced by the cloud yielded a column mass of 5.3 $\times 10^{-4}$ g N m^{-2}. Table 4.1 gives estimates of the column mass of N in NO_x computed using model results sampled in the same way described above for the pdfs and computing layer means. The assumption of Price et al. [1997] that an IC flash produces only 10% as much NO as a CG flash results in a large underestimation of the observed column mass. Assuming that on average, an IC flash produces 75% as much NO as a CG flash produces yields the best comparison with column mass estimated from observations. Figure 4.9 compares simulated pdfs and observed NO_x for 11.5, 12.5 and 13.5 km AGL. At 11.5 and 12.5 km, the simulation assuming that P_{IC} is 75% of P_{CG} reproduces the distribution of lower values but overestimates the maximum values. At 13.5 km, the model reproduces the distribution of observed values well below 0.5 ppbv, underestimates the distribution for NO_x mixing ratios between 0.5 and 2.75 ppbv, and then produces higher NO_x mixing ratios than observed at the upper end of the distribution. Figure 4.10 shows that the maximum in the observed mean profile of 2 ppbv is found at 14 km, while the simulated maximum of 1.9 ppbv is found at 13 km. The production scenario in which an IC flash produces on average 525 moles NO and a CG flash produces on average 700

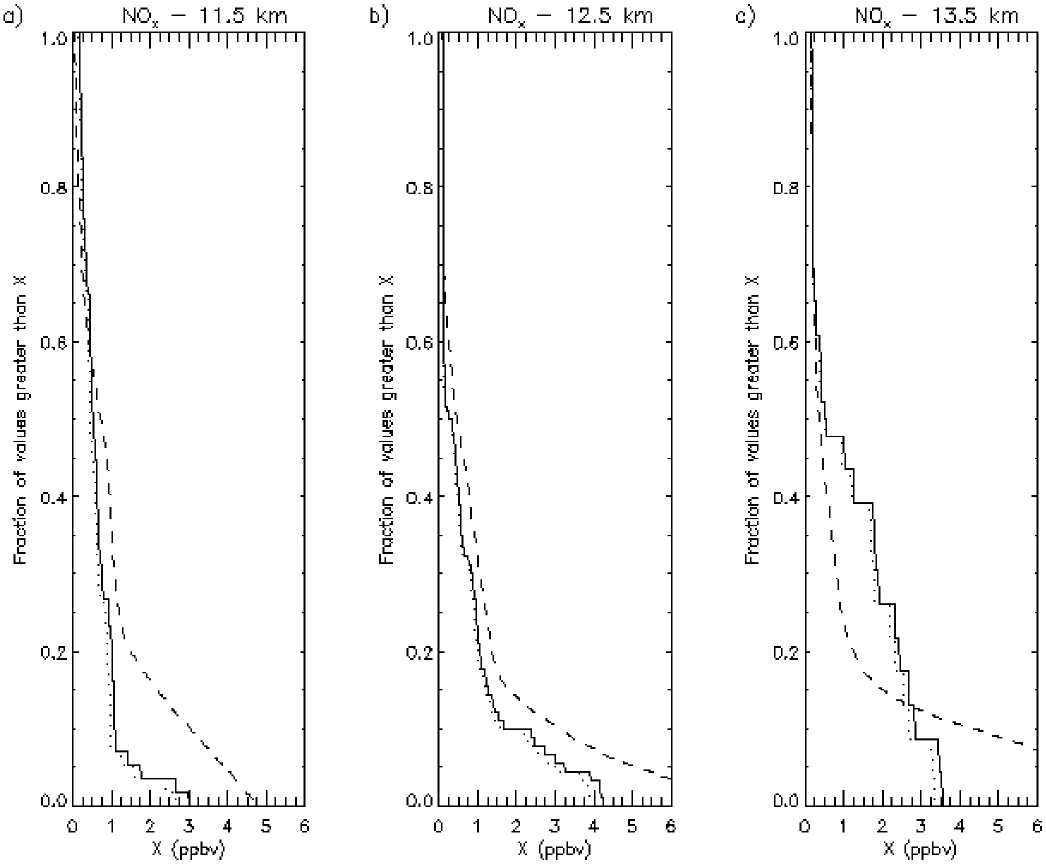

Figure 4.9. Pdfs of simulated (dashed) and observed (assuming cloud enhanced photolysis rates – dotted, assuming clear sky photolysis rates –solid) NO_x at (a) 11.5, (b) 12.5, and (c) 13.5 km in the July 16 CRYSTAL-FACE storm.

moles NO was selected as the best fit because it compared most favorably with column mass. The model could not reproduce the spiky shape of the observed mean profile shown in Figure 4.10. Due to the changes in cloud top height in the ARPS simulation of the storm, the CSCTM was also unable to reproduce the height of the maximum at 14 km, though with the modified lightning scheme was able to produce a peak only 1 km below. The overestimation of maximum NO_x values seen in the pdfs in Figure 4.9 may be due in part to the weakening of the storm between assimilation cycles. At each level, lightning NO_x is placed throughout the 20 dBZ contour. As the storm weakens, the size

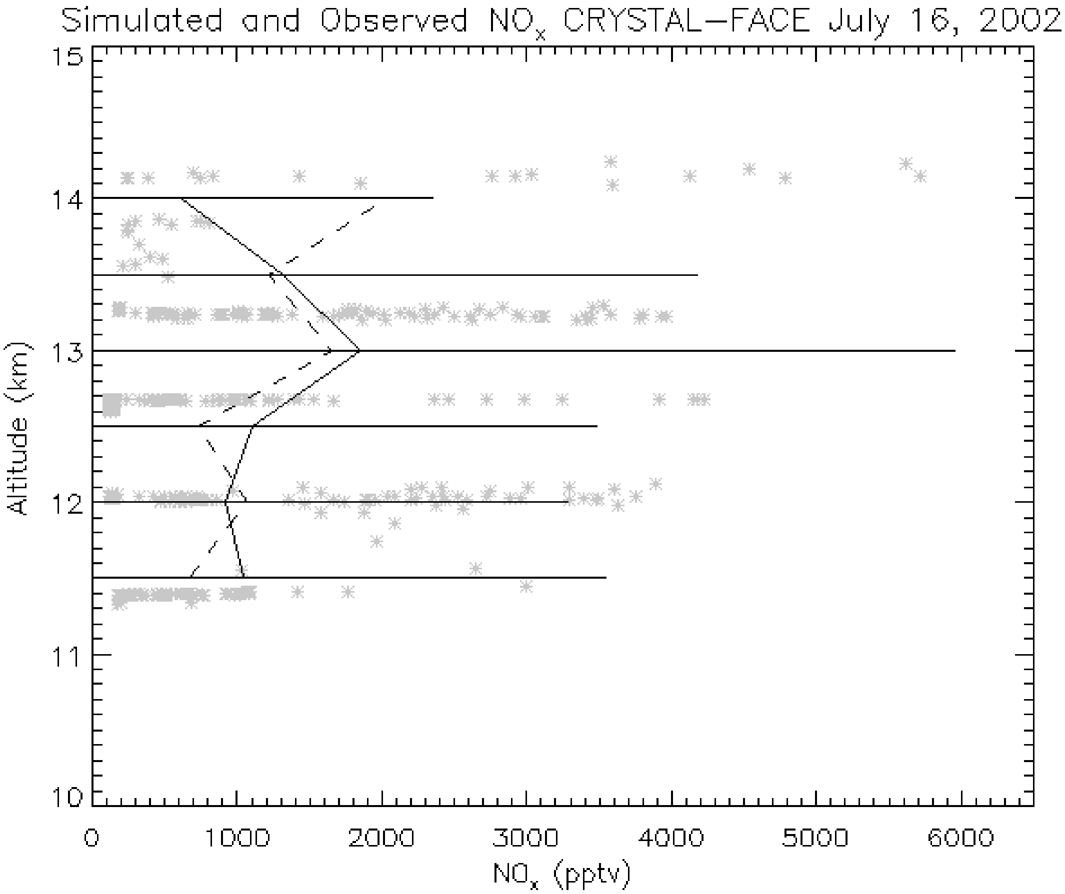

Figure 4.10. Mean in-cloud simulated (solid) and observed (dashed - assuming clear sky photolysis rates-solid) NO_x. Asterisks represent observed NO_x (calculated assuming clear sky photolysis rates) averaged over 14-second intervals. Solid bars show the standard deviation of simulated in-cloud NO_x at each level.

of this area shrinks. If this area is smaller than the size of the observed cell, lightning NO_x may be placed into too few cells, creating values that are higher than observations. Excessive upward transport in the simulation as suggested by the CO pdfs may also contribute to the overestimation of the maximum NO_x values at each level.

4.2.5 Simulation of the chemical environment of the storm

The CSCTM with chemical reactions included was run for the July 16 CRYSTAL-FACE storm. The reaction scheme was the same as described in DeCaria et al. [2005] with the addition of isoprene, its products, and propene. Dr. Rokjin Park from Harvard University provided a mean July profile for the latitude and longitude of south Florida calculated from a global 3-D UMD-CTM [Park et al., 2004] simulation which included C_2H_4, C_3H_6, C_2H_6, C_3H_8, isoprene, PAN, CH_3CO_3, CH_3OOH, H_2O_2, HCHO, and HNO_3. The single column "spin-up" version of the CSCTM was run for 15 minutes to allow the NO, NO_2, O_3, and CO profiles constructed from observations to come into chemical equilibrium with the profiles from the global model prior to the simulation of the storm.

The CSCTM with chemistry was run assuming that a CG flash produces 700 moles NO and an IC flash is on average 75% as productive of NO as a CG flash. As in the simulations of the July 21 EULINOX and July 10 STERAO storms, the inclusion of chemical reactions resulted in a decrease in NO_x as it was converted to reservoir species. The column mass of N in NO_x was estimated to be 4.5 x 10^{-4} g N m^{-2} when chemical reactions were accounted for which is less than the range of column mass calculated from observations of 5.0 to 5.3 x 10^{-4} g N m^{-2}. In order to match the observed column mass, the P_{IC}/P_{CG} ratio was increased from 0.75 to 0.9. When a P_{IC}/P_{CG} ratio of 0.9 was assumed, the calculated column mass was 5.2 x 10^{-4} g N m^{-2}. Figure 4.11 shows the simulated NO_x mixing ratios at 10 km at the end of the 240-minute simulation assuming a P_{IC}/P_{CG} ratio of 0.9. At this time, the convective plume of enhanced NO_x is visible approximately 180 km off the coast of Florida. Maximum NO_x mixing ratios exceed 3.6 ppbv.

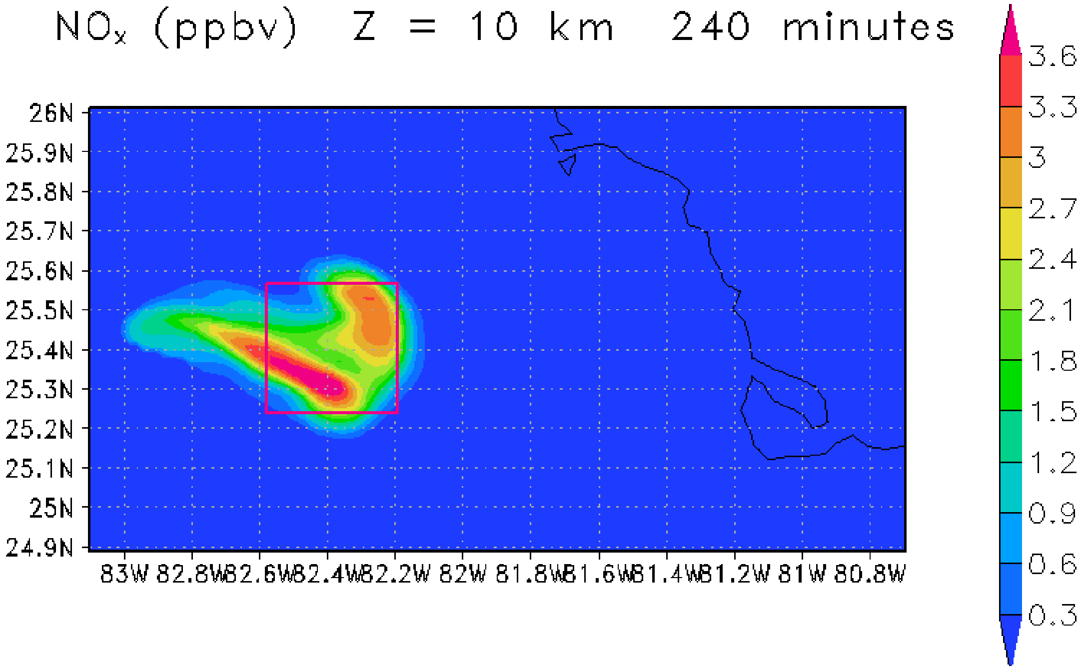

Figure 4.11. Simulated NO$_x$ mixing ratios (assuming P_{CG}=700 and P_{IC}=630 mol NO) in ppbv at 10 km, 240 minutes into the simulation of the July 16 CRYSTAL-FACE storm. The box indicates the area over which ozone averages were computed.

The version of the CSCTM including chemical reactions was also run without lightning. The change in ozone mixing ratios was averaged over the 40 km by 40 km box shown in Figure 4.11 and the change in ozone during the storm due to lightning NO$_x$ production calculated by subtracting the average from the simulation which did not include lightning from the lightning simulation average. The results are shown in Figure 4.12. The largest mean increase in ozone mixing ratios due to lightning NO$_x$ of ~ 1 ppbv occurs at 10.5 km. The maximum increase of any grid cell within the sampling area is 3.5 ppbv at 5.5 km. At levels below 4 km, lightning NO$_x$ has very little impact on O$_3$

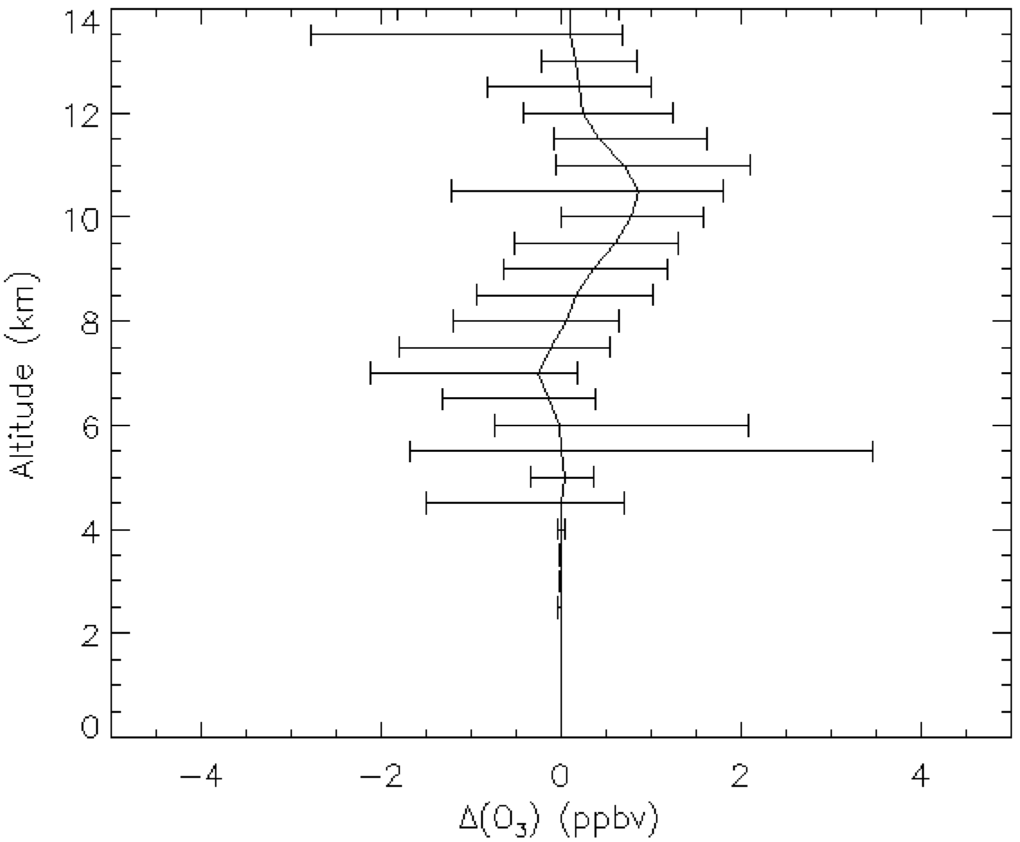

Figure 4.12. Solid line is average change in ozone mixing ratios due to lightning during the 240-minute simulation of the July 16 CRYSTAL-FACE storm. Bars indicate the maximum and minimum ozone change within the averaging box at each level.

mixing ratios which was not the case in the July 21 EULINOX and July 10 STERAO simulations. This results from the strengthening and weakening of the simulated storm which occurs with the cycle of data assimilation. When the storm is weakening, the cloud base is higher than in the other simulated cases and less lightning NO_x is reaching the altitudes below 4 km to affect O_3 mixing ratios.

4.2.6 Simulation of chemistry in the convective plume

Chemical fields from the end of the 240-minute simulations which did and did not include lightning NO_x production were used to initialize the chemistry-only version of the

CSCTM which estimates chemistry in the downstream convective plume. The mean change in net ozone production was calculated by averaging the change in ozone in both cases over the averaging area shown in Figure 4.11 and subtracting the mean 24-hour change in ozone in the "no lightning" case from the 24-hour change in ozone in the lightning simulation. The mean change in net ozone production is shown in Figure 4.13. On average, the inclusion of lightning NO_x results in a small increase in net ozone production, maximizing at 3 ppbv day^{-1} at 9.5 km. A maximum increase in net ozone

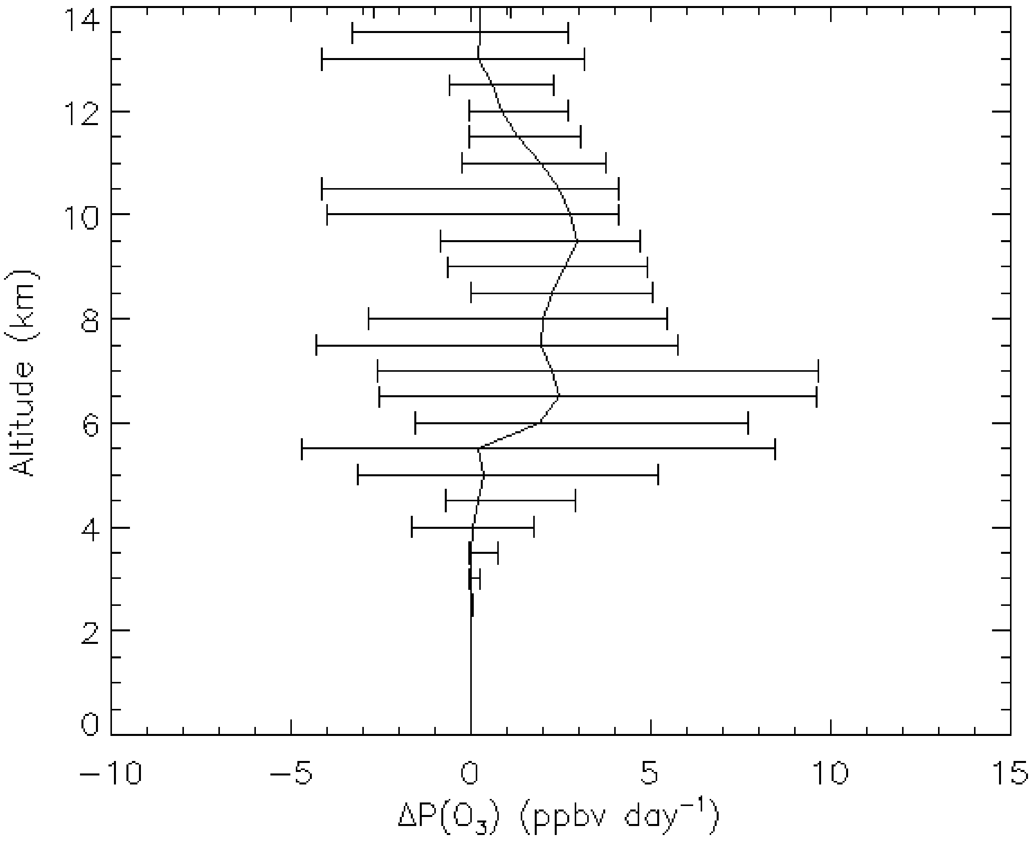

Figure 4.13. Solid line is the average change in net ozone production due to lightning in the 24 hours following the July 16 CRYSTAL-FACE storm. Bars show the maximum and minimum change within the averaging box at each level.

Table 4.2. Average Species Concentrations at 10 km AGL at the Beginning and End of the Chemistry-Only Simulation of the July 16 CRYSTAL-FACE storm

Species	Average Mixing Ratio Immediately Following Convection (ppbv)	Average Mixing Ratio 24 hours after Convection (ppbv)
NO_x	1.72	0.980
O_3	92.4	94.5
HNO_3	0.881	1.35
HCHO	0.181	7.69×10^{-2}
H_2O_2	0.961	0.586
CH_3OOH	0.335	0.151
$CH_3CO_3NO_2$	0.462	0.465
OH	1.93×10^{-4}	3.08×10^{-4}
HO_2	1.84×10^{-3}	3.09×10^{-3}
RO_2	3.82×10^{-4}	5.37×10^{-4}

* Averages are computed over the sampling box shown in Figure 4.11.

production of ~10 ppbv day^{-1} is seen at 6.5 and 7 km. As was the case during the 240-minute simulation of the storm, lightning NO_x had very little impact on O_3 mixing ratios below 4 km.

Table 4.2 gives the average mixing ratios over the sampling area shown in Figure 4.11 of a number of species at the beginning and end of the chemistry-only simulation. O_3 has increased by 2.1 ppbv entirely due to lightning NO_x. If lightning NO_x were not considered, a small loss of O_3 would occur at the 10 km level in the 24 hours following convection due to convective transport alone.

4.3 The July 29 CRYSTAL-FACE storm

4.3.1 Observed storm evolution

At 1700 UTC on July 29, 2002, a powerful thunderstorm developed along the west coast of Florida near Fort Myers and was observed as part of CRYSTAL-FACE. The storm intensified and moved north along the coast (see Figure 4.14). The coastal convection later merged with convection originating near Lake Okeechobee. The area in and above the coastal storm was sampled by the WB-57 from 1845 to 2013 UTC at altitudes ranging from 12.5 to 13.8 km. Figure 4.15 shows a visible image from the GOES-8 satellite taken at 1815 UTC with the WB57 flight track overlaid.

Figure 4.16 shows the time series of CG flashes recorded by the NLDN from 1700 to 2300 UTC. In contrast to the July 16 CRYSTAL-FACE storm, the July 29 storm was an exceptionally strong lightning producer with 4168 CG flashes associated with the coastal storm recorded by the NLDN during this period. Maximum CG flash rates exceeded 30 flashes per minute during the most electrically active period from 1900 to 2000 UTC. Because the NLDN only records the occurrence of CG flashes, it was necessary to estimate IC flashrates. NLDN flashes with positive peak current less than 10 kA are thought to be IC flashes [Cummins et al., 1998]. The percentage of weak positive flashes was calculated during the July 29 storm and during the month of July as a whole and was larger by a factor of 2.5 for the July 29 storm. The south Florida climatological value for the IC/CG ratio of 2 from Boccippio et al. [2001] was multiplied by 2.5 to estimate an IC/CG ratio of 5 for the July 29 coastal storm. CG flash rates were estimated by removing weak positive flashes and adjusting for the network's detection efficiency as shown in Cummins et al. [1998].

4.3.2 Simulated storm evolution

The July 29 CRYSTAL-FACE storm was simulated by Dr. Ruei-Fong Lin from NASA Goddard Space Flight Center using the NASA Goddard version of the non-hydrostatic PSU/NCAR (MM5) mesoscale model [Tao et al., 2003] with a horizontal resolution of 2 km and vertical resolution of 0.5 km. The MM5 model was initialized

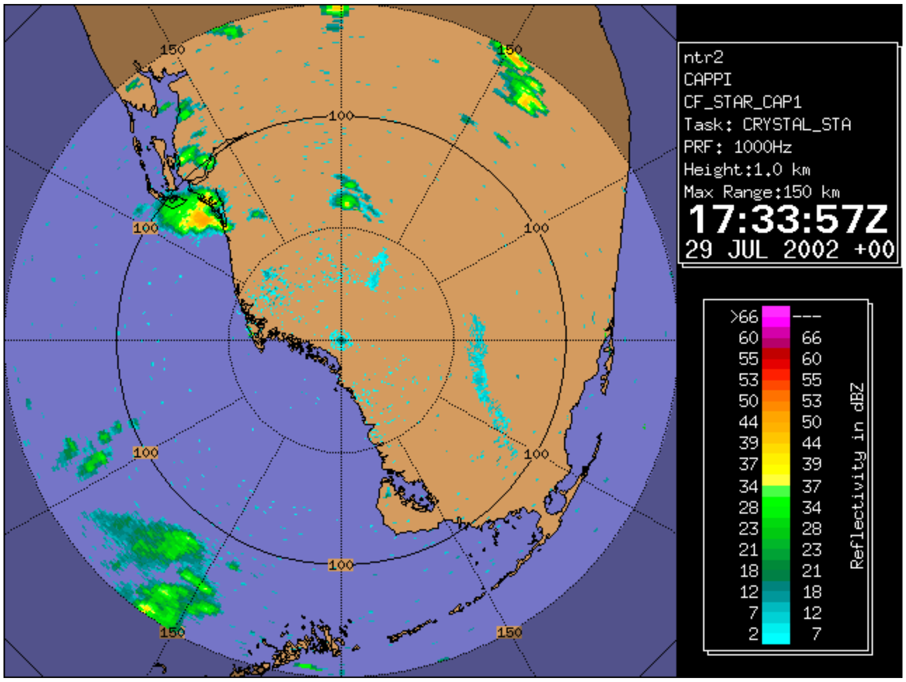

Figure 4.14. CAPPI reflectivty image from 1733 UTC on July 29, 2002 at 1km elevation.

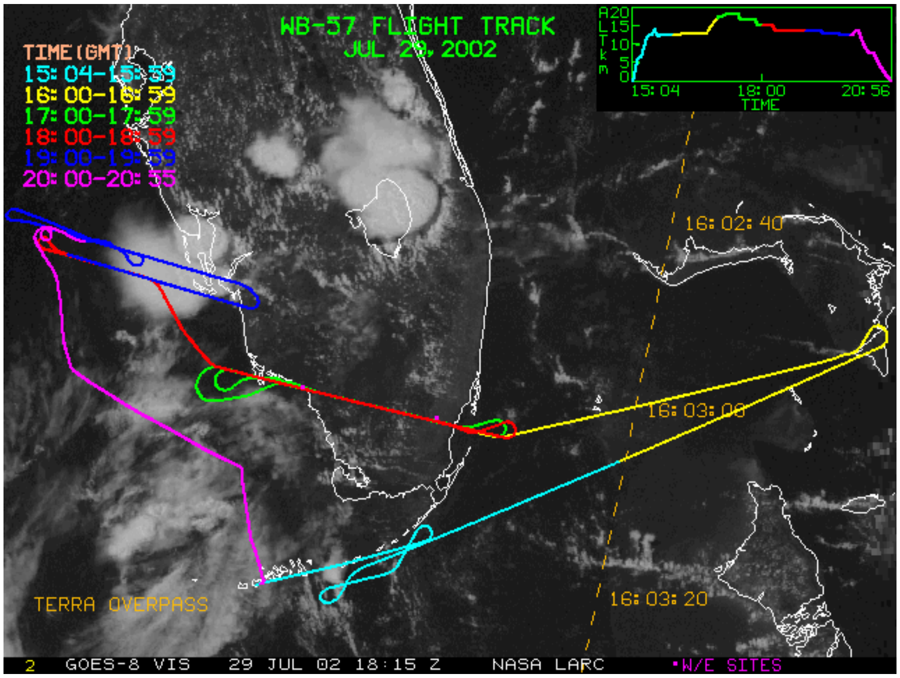

Figure 4.15. GOES-8 visible image at 1815 UTC on July 29, 2002 overlaid with the WB57 flight track.

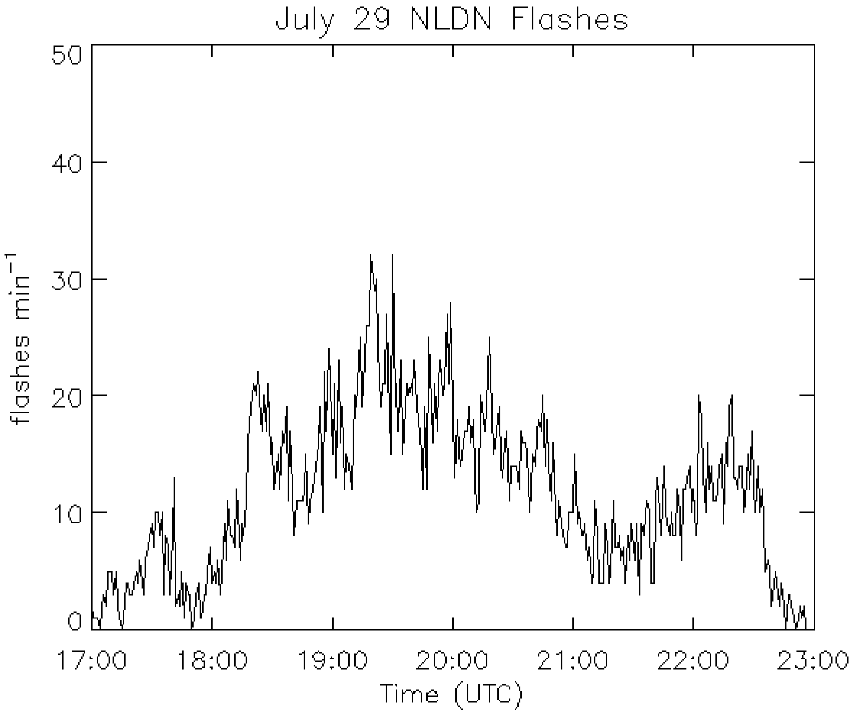

Figure 4.16. Observed CG flashrates in the July 29 CRYSTAL-FACE storm.

with fields from the NCEP Eta model and run for 8 hours from 1400 to 2200 UTC. Simulated convection began along the coast approximately 3 hours earlier than observed. Figure 4.17 shows the 1 km plot of radar reflectivity computed using hydrometeor fields from the MM5 simulation at 1430 UTC. The location of the simulated convection matches the location of the observed convection well, though at this time (30 minutes after convection has begun), the simulated convection covers a larger area than the observed. Precipitation top heights, typically from 13 to 13.5 km, compared favorably with precipitation top heights observed by the EDOP cloud radar aboard the ER-2 aircraft. The duration of the coastal convection, as well as the direction of the system's movement were effectively reproduced by the MM5 simulation, though the movement of the system was slightly slower than observed.

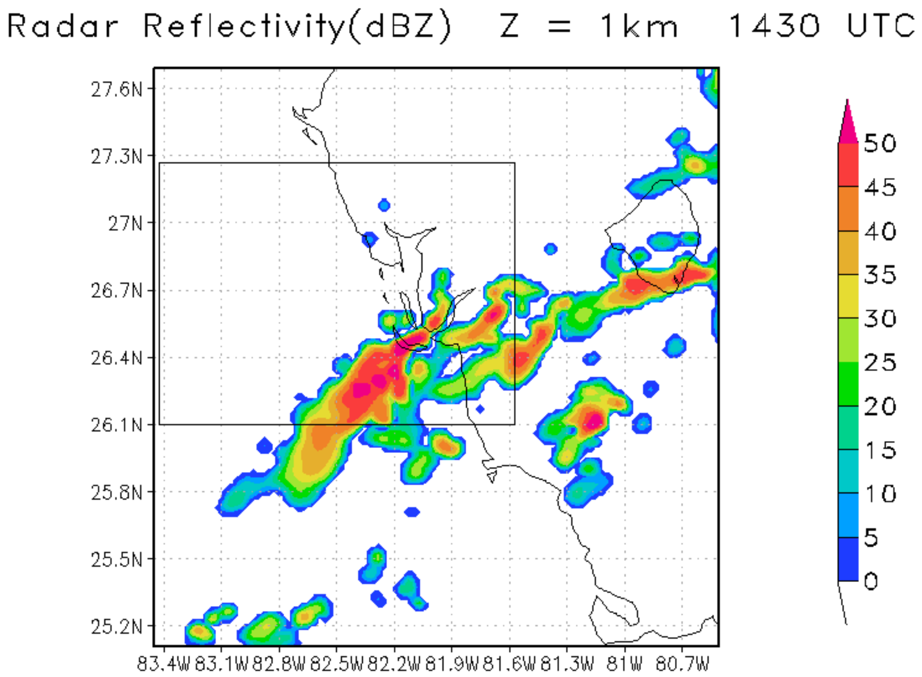

Figure 4.17. Radar reflectivity at 1 km calculated from MM5 hydrometeor fields at 1430 UTC on July 29, 2002. The box indicates the areas of the domain used in calculating lightning NO_x production.

4.3.3 Tracer transport

The passive version of the CSCTM was run to study the transport of CO and O_3 and to obtain a first estimate of lightning NO_x production. Initial condition profiles of CO, NO_x and O_3, shown in Figure 4.18, were constructed using data from the ascent and descent of the WB57, portions of the flight which were not affected by convection, and fields from the global University of Maryland Chemical Transport Model (UMD-CTM) where necessary. CO data from the Twin Otter aircraft were available in the vicinity of the coastal storm and CO mixing ratios greater than 150 ppbv were observed in the boundary layer. Given these measurements and the intensity of the convection, CO mixing ratios in the 120-150 ppbv range were expected in the anvil observations of the

WB57. However, the greatest value observed in the anvil was approximately 100 ppbv. This is likely the result of cleaner air from the marine boundary layer entering the storm. Westerly surface winds from the Gulf of Mexico observed at Fort Myers support this conclusion.

For comparison with model results, observations from 1845 to 2013 UTC were averaged over 14 second intervals in order to match the 2 km spatial resolution of the model. CAPS observations were used to determine in-cloud flight segments. In-cloud aircraft observations were then binned into 0.5 km thick layers centered on 12.5 and 13 km and mean values and pdfs were calculated in each layer for each tracer species. The CSCTM output was sampled from 1550 to 1710 UTC because convection along the coast

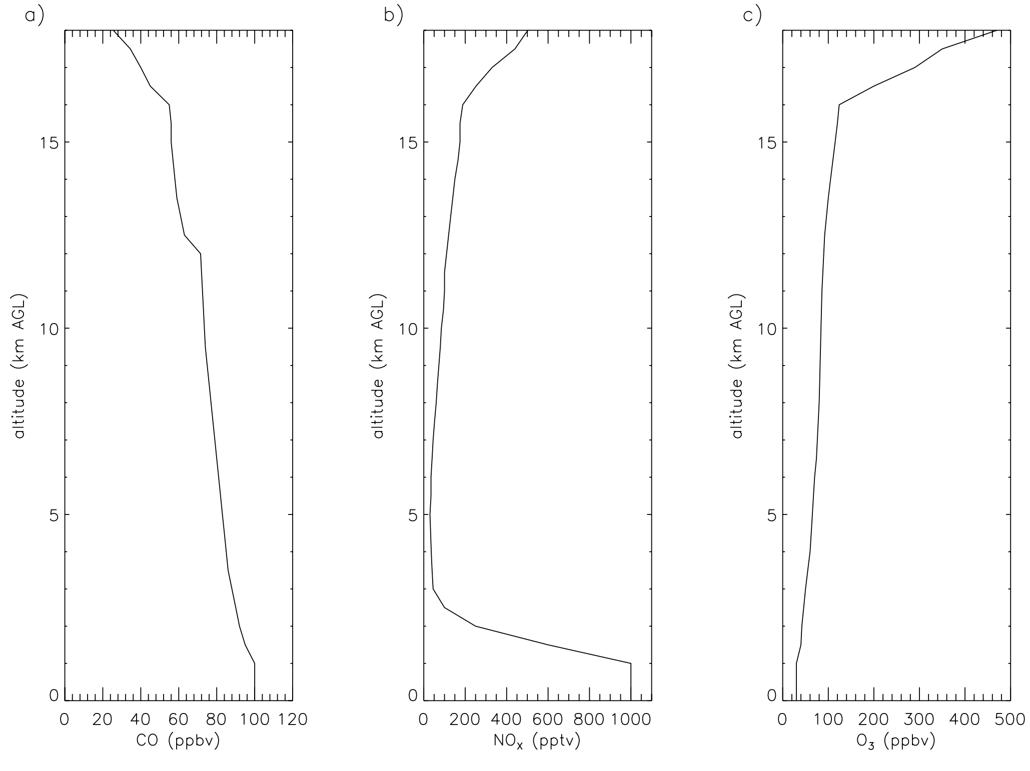

Figure 4.18. Initial condition profiles of (a) CO, (b) NO$_x$, and (c) O$_3$ in the July 29 CRYSTAL-FACE storm.

began 3 hours earlier in the simulation than the actual start of convection. Grid cells with computed radar reflectivity between 0 and 30 dBZ were included because the aircraft did not fly in the higher reflectivity storm core.

Figure 4.19 compares pdfs of simulated and observed CO mixing ratios at 12.5 and 13 km. At both levels, the model overestimates CO mixing ratios suggesting that upward transport in the model may be too large. Figure 4.20 shows a similar plot of simulated and observed O_3 mixing ratios at 12.5 and 13 km. The model also overestimates O_3 at these levels, suggesting that too much ozone rich air is being transported downward in the model. However, the intense lightning activity in the storm and extremely elevated NO mixing ratios observed in the anvil (up to 10 ppbv) indicate that the lightning NO_x source in this particular storm was extraordinarily strong. Errors

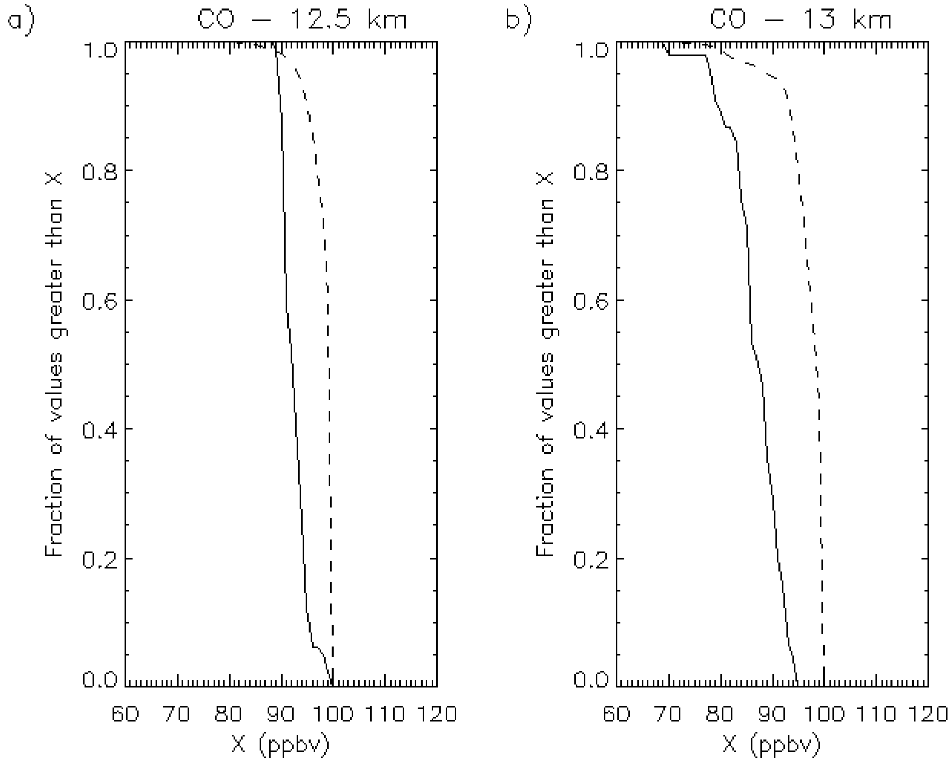

Figure 4.19. Pdfs of simulated (dashed) and observed (solid) CO at (a) 12.5 and (b) 13 km in the July 29 CRYSTAL-FACE storm.

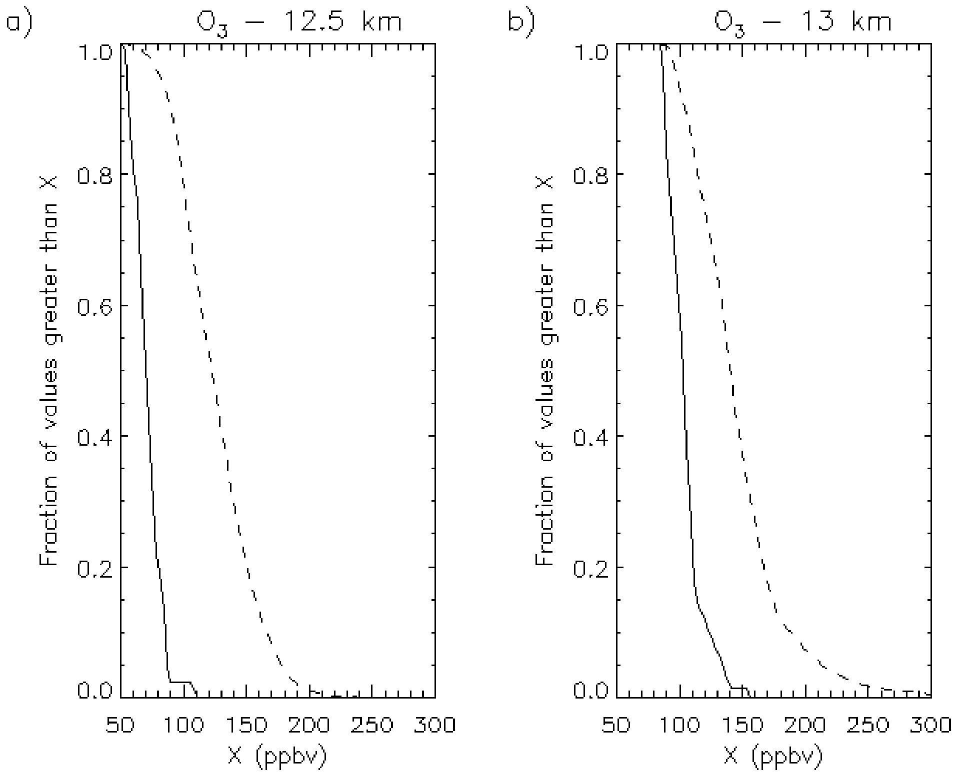

Figure 4.20. Pdfs of simulated (dashed) and observed (solid) O_3 at (a) 12.5 and (b) 13 km in the July 29 CRYSTAL-FACE storm.

in the amount of boundary layer NO_x transported to the anvil are unlikely to significantly affect the quality of the lightning NO_x production estimate.

4.3.4 Lightning NO_x production

Lightning NO_x production was calculated in the model beginning at 1400 UTC but using flashrates for the coastal storm from 1700 UTC because simulated convection began earlier than the observed storm. In order to avoid placing lightning NO_x into too large an area and diluting it, a smaller region of the domain was designated to receive lightning NO_x and is shown in Figure 4.17. On average, the area covered by convection within this region was approximately equal to the area of the coastal storm as estimated by visual inspection of radar and satellite plots. Mean peak current was calculated from

CG flashes recorded by the NLDN and using the relationship between peak current and energy dissipated from Price et al. [1997], P_{CG} was estimated to be approximately 590 moles NO per flash. The upper mode of the vertical distribution of IC NO_x was assumed to be at the height of the -45° C isotherm, while the lower mode was assumed to be at the height of the -15° C isotherm. Various values of the P_{IC}/P_{CG} ratio were simulated and the results compared with aircraft NO observations. NO_2 was estimated using NO and O_3 observations and the photostationary state assumption. The observed column mass of N in NO_x was calculated for the 1 km thick layer extending from 12.25 to 13.25 km by computing layer mean NO_x mixing ratios. Assuming that photolysis rates were enhanced by the cloud by a factor of 2 yielded a column mass of 6.6×10^{-4} g N m^{-2} while assuming that photolysis rates were unaltered by the cloud yielded a column mass of 7.0×10^{-4} g N m^{-2}. Table 4.3 gives estimates of column mass calculated from the CSCTM simulation. In this storm, assuming that an IC flash is on average 60% as productive of NO as a CG flash yields the most favorable comparison with column mass.

Figure 4.21 shows the pdfs of observed and simulated NO_x assuming that P_{IC} equals 50 and 60% of P_{CG}. When compared with observed pdfs at both 12.5 and 13 km, the production scenario which assumes a P_{IC}/P_{CG} ratio of 0.5 compares more favorably

Table 4.3. Calculated column mass of N in NO_x in the July 29 CRYSTAL-FACE storm, assuming an IC/CG ratio of 5

P_{CG} (moles NO per flash)	P_{IC}/P_{CG}	Column Mass (g N m^{-2})
590	0.1	2.3×10^{-4}
590	0.5	6.0×10^{-4}
590	0.6	6.9×10^{-4}
590	0.75	8.3×10^{-4}
590	1.0	1.0×10^{-3}

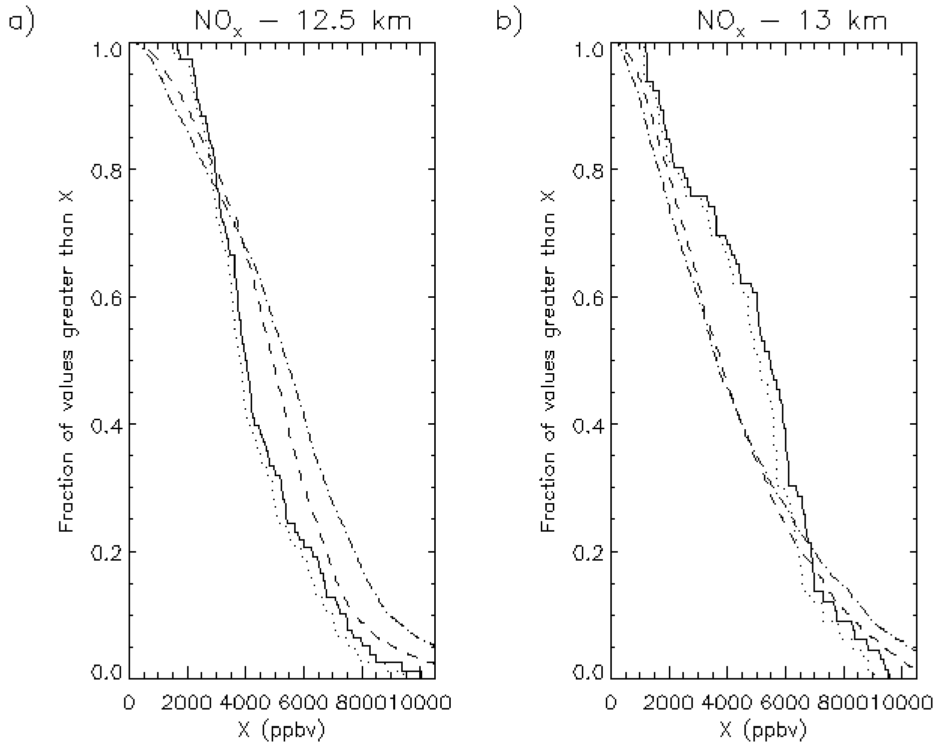

Figure 4.21. Pdfs of simulated (assuming P_{IC}/P_{CG}=0.5 – dashed, assuming P_{IC}/P_{CG}=0.6 – dot dashed) and observed (assuming cloud enhanced photolysis rates – dotted, assuming clear sky photolysis rates – solid) NO$_x$ at (a) 12.5 and (b) 13 (km) in the July 29 CRYSTAL-FACE storm.

than assuming a P_{IC}/P_{CG} ratio of 0.6. The underestimation of the simulated column mass when the production scenario assuming a P_{IC}/P_{CG} ratio of 0.5 results from the inclusion of gridcells with background NO$_x$ concentrations as well as the underestimation of the distribution at 13 km between 2 and 6 ppbv. Based on the comparison of simulated and observed pdfs and computed column mass, it was estimated that in the 7/29 CRYSTAL-FACE storm, an IC flash on average produced 50-60% as much NO as a CG flash while, on average, a CG flash produced 590 moles NO. It should be noted that this production scenario was deduced assuming that the IC/CG ratio in this particular storm was greater than the climatological IC/CG ratio for south Florida by a factor of 2.5. Because many more weak positive flashes (which are believed to be IC flashes) were recorded in this storm than was typical for the South Florida area during the month of July, it is likely that the IC/CG ratio was elevated above the climatological value. However, because of the uncertainty surrounding this assumption, the storm was also simulated assuming the climatological IC/CG ratio of 2. Estimates of column mass for a number of different production scenarios are shown in Table 4.4 assuming an IC/CG ratio of 2. If there are twice as many IC flashes as CG flashes, than an IC flash on average must produce 25-50% more NO than a CG flash to match observed NO_x mixing ratios.

4.3.5 Simulation of the chemical environment of the storm

The July 29 CRYSTAL-FACE storm was also simulated using the version of the CSCTM which includes chemical reactions as well as convective transport and lightning NO_x production. Initial conditions of a number of species were taken from the same mean July profile for south Florida used to provide initial conditions for the July 16 storm simulation. The "spin-up" version of the model was run for 15 minutes prior to the simulation of the chemical environment of the storm.

Table 4.4. Calculated column mass of N in NO_x in the July 29 CRYSTAL-FACE storm, assuming an IC/CG ratio of 2

P_{CG} (moles NO per flash)	P_{IC}/P_{CG}	Column Mass (g N m^{-2})
590	0.1	1.8×10^{-4}
590	0.5	3.2×10^{-4}
590	0.6	3.6×10^{-4}
590	0.75	4.2×10^{-4}
590	1.0	5.1×10^{-4}
590	1.25	6.0×10^{-4}
590	1.5	$6.9 \times 10^{-4}1$

A production scenario in which a CG flash produces on average 590 moles NO and an IC flash produces 50% as much NO as a CG flash was assumed (with an IC/CG ratio of 5) for the CSCTM simulation that included chemistry. The inclusion of chemical reactions resulted in a decrease in NO_x when compared to the passive simulation because some NO_x is converted to reservoir species. With chemical reactions simulated, the column mass of N in NO_x was 5.7×10^{-4} g N m^{-2} for the 1-km thick layer extending from 12.25 to 13.25 km. Assuming instead a P_{IC}/P_{CG} ratio of 0.6 produced a column mass of 6.6×10^{-4} g N m^{-2} which was within the estimated range of observations (6.6-7.0 x 10^{-4}

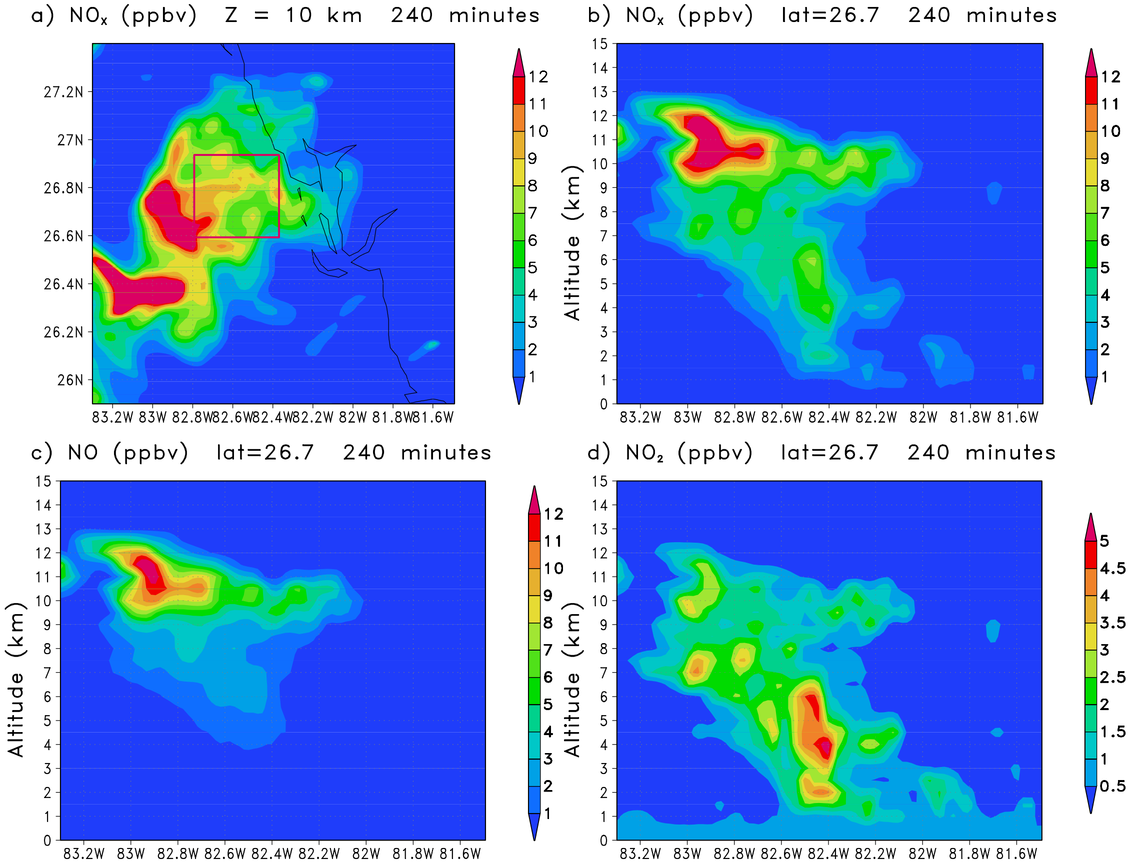

Figure 4.22. (a) Simulated NO_x mixing ratios in ppbv at 10 km, 240 minutes into the simulation of the July 29 CRYSTAL-FACE storm. The box indicates the area over which ozone averages were computed. Vertical cross sections at 26.7° latitude of (b) NO_x, (c) NO, and (d) NO_2 are also shown.

g N m^{-2}). As a result, the production scenario in which an IC flash produces on average 60% as much NO as a CG flash was selected as the most likely for this storm. Figure 4.22a shows the NO_x mixing ratios calculated by the CSCTM with chemical reactions assuming a P_{IC}/P_{CG} ratio of 0.6 at 10 km at the end of the 240 minute simulation. Maximum NO_x mixing ratios exceed 12 ppbv in areas of the anvil outflow due to the intense lightning activity associated with the coastal convection. Figures 4.22b-d show vertical cross sections of NO_x, NO and NO_2 at 26.7° latitude at the end of the simulation. The highest NO_2 mixing ratios reside below 7 km. The highest NO mixing ratios (greater than 12 ppbv) are found between 9 and 12 km where NO_2 mixing ratios are less than 3.5 ppbv.

The CSCTM with chemical reactions was also run without lightning NO_x production. The average change in ozone due to lightning was calculated by computing the mean change in ozone over the averaging area shown in Figure 4.22a in the lightning and “no-lightning”simulations and subtracting the “no-lightning” average from the lightning average. The results are shown in Figure 4.23, along with the maximum and minimum change within the averaging box at each level. Lightning NO_x causes a small loss of ozone during the lifetime of the storm averaging less than 2 ppbv at all levels. The maximum loss of ozone due to lightning during the storm is 7 ppbv at 8.5 km.

4.3.6 Simulation of chemistry in the convective plume

Chemical fields from the end of 240-minute simulations which did and did not include lightning were used to initialize the chemistry-only version of the CSCTM. The mean change in net ozone production due to the introduction of lightning NO_x in the day following the storm was computed by averaging the change in ozone in the day following convection in both the lightning and "no-lightning" cases over the averaging box shown in Figure 4.22 and subtracting the "no-lightning average" from the lightning average. On average, the increase in net ozone production due to lightning NO_x was very small, maximizing at only 3 ppbv day^{-1} though individual grid cells showed much a greater increase in production or destruction.

Table 4.5 gives the mixing ratios of a number of species at the beginning of the chemistry-only run (immediately following convection) and 24 hours later at 10 km

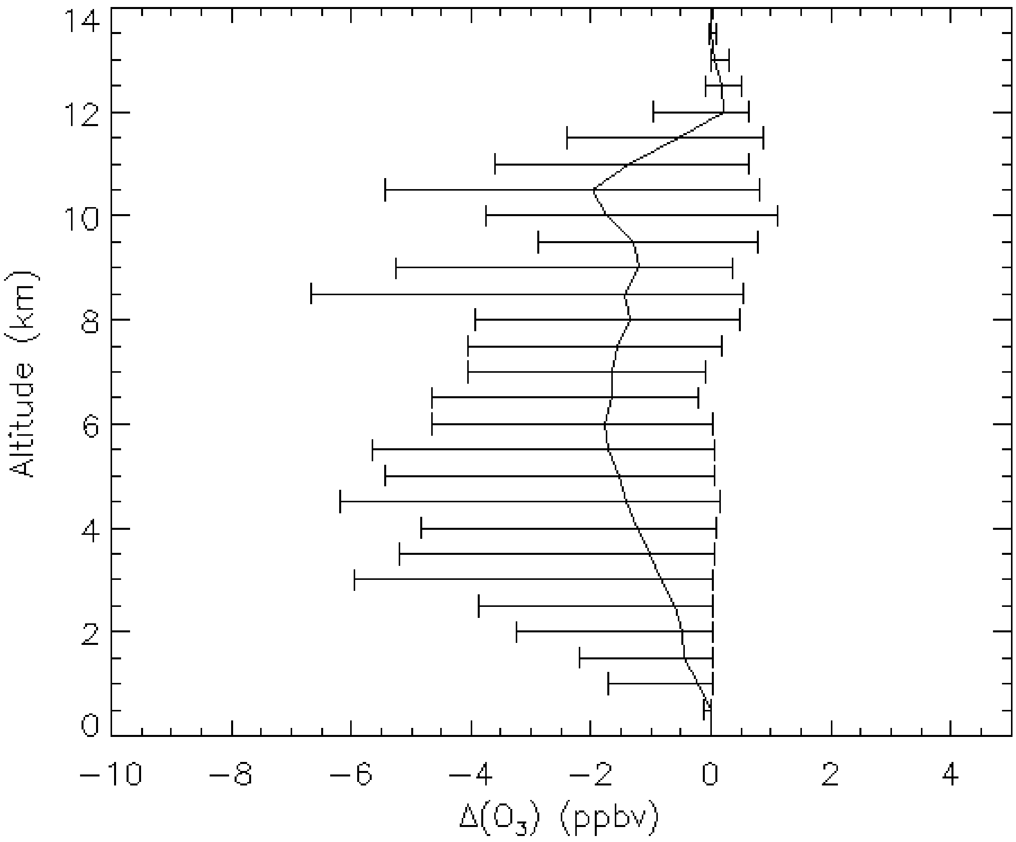

Figure 4.23. Solid line is the average change in ozone mixing ratios due to lightning during the 240-minute storm simulation of the July 29 CRYSTAL-FACE storm. Bars indicate the maximum and minimum ozone change within the averaging box at each level.

averaged over the averaging area shown in Figure 4.22. In the 24 hours following convection, average ozone mixing ratios have increased 11 ppbv mainly due to convective transport of ozone precursors. NO_x mixing ratios have decreased by 3 ppbv, but still remain extremely elevated over background concentrations.

Table 4.5. Average Species Concentrations at 10 km AGL at the Beginning and End of the Chemistry-Only Simulation of the July 29 CRYSTAL-FACE storm

Species	Average Mixing Ratio Immediately Following Convection (ppbv)	Average Mixing Ratio 24 hours after Convection (ppbv)
NO_x	7.95	4.93
O_3	111.0	122.0
HNO_3	0.818	2.32
HCHO	0.416	8.46×10^{-2}
H_2O_2	1.34	0.821
CH_3OOH	0.857	0.418
$CH_3CO_3NO_2$	0.480	0.488
OH	5.71×10^{-4}	1.62×10^{-4}
HO_2	4.44×10^{-4}	1.78×10^{-4}
RO_2	6.88×10^{-5}	2.64×10^{-5}

* Averages are computed over the sampling box shown in Figure 4.22a.

Chapter 5. Discussion and implications for global modeling

In order to adequately represent the lightning NO_x source in global 3-D CTMs, the geographic distribution of flashes, average production of NO per flash, and vertical distribution of lightning NO_x after convection must be specified. Each of these aspects is discussed in this chapter.

5.1 Vertical distributions of lightning NO_x mass

Pickering et al. [1998] presented vertical profiles of lightning NO_x for use in 3-D CTMs based on the results of 2-D cloud-resolving model simulations of seven convective events. These simulations assumed the production scheme of Price et al. [1997] in which a CG flash produces 1100 moles NO and an IC flash is 10% as productive of NO as a CG flash. NO_x produced by CG flashes was distributed in the simulated storms from the surface to the -15°C isotherm while NO_x produced by IC flashes was distributed above -15°C.

Average profiles of lightning NO_x mass computed for the midlatitude continental, tropical continental, and tropical marine regimes in the Pickering et al. [1998] analysis showed peaks in mass near the surface and in the upper troposphere, leading many global CTMs to adopt a C-shaped vertical distribution of lightning NO_x mass. The passive version of the 3-D CSCTM allows IC and CG lightning NO_x to be isolated from pre-existing transported NO_x. I calculated vertical profiles of lightning NO_x mass based on the four case studies presented in Chapters 2-4, the 3-D simulation of the July 12 STERAO storm from DeCaria et al. [2005], and the simulation of a squall line observed during PRE-STORM. These profiles are intended to update the profiles presented in Pickering et al. [1998] for use in regional and global CTMs.

5.1.1 Subtropical events

The July 16 and July 29 storms were the only two subtropical storms simulated. Figure 5.1 shows the percentage of the mass of N in lightning NO_x at each model level for both the July 16 and 29 CRYSTAL-FACE storms. Following the July 29 storm, the maximum in the vertical mass distribution is found at anvil levels (~10 – 10.5 km). In the case of the July 16 storm, the maximum is found in the 6-7 km layer, coincident with the lower mode of the vertical distributions of the lightning NO_x source in the CSCTM.

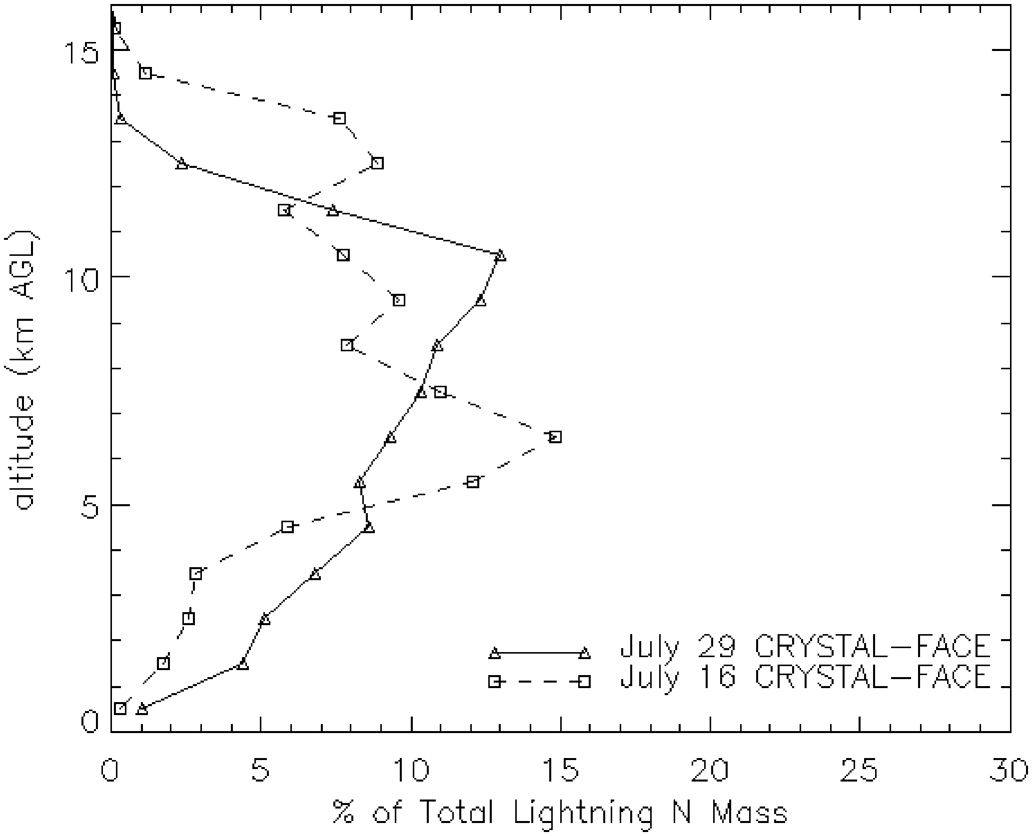

Figure 5.1. Vertical distributions of percentage of lightning NO_x mass following convection for two simulated subtropical storms.

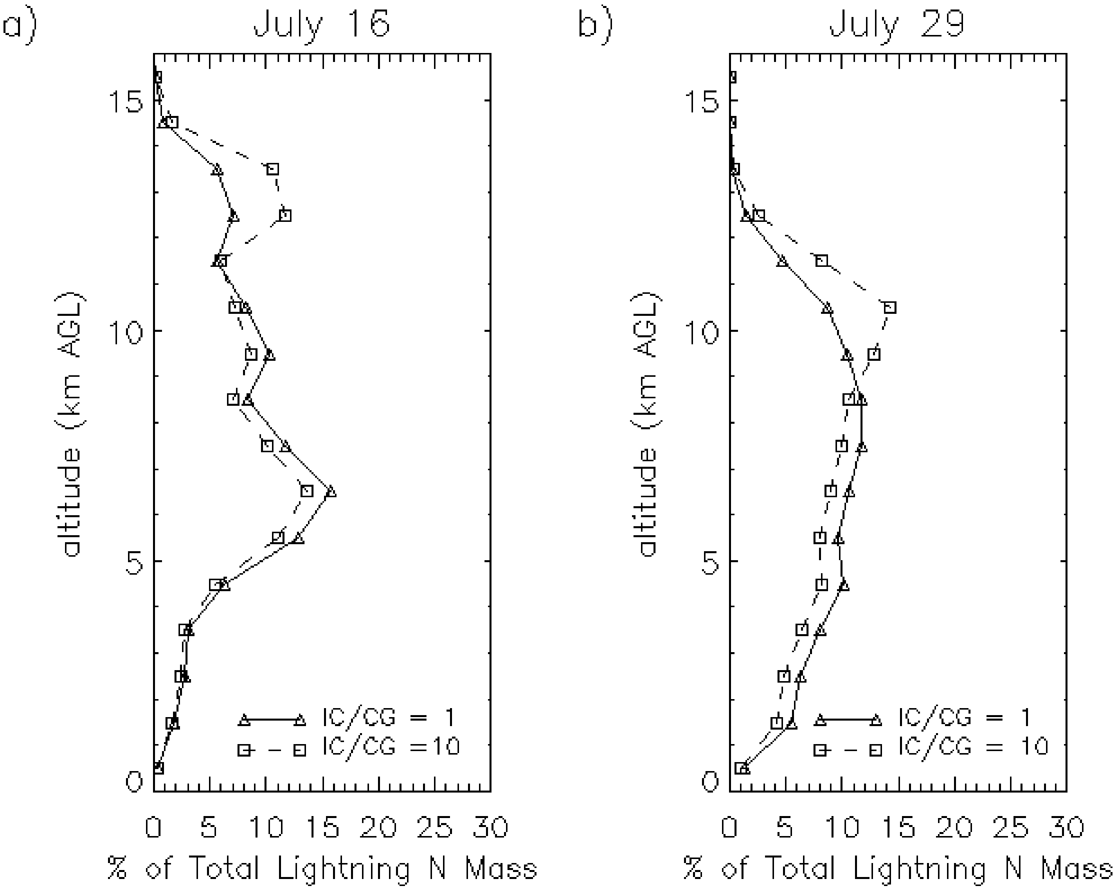

Figure 5.2. Vertical distributions of the percentage of lightning NO_x mass following convection for (a) the July 16 and (b) the July 29 CRYSTAL-FACE simulations assuming IC to CG ratios of 1 and 10.

A smaller peak is found in the 9-10 km layer, the height of the upper mode of the distribution, and another peak at 12-13 km, near the top of the cloud. These vertical lightning NO_x mass distributions were based on the assumed IC to CG ratios of 2 and 5 for the July 16 and 29 storms respectively. Since the IC to CG ratio may be highly variable and was estimated (not known with certainty) for these simulations, the results of a sensitivity test of the assumption of IC to CG ratios of 1 and 10 are shown for the July 16 storm in Figure 5.2a and for the July 29 storm in Figure 5.2b. For both storms, assuming an IC to CG ratio of 1 results in a greater percentage of lightning NO_x mass lower in the cloud, while assuming the higher IC to CG ratio of 10 causes more lightning

NO_x to reside in the uppermost portions of the cloud. However, these differences are substantial only in the 12-14 km altitude range in the July 16 case and in the 10-12 km range for the July 29 storm.

Vertical profiles of NO_2 following convection are also of interest because of the development of satellite instruments (including GOME, SCIAMACHY, OMI) capable of measuring column NO_2 amounts in the troposphere. Mean vertical profiles of NO_2 after convection are shown in Figure 5.3 for the July 16 and 29 CRYSTAL-FACE storms. The profiles were calculated over the 40 by 40 km area positioned in the convective region of the model domain (shown in Figure 4.11 for the July 16 storm and Figure 4.22a for the July 29 storm). The July 29 profile shows extremely elevated NO_2 mixing ratios

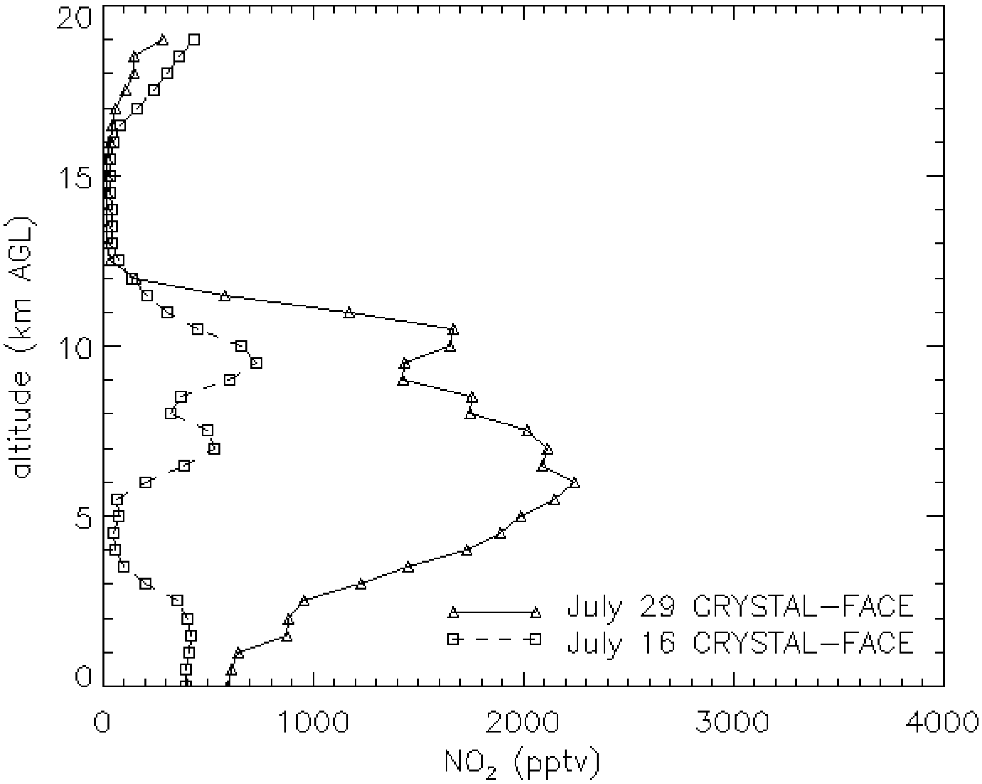

Figure 5.3. Average vertical profile of NO_2 mixing ratio in the convective region following two simulated subtropical storms.

exceeding 2 ppbv from 5 to 7.5 km, while the July 16 profile maximizes at only 0.7 ppbv at 9.5 km. The disparity in profiles is due to the large difference in flash rates in the two storms with over 4000 CG flashes recorded by the NLDN in the July 29 storm, and only 300 CG flashes recorded in the July 16 storm. Very little NO_2 resides above 12 km in these cases, whereas NO enhancements extend to 13.5 km in the July 29 storm and over 14 km in the July 16 storm. Typical NO_2 profiles from the model may prove useful in improving NO_2 retrievals from satellite instruments.

5.1.2 Simulation of the June 10-11 PRE-STORM squall line

The PRE-STORM field campaign was conducted from May to June, 1985 in order to observe the evolution and structure of mesoscale convective systems in the Oklahoma-Kansas region [Rutledge and MacGorman, 1988]. During the project, the occurrence of CG lightning flashes was recorded by the National Severe Storms Laboratory's Lightning Location Network. Storms were observed by satellite and several radar systems. Chemical measurements in the anvils of some storms were made (e.g. Dickerson et al., 1987; Luke et al., 1992; Pickering et al., 1988), although not in the case of the June 10-11 squall line. The lack of chemical observations prevented the same method of estimating lightning NO_x production used in the other four case studies to be applied to this system. However, it was of interest to study the vertical distribution of lightning NO_x in this squall line because its structure was unlike the other storms simulated and also because the vertical distribution of lightning NO_x in this storm was estimated using a 2-D model with a simpler lightning scheme in Pickering et al. [1998].

At approximately 2300 UTC on June 10, a squall line developed in western Kansas as a group of convective cells organized in a roughly northeast to southwest line

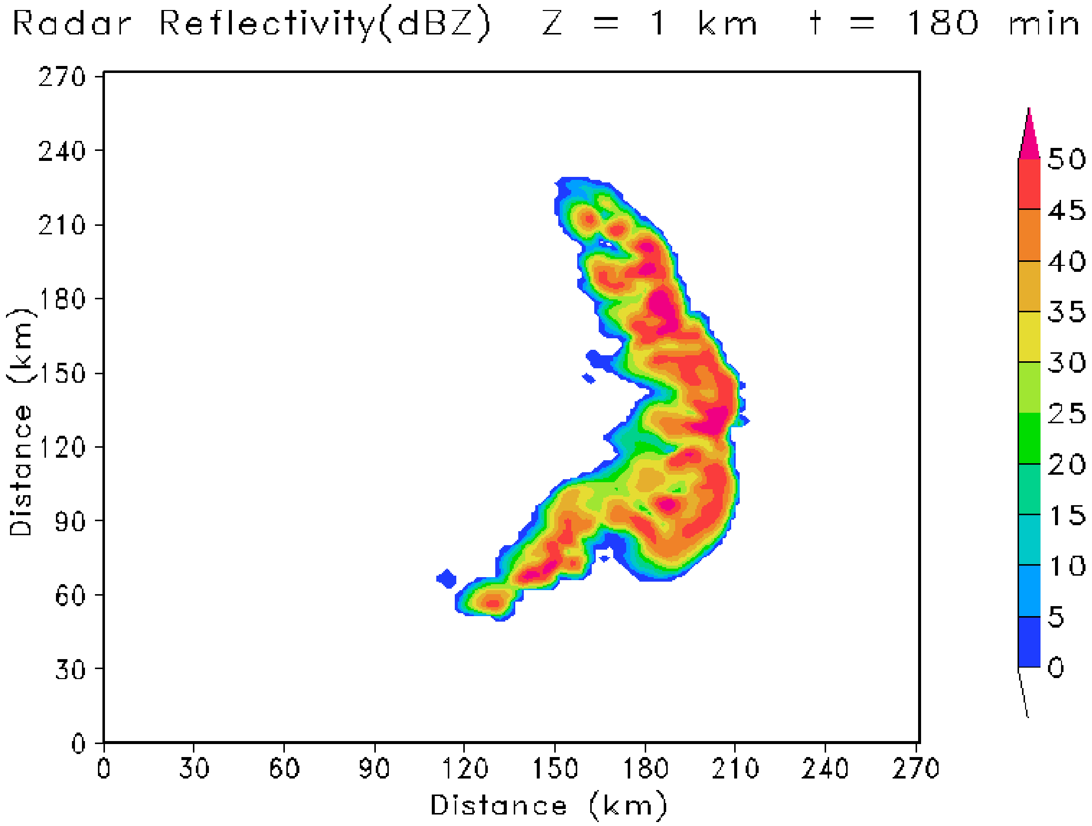

Figure 5.4. Radar reflectivity computed from GCE hydrometeors at 1 km elevation, 180 minutes into the simulation of the June 10-11 PRESTORM squall line.

[Rutledge and MacGorman, 1988]. The June 10-11 squall line has been documented extensively in the literature (e.g. Johnson and Hamilton, 1988) and has previously been simulated using the 2-D version of the GCE [Tao et al., 1993] and with MM5 (Zhang et al., 1989; Wang et al., 1996). A segment of the squall line was simulated more recently by Steve Lang of NASA Goddard Space Flight Center using the 3-D GCE model with a horizontal resolution of 1.5 km and vertical resolution varying from approximately 0.25 km near the surface to slightly more than 1 km near the top of the domain at 21.4 km. The width of the storm compared favorably with radar observations presented in Rutledge and MacGorman [1988]. Figure 5.4 shows a plot of radar reflectivity computed from the GCE simulated hydrometeor fields at 1 km elevation, 180 minutes into the simulation.

Because no chemical observations were available in the storm anvil, the transport of CO, pre-existing NO_x, and O_3 were not calculated. The passive version of the CSCTM was used to simulate lightning NO_x production and the transport of lightning NO_x only. Based on time series of positive and negative CG flash rates from Nielsen et al. [1994], approximately 6500 CG flashes occurred during the storm's lifetime. Observations of total lightning activity were unavailable, so the climatological IC to CG ratio of 3 for the region [Boccippio et al, 2001] was assumed to estimate IC flash rates. The simulated storm was a squall line with a large trailing stratiform precipitation area. Plots of observed radar reflectivity overlaid with the locations of CG flashes typically show flashes occurring over the length of the squall line and extending no more than 100 km in the x-direction. In order to avoid placing lightning NO_x throughout the entire stratiform region and diluting it excessively, the lightning parameterization was modified to restrict lightning NO_x placement to an area of approximately this size. It was not possible to estimate a production scenario for IC and CG flashes as in the other storms presented. Instead, the average value of P_{IC} and P_{CG} was calculated over the five other storms. P_{CG} was estimated to be approximately 500 moles of NO and P_{IC} was estimated to be 85% of P_{CG}, or 425 moles of NO. Figure 5.5 shows the vertical profiles of lightning NO_x mass calculated from the 3-D CSCTM simulation and in the 2-D simulation of the same squall line presented in Pickering et al. [1998]. The 2-D simulation places most lightning NO_x below 1 km and between 9 and 15 km. In contrast, the 3-D simulation distributes lightning NO_x mass fairly evenly between 1 and 10 km, and then drops off in the upper

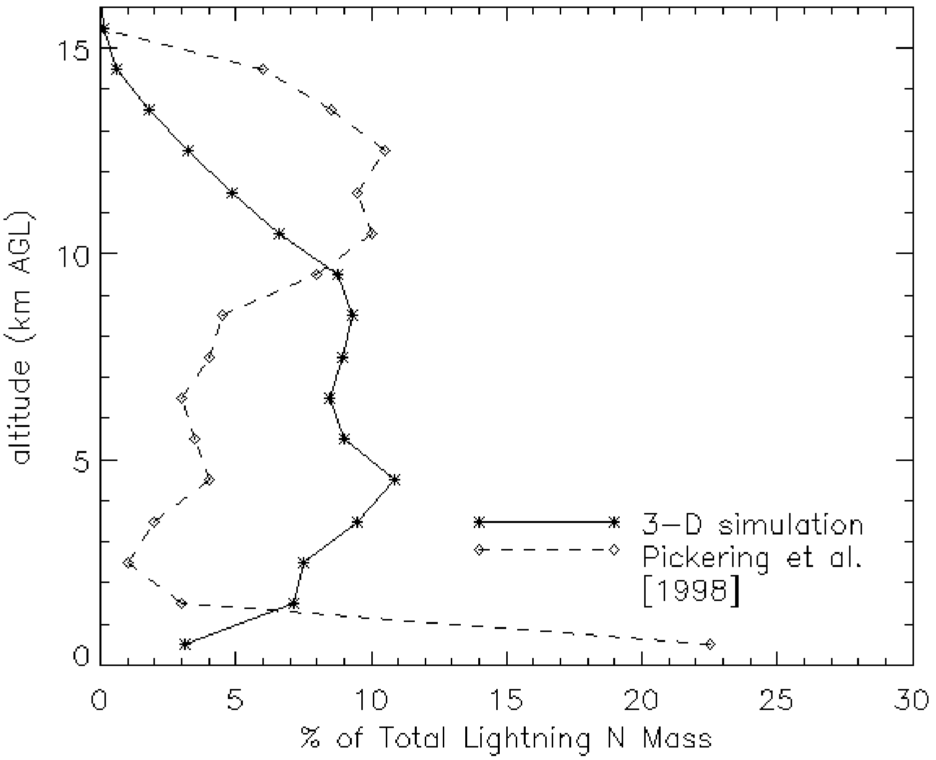

Figure 5.5. Vertical distributions of the percentage of lightning NO_x mass following convection for the 3-D simulation of the June 10-11 PRESTORM squall line and the 2-D Pickering et al. [1998] simulation of the same storm.

troposphere where the secondary maxima in the 2-D profile is found.

5.1.3 Midlatitude continental events

Midlatitude continental events simulated using the 3-D CSCTM include the July 10 STERAO storm, the July 21 EULINOX storm, the June 10-11 PRESTORM squall line, and the July 12 STERAO storm simulated by DeCaria et al. [2005]. Figure 5.6 shows the vertical distribution of the mass of N in lightning NO_x for the four midlatitude continental storms. The distributions for the four storms all reflect the double peaked distribution of lightning NO_x produced by IC flashes in the model. There is variation between the simulations in which mode of the lightning distributions is dominant. In the

EULINOX and PRESTORM storms whose IC to CG ratios were on average 5 and 3, respectively, a higher percentage of lightning NO_x mass is found near the height of the lower mode of the IC distribution which is also the mode of the CG distribution. In the simulations of the July 10 and July 12 STERAO storms, which had average IC to CG ratios of 33 and 8, a greater percentage of lightning NO_x mass resides near the height of the upper mode of the IC vertical distribution following convection. In addition to the IC to CG ratio, the dominance of the modes is likely affected by storm dynamics and the timing of IC and CG flashes in relation to the evolution of the storm.

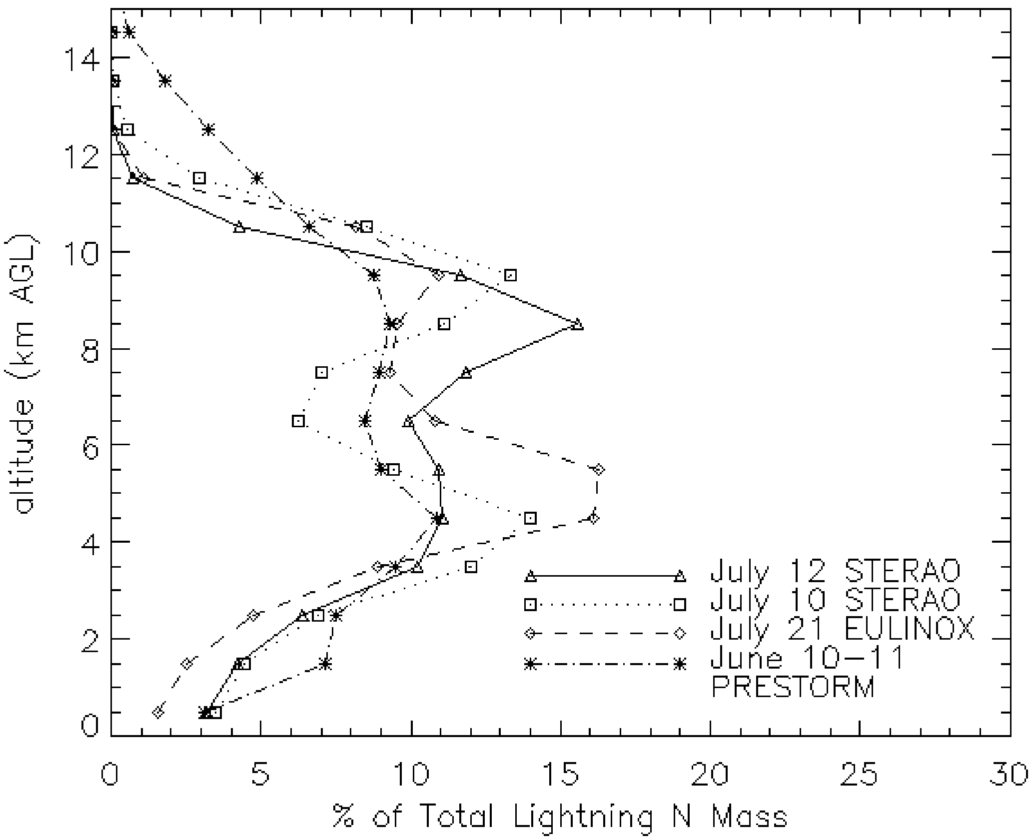

Figure 5.6. Vertical distributions of percentage of lightning NO_x mass following convection for four simulated midlatitude continental storms.

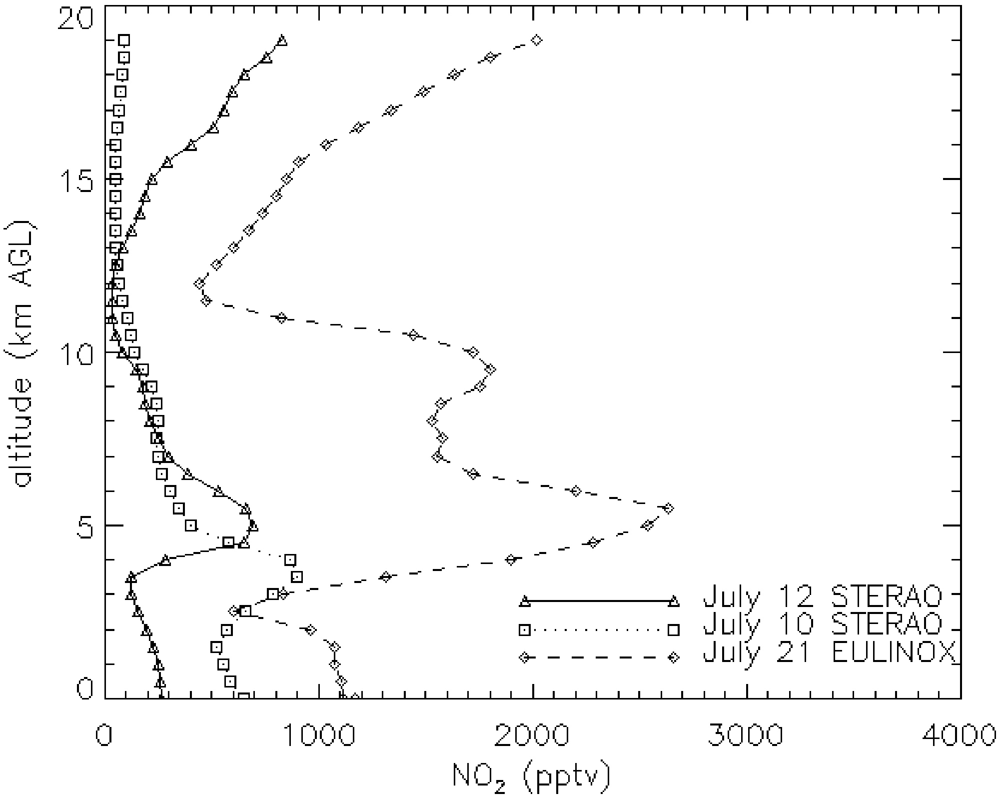

Figure 5.7. Average vertical profile of NO_2 mixing ratio in the convective region following three simulated midlatitude continental storms.

The version of the CSCTM including chemical reactions was used to simulate the two STERAO storms and the July 21 EULINOX storm. The PRESTORM case was not simulated with chemical reactions due to a lack of in-cloud data to estimate a lightning NO_x production scenario. Figure 5.7 shows average vertical profiles of NO_2 calculated over a 40 by 40 km area in the convective region of the model domain following convection (shown in Figure 2.12b for the July 21 EULINOX storm and Figure 3.11 for the July 10 STERAO case). The values in the vertical profile of NO_2 from the EULINOX storm are much larger than in either of the STERAO storms with a maximum of nearly 2.5 ppbv at 5.5 km.

5.1.4 Average vertical profiles of lightning NO_x mass

Figure 5.8a shows the average vertical distribution of the mass of N in lightning NO_x calculated by averaging the case studies in the subtropical regime and Figure 5.8b shows the average vertical distribution for storms in the midlatitude continental regime. Both plots are overlaid with smooth curves fit to the regime average. Table 5.1 lists the percentages of lightning NO_x mass in each 1-km layer taken from the smoothed curves in Figure 5.8. In both regimes on average, only a small percentage of lightning NO_x resides in the boundary layer following the convective event. A greater percentage of lightning NO_x remains in the middle and upper troposphere where the lightning NO_x was originally

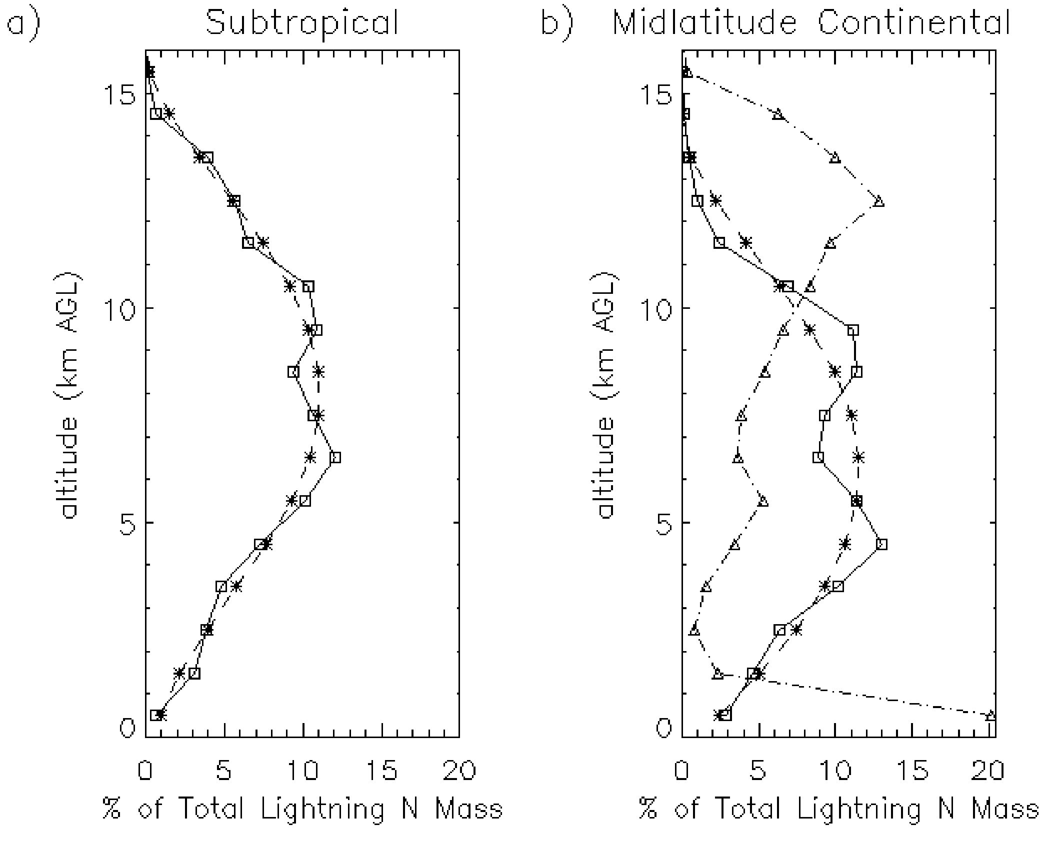

Figure 5.8. Average vertical distribution of percentage of lightning NO_x mass following convection (solid) for the (a) subtropical and (b) midlatitude continental regimes fit with smooth curves (dashed). The Pickering et al. [1998] profile for the midlatitude continental regime (dash-dot) is also shown in (b).

Table 5.1. Average Profiles of Lightning NO_x Mass in Percent

Altitude Range, km	Subtropical	Midlatitude
0-1	1.0	2.4
1-2	2.1	5
2-3	3.9	7.4
3-4	5.8	9.3
4-5	7.7	10.6
5-6	9.3	11.4
6-7	10.5	11.5
7-8	11.0	11
8-9	11.0	9.9
9-10	10.4	8.3
10-11	9.2	6.3
11-12	7.5	4.2
12-13	5.5	2.2
13-14	3.4	0.5
14-15	1.5	0
15-16	0.2	0

produced. These average vertical distributions are in marked contrast to the C-shaped profiles presented in Pickering et al. [1998] based on 2-D cloud-resolving model simulations in which a significant percentage of lightning NO_x mass was transported to the boundary layer and relatively little lightning NO_x mass was found between 1.5 and 6.5 km after convection concluded.

Assuming the density profile of the standard atmosphere, the total mass of lightning NO_x averaged over the EULINOX and STERAO storms, and that NO_x is distributed uniformly over a 400 km^2 region (typical of a global model grid cell), the average midlatitude profile shown in Table 5.1 corresponds to a maximum increase in NO_x mixing ratios of ~ 185 pptv between 7 and 9 km immediately following convection (~2 km higher than the maximum of the lightning NO_x mass distribution). Because the lifetime of NO_x increases with altitude, lightning NO_x will be converted to reservoir species such as PAN and HNO_3 more rapidly in the 7-9 km layer than at higher altitudes.

As the time after convection increases, the maximum increase in NO_x mixing ratios due to lightning would be seen at higher altitudes which is consistent with the C-shaped profile of NO_x typically observed in the troposphere. Downward transport from the stratosphere also contributes to the upper tropospheric maximum in observed NO_x mixing ratios, while the maximum near the surface results from emissions from surface sources such as fossil fuel combustion and soil.

5.2 Global lightning NO_x production

Chapters 2 through 4 presented results of the simulations of four thunderstorms using the 3-D CSCTM. Best-fit production scenarios of P_{IC} and P_{CG} were estimated by comparing in-cloud aircraft observations with model output for these storms. This method was also used by DeCaria et al. [2005] to estimate production per IC flash and per CG flash in the July 12 STERAO storm. Figure 5.9 shows the production scenarios estimated for these five storms, the production scenario from Price et al. [1997] which was used in calculating the vertical profiles of lightning NO_x mass presented in Pickering et al. [1998], and the production scenario estimated for the July 21 EULINOX storm by Fehr et al. [2004]. In all storms simulated, P_{CG} was estimated to be less than the 1100 moles per CG flash given in Price et al. [1997]. In addition, the ratio of P_{IC} to P_{CG} was greater than the commonly assumed value of 0.1 presented by Price et al. [1997]. Over the five storms simulated by the CSCTM, the average estimated P_{CG} was 500 moles NO and the average P_{IC}/P_{CG} was 0.85 (assuming a P_{IC}/P_{CG} ratio of 1 for the July 12 STERAO storm and 0.6 for the July 29 CRYSTAL-FACE storm).

Production of approximately 500 moles NO per flash has been verified by the recent modeling studies of Cooper et al. [2006] and Hudman et al. [2006]. Cooper et al.

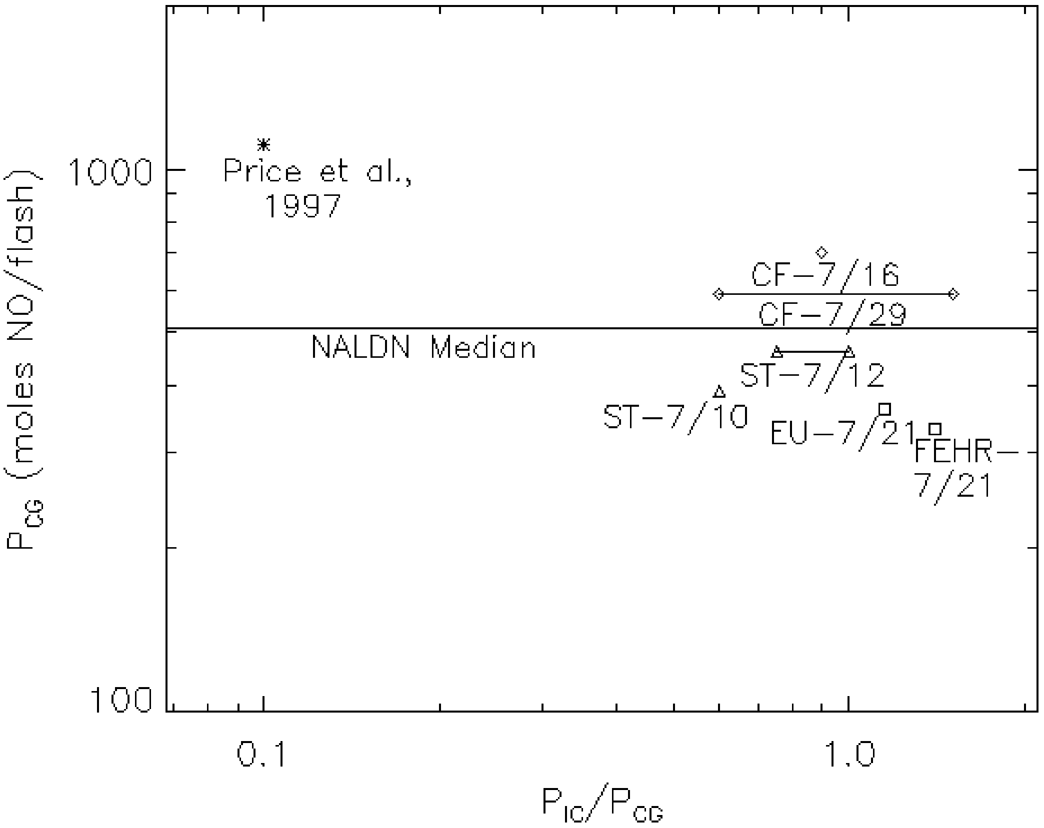

Figure 5.9. Estimated lightning NO_x production scenarios for the July 16 CRYSTAL-FACE (CF-7/16), July 29 CRYSTAL-FACE (CF-7/29), July 10 STERAO (ST-7/10), July 12 STERAO (ST-7/12), and July 21 EULINOX (EU-7/21) storms. The Price et al., [1997] and Fehr et al. [2004] (FEHR-7/21) production scenarios are also shown, as is the estimated value of P_{CG} calculated assuming the NALDN median peak current from Orville et al. [2002].

[2006] assumed the DeCaria et al. [2005] lightning NO_x production scenario (P_{IC}=P_{CG}=460 moles NO) in their simulation of the global transport and dispersion of North American NO_x emissions using the FLEXPART Lagrangian particle dispersion model. Simulated NO_x values were compared with NO_x observed by aircraft over the continental U.S. during the ICARTT (International Consortium for Atmospheric Research on Transport and Transformation) study conducted in July and August of 2004. The assumption of the DeCaria et al. [2005] lightning production scenario yielded good agreement with aircraft observations [Cooper et al., 2006]. Hudman et al. [2006] compared ICARTT observations with output from the 3-D global GEOS-Chem CTM to constrain NO_y sources from North America. Simulated flash rates calculated using the Price and Rind [1992] parameterization compared favorably with NLDN observations, yet upper tropospheric NO_x observations were underestimated by the model. Adjusting the production per flash from the initial value of 125 to 500 moles NO per flash was necessary to obtain a good agreement with aircraft observations during ICARTT.

The median peak current (16.5 kA for negative flashes and 19.8 kA for positive flashes which account for 10.9% of the total) of the North American Lightning Detection Network (NALDN) presented in Orville et al. [2002] corresponds to a P_{CG} value of 508 moles NO when using the Price et al. [1997] relationship between peak current and energy dissipated which agrees well with the estimate of 500 moles NO per CG flash calculated over the five storms simulated using the CSCTM. Therefore, the cases simulated appear to be representative of midlatitude and subtropical storms. Assuming the average production scenario over these five storms (500 moles NO per CG flash and P_{IC}/P_{CG}=0.85), an average global IC to CG ratio of 3 (extrapolating the Boccippio et al. [2001] result for the U.S. to the globe) and a global flash rate of 44 flashes s^{-1} [Christian et al., 2003] yields a global lightning NO source of 8.6 Tg N yr^{-1}.

Estimates of the global lightning NO source range from 2-20 Tg N yr^{-1} [IPCC, 2001], though most recent studies are confined to the lower half of this range. Levy et al. [1996] estimated global lightning NO_x production between 2 and 6 Tg N yr^{-1} with a most likely range of 3 to 5 Tg N yr^{-1} by comparing global CTM simulations and NO_x and NO_y

observations. Lee et al. [1997] estimated a global lightning NO_x source of 5 Tg N yr^{-1} which is assumed in many global CTMs [Zhang et al. 2003]. A number of other studies have attempted to estimate global lightning NO_x production based on NO_x observations. Huntrieser et al. [1998] used aircraft NO measurements taken in thunderstorm anvils over Europe during the LINOX (lightning-produced NO_x) project to estimate average lightning NO_x production per thunderstorm, and extrapolated to the global scale to yield an estimate of 4 Tg N yr^{-1}. A similar approach using measurements obtained during EULINOX led to an estimate of 3 Tg N yr^{-1} [Huntreiser et al., 2002]. Beirle et al. [2005] used tropospheric column NO_2 measurements from the GOME instrument and NLDN data for a storm observed in the Gulf of Mexico to estimate production per flash and extrapolated to a global lightning NO_x source of 1.7 Tg N yr^{-1}. All of these estimates are less than the estimate presented in this work of 8.6 Tg N yr^{-1}. This may be due to the fact that each of these observational studies relied upon thunderstorms observed in a relatively small region occurring close together in time which may be less representative of a typical thunderstorm than the sample of storms I have used in this analysis. Estimating global lightning NO_x production based on storms observed in a number of different locations is likely better suited to extrapolating to a global source. Because of satellite observations of total lightning activity from instruments such as the Optical Transient Detector (OTD; Christian et al., 2003), uncertainty in the global flashrate (44 ± 5) has been greatly reduced while the number of thunderstorms occurring globally remains uncertain.

In this analysis, the average production scenario was calculated using data from midlatitude continental and subtropical storms observed in large field campaigns. No tropical storms were simulated because of a lack of data from any comparable field project in the tropics. Because 78% of lightning flashes occur in the tropics between 30°S and 30°N [Christian et al., 2003], further investigation of the properties of tropical lightning flashes and their production of NO is needed. If lightning flashes occurring in the tropics on average have weaker peak current than flashes occurring in the subtropics and midlatitudes, the estimate of the global source strength of lightning NO_x production would likely decrease. Data are just now becoming available from tropical field projects such as TROCCINOX (Tropical Convection, Cirrus and Nitrogen Oxides Experiment) in Brazil and SCOUT-O3/ACTIVE (Stratospheric-Climate Links with Emphasis on the Upper Troposphere and Lower Stratosphere/Aerosol and chemical transport in tropical convection) in Australia.

5.3 Lightning NO_x production per unit flash length

In addition to estimating NO_x production per lightning flash, I modified the lightning NO_x scheme to allow production per meter flash channel length to be estimated in the July 21 EULINOX and the July 10 STERAO storms. The estimated production for the July 21 EULINOX storm was 1.42 x 10^{-2} moles NO per meter flash channel length while the estimate for the July 10 STERAO storm was 2.1 x 10^{-2} moles NO per meter flash length, both of which compare favorably with other estimates of NO production per meter available in the literature. The July 21 EULINOX storm estimate is within the range of 3.3 x 10^{-4} and 1.7 x 10^{-2} moles NO per meter flash channel length from Stith et al. [1999] based on the July 10 STERAO storm. Estimates for both storms are significantly larger than the value of 1.7 x 10^{-3} moles NO per meter flash channel length estimated by Skamarock et al. [2003] which included a number of short duration interferometer flashes not included in the simulation of the July 10 STERAO case presented in Chapter 3 and other studies of STERAO storms (e.g. DeCaria et al, 2005). These estimates are also larger than the estimate of 4.5 x 10^{-3} moles NO per meter flash length obtained by Huntrieser et al. [2002] for the EULINOX field project.

5.4 Global flash rate parameterizations

In addition to the average production per flash and the vertical profile of lightning NO_x following convection, the locations of lightning flashes must also be specified in global models. Satellite-based instruments which monitor total lightning activity, including the OTD and Lightning Imaging Sensor (LIS), provide information on the global distribution of lightning and have allowed global lightning climatology to be studied (e.g. Christian et al., 2003). However, gridded average flash frequencies are not suitable for use in global CTMs which must parameterize convective transport because satellite-observed lightning is not necessarily collocated in space and time with the representation of convection in the model. Ozone production is highly variable and depends on the presence of ozone precursors such as NO_x and NMHCs. In order for a global CTM to produce an accurate representation of ozone mixing ratios following convection, lightning produced NO_x must be placed in the same locations in the model domain as convectively transported ozone precursors [Allen and Pickering, 2002].

A number of methods have been developed in order to parameterize lightning flash rates in global CTMs. Price and Rind [1992] developed separate parameterizations for marine and continental locations which scaled flash rates to the fifth power of convective cloud top heights. Allen and Pickering [2002] evaluated the cloud top height parameterization of Price and Rind [1992], as well as parameterizations based on convective precipitation and upward convective mass flux by comparing simulated and observed distributions of flash rates. Their results showed that of the three parameterizations, the parameterization based on convective mass flux compared best at most locations, though it resulted in an overestimation of flash rates in the equatorial western Pacific and an underestimation of flash rates in parts of Africa. The cloud top height method of Price and Rind [1992] was unable to adequately reproduce the variability of observed flash rates which would likely result in the overestimation of the amount of ozone produced by lightning NO_x [Allen and Pickering, 2002].

Ridley et al. [2004] evaluated the relationship between cloud top height and flash rates in the July 16 and 29 CRYSTAL-FACE storms. The results indicated that flash rates in these storms did not scale to the fifth power of cloud top height as previous studies had indicated for continental thunderstorms [e.g. Ushio et al., 2001] and as the Price and Rind [1992] method of parameterizing flash rates assumes. In fact, the maximum cloud top height of 15.2 km was greater in the July 16 storm, which was a relatively weak lightning producer, than in the July 29 storm which produced over 4000 CG flashes but reached only 13.8 km. In addition, Ridley et al. [2004] noted that the cloud top heights observed during CRYSTAL-FACE were within the narrow range of ~14-15 km, yet CG flashes observed per storm ranged from a few hundred to thousands. The cloud top height method of Price and Rind [1992] is unable to reproduce this observed variability as was previously noted by Allen and Pickering [2002].

A relationship between lightning flash rates and various ice parameters is thought to exist because of the mechanism believed to be responsible for producing charge separation in thunderstorms [e.g. Baker et al., 1999; Blyth et al., 2001; Petersen and

Rutledge, 2001]. When precipitation sized ice particles collide with smaller ice crystals in the mixed phase region of a cloud, positive charge is transferred to the smaller ice crystals. The smaller, lighter, ice crystals are carried upwards, creating a positive charge region in the upper part of the cloud, while the heavier, precipitation sized particles travel downwards, establishing a negative charge region near the cloud base. These processes eventually result in electric fields sufficient in strength to initiate lightning. A recent study by Petersen et al. [2005] noted a relationship between precipitation ice mass and lightning flash density based on an analysis of Tropical Rainfall Measurement Mission (TRMM) lightning and radar observations. Their results indicate that this relationship is invariant between land, ocean, and coastal regimes on a global scale. These findings suggest that the possibility of parameterizing flash rates in global CTMs using ice mass be examined. The Petersen et al. [2005] study focused on the relationship between precipitation ice mass and lightning. However, cloud microphysics in most general circulation models (GCMs) is rather primitive. Several GCMs have recently developed more advanced microphysics but precipitation ice mass may still not be a common product of the convective parameterizations in these GCMs. Total ice mass, which includes both precipitation ice and cloud ice, may be a more common output field. The relationships between precipitation ice mass and lightning, and total and precipitation ice mass have been examined in the July 10 and 12 STERAO, July 16 and 29 CRYSTAL-FACE, and July 21 EULINOX storms.

In each storm, the total mass of precipitation-sized ice hydrometeors (hail/graupel and snow) was calculated throughout the model domain at each output time step, as was the total ice mass. The average flash density per storm was estimated by calculating the total number of IC and CG flashes associated with each storm and dividing by the size of the model domain. Figure 5.10 shows the relationship between the precipitation ice mass, averaged over the lifetime of the storm, and flash density in each of the five storms. The results suggest a near linear relationship in four of the five storms. The July 21 EULINOX storm appears to have a higher ratio of precipitation ice mass to flash density than the CRYSTAL-FACE and STERAO storms. The relationship is uncertain, however, due to the lack of storms with moderate flash rates and precipitation ice content. Figure 5.11 shows the relationship between precipitation and total ice mass, both averaged over the lifetime of the storm. Over all five storms, the relationship between total and precipitation sized ice mass appears to be linear. These results suggest the possibility that

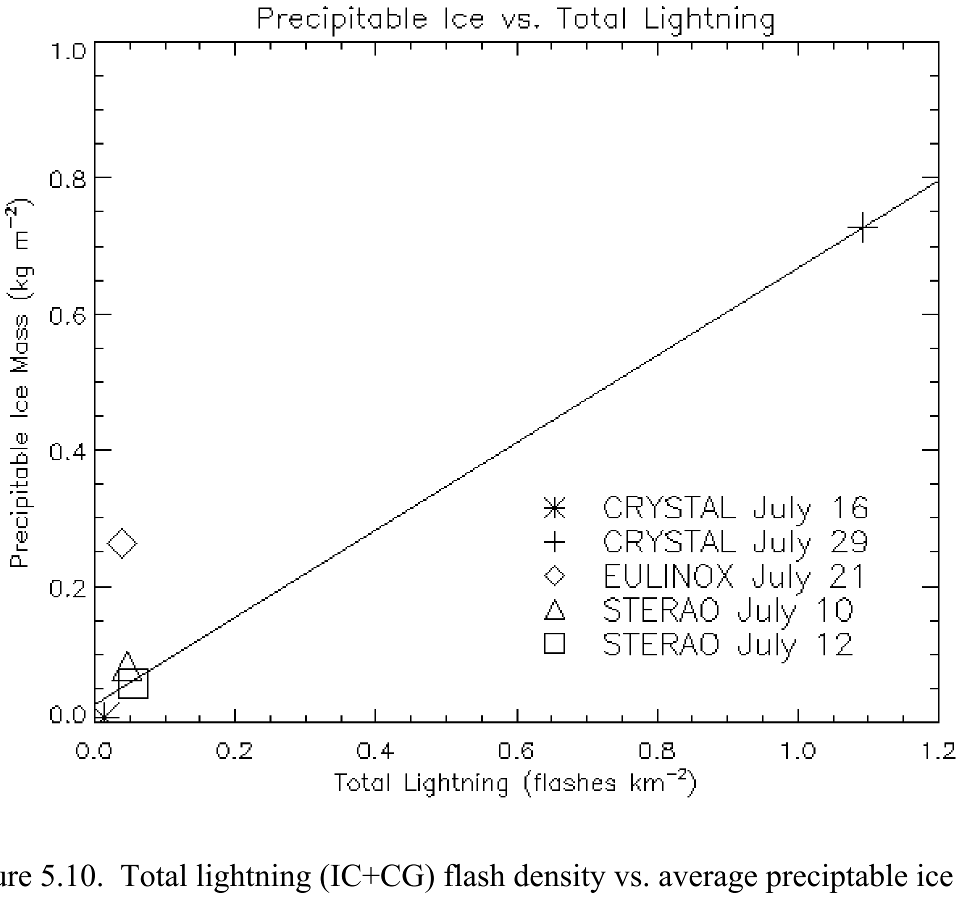

Figure 5.10. Total lightning (IC+CG) flash density vs. average preciptable ice mass for five simulated storms. Best-fit line through the CRYSTAL and STERAO storms is also shown.

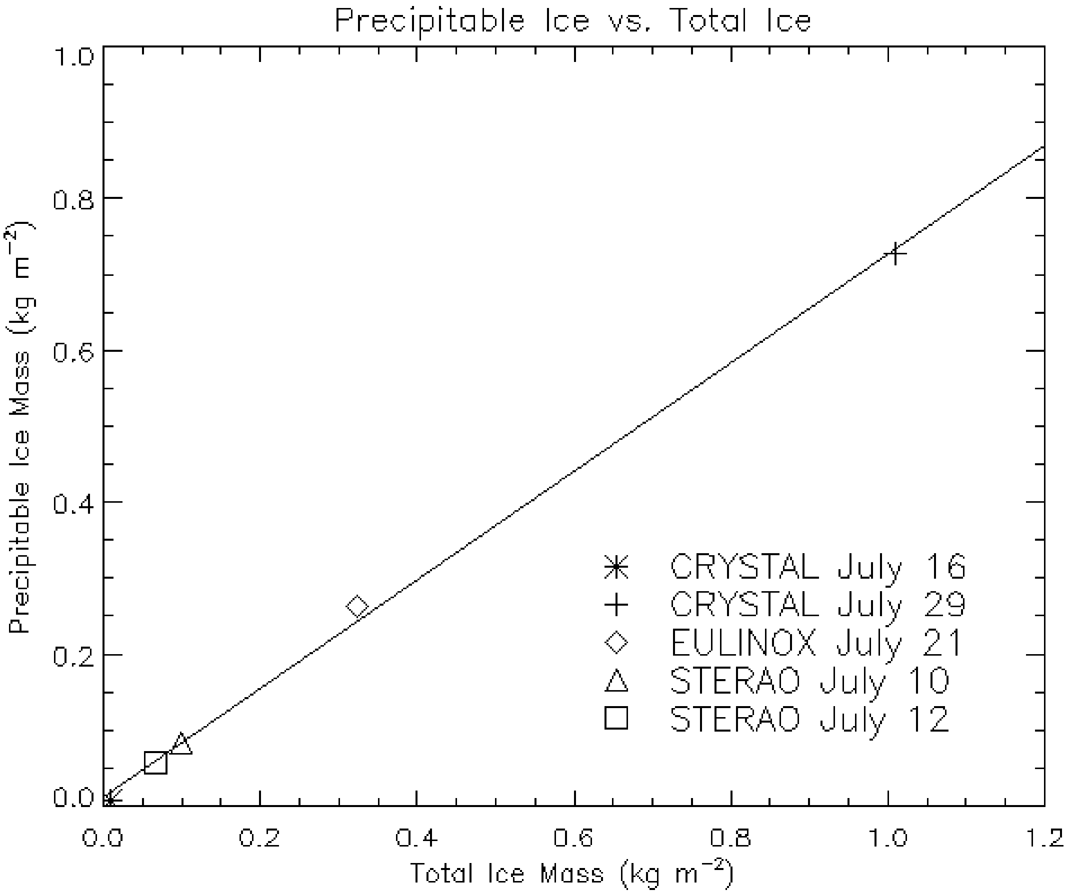

Figure 5.11. Average preciptable ice mass vs. average total ice mass for five simulated storms. Best-fit line is also shown.

parameterizations may be developed for global CTMs which use total ice mass to predict lightning flash density and flash rates. However, much more research is needed to determine the robustness of the potential relationship between total and precipitation ice mass, especially in tropical thunderstorms.

5.5 Ozone production due to lightning NO$_x$

The effect of lightning NO$_x$ on ozone during and following convection was also investigated. Table 5.2 gives the mean NO$_x$ at the end of convection, the change in O$_3$ due to lightning during the lifetime of the storm, the 24-hour change in O$_3$, and the 24-

Table 5.2. Mean NO_x and Ozone Production at 10 km AGL

Storm	Average NO_x immediately following convection (ppbv)	Average change in O_3 during the storm due to lightning (ppbv)	Average O_3 production in the 24-hours following convection (ppbv day^{-1})	Change in O_3 production due to lightning in the 24-hours following convection (ppbv day^{-1})
July 21 EULINOX	3.51	-1.6	10.3	0.6
July 10 STERAO	1.01	2.5×10^{-2}	8.5	2.8
July 16 CRYSTAL-FACE	1.72	0.8	2.1	2.8
July 29 CRYSTAL-FACE	7.95	-1.8	11.0	-2.3

* Averages calculated over the boxes shown in Figures 2.12b, 3.11, 4.11, and 4.22a.

hour change in O_3 due to lightning NO_x for the four case studies presented in Chapters 2-4 at 10 km AGL. During the July 21 EULINOX and July 29 CRYSTAL-FACE storms which contained the greatest NO_x mixing ratios, a decrease in ozone of less than 2 ppbv occurred during the lifetime of the storm due to lightning NO_x injection. During the July 16 CRYSTAL-FACE storm, lightning NO_x increased ozone mixing ratios by 0.8 ppbv, while during the July 10 STERAO storm, lightning NO_x caused a negligible change in ozone mixing ratios.

In all cases, net ozone production occurred in the convective plume at 10 km in the 24 hours following convection due to the redistribution of ozone precursors. In the July 10 STERAO and July 16 CRYSTAL-FACE cases, lightning NO_x increased net ozone production in the day following the storm by nearly 3ppbv day^{-1}. In contrast, lightning NO_x caused a decrease in ozone production in the day following convection at

10 km in the July 29 CRYSTAL-FACE storm and only a small increase in production in the July 21 EULINOX storms. These results suggest that highly electrified storms which produce extremely elevated NO_x mixing ratios may reduce O_3 production in the convective plume. Dilution of these convective plumes as they are advected farther downwind will result in a transition to increased O_3 production. It appears that net O_3 production over the first 24 hours in outflow from storms with large flash rates may be less than in the outflow from moderate flash rate storms. If a period longer than 24 hours were studied using a larger scale model, large flash rate storms may produce more ozone than moderate flash rate storms.

5.6 Simulated transport characteristics

Output from three different cloud resolving models has been used to drive offline CSCTM simulations of four thunderstorms. GCE model output was used to drive simulations of convective transport in both the July 21 EULINOX and July 10 STERAO storms. In the EULINOX storm, model output was compared with in-cloud aircraft observations taken in the core region of the storm from 8 to 9 km. Simulated distributions of in-cloud CO_2 mixing ratios compared well with observations, though the maximum values of CO_2 were overestimated by the model, indicating that upward motion in the GCE simulation may have been slightly larger than in the observed storm. A comparison of the distributions of simulated and observed O_3 showed that the maximum observed values of O_3 at 8 and 9 km were not reproduced by the model, suggesting that downward motion in the GCE simulation may have been weaker than observed. The underestimation of downward transport suggested by an analysis of the O_3

pdfs was inconsistent with the analysis of the CO_2 pdfs which may have been due to a lack of observations in the tropopause region to define initial condition profiles.

In the July 10 STERAO storm, anvil aircraft observations were available between 8 and 12.5 km. The CSCTM simulation, driven by GCE model output was able to reproduce the distribution of observed CO mixing ratios in the anvil fairly well from 11 to 11.5 km. Below 11 km, the model underestimated the distribution of observed CO mixing ratios, while above 11.5 km, the model overestimated CO. These results suggest that the GCE simulation may contain excessive upward motion which resulted in too much CO being transported above 11.5 km, while either too little CO remained at levels below 11 km, or too little CO was detrained into the storm's anvil region. An analysis of simulated and observed O_3 distributions showed an underestimation of O_3 mixing ratios, indicating inadequate downward motion in the simulation of the storm.

The ARPS model was used to simulate the July 16 CRYSTAL-FACE storm and the output used to drive the CSCTM. Data were assimilated into the model hourly which caused periodic changes in the horizontal and vertical extent of the storm. Aircraft observations taken in the storm anvil from 11.5 to 14 km were compared with simulated CO and O_3 mixing ratios at the same altitudes. Below 13.5 km, the simulation overestimated CO mixing ratios, indicating excessively strong upward motion. At 13.5 km and above, observed CO mixing ratios were underestimated by the model. Observed O_3 mixing ratios were reproduced fairly well by the simulation at all levels, though the maximum O_3 mixing ratios were overestimated below 13.5 km. The comparison of simulated and observed CO and O_3 mixing ratios suggests that the ARPS simulated storm may contain upward and downward motion greater than observed. The periodic decrease in simulated cloud top height (below the observed height of 14 km) results in too little CO being transported to 13.5 km and above.

The MM5 was used to simulated the July 29 CRYSTAL-FACE storm. Aircraft observations were made in the storm anvil from 12.5 to 13 km. At these levels, a comparison of the distributions of observed and simulated CO and O_3 mixing ratios showed that the model significantly overestimated observations of both species. These results indicate that both upward and downward motion in the MM5 simulation of the storm may have been larger than in the observed storm.

Generally, the two storms simulated by the GCE model evidenced the most reasonable transport of tracer species. In both cases, downward motion was most likely slightly underestimated, while upward motion was slightly overestimated. The ARPS simulated cloud top height in the July 16 CRYSTAL-FACE storm varied periodically, increasing above the observed height of 14 km immediately following the assimilation of data, and then decreasing below 14 km. This resulted in inadequate upward transport above 13.5 km, while below this level, both upward and downward transport were too strong. The MM5 simulation overestimated both upward and downward motion which caused simulated CO and O_3 mixing ratios in the upper levels of the storm in excess of observations.

Chapter 6. Summary

Four storms observed during three different field projects in the midlatitudes and subtropics have been simulated using the 3-D CSCTM which includes a source of lightning NO_x. An analysis of the mean peak current in these storms indicated that the average over all storms was nearly equivalent to the median peak current of flashes observed over North America, indicating that these storms comprise a sample representative of midlatitude and subtropical convection which may be used to examine characteristics of lightning NO production. Lightning NO_x production per flash was estimated in each storm by specifying different values of P_{IC} and P_{CG} and comparing the results with in-cloud aircraft observations of NO_x. In all four cases, IC flashes were estimated to produce, on average, 60-115% as much NO as CG flashes. This finding contradicts the assumption of Price et al. [1997] that IC flashes are only 10% as efficient as CG flashes at producing NO because IC flashes are less energetic than CG flashes. A recent study by Zhang et al. [2003] suggested that an IC flash typically is 50-100% as energetic as a CG flash which agrees favorably with the estimates of P_{IC} presented in these cases. IC flashes may produce less NO per meter flash channel length than CG flashes because IC flashes typically occur in lower pressure levels of the atmosphere. If average IC flash lengths are longer than CG flash lengths, then production per flash may be roughly equivalent.

Average values of P_{CG} and P_{IC} (500 and 425 moles NO per flash, respectively) have been computed over the four storms presented here, and the July 12 STERAO storm simulated by DeCaria et al. [2005]. Along with an assumed global flash rate and IC/CG ratio, this scenario has been used to estimate a global annual lightning NO_x source of 8.6 Tg N yr^{-1}. In addition, the results from six simulations have been used to calculate the average vertical profiles of lightning NO_x following convection for the subtropical and midlatitude continental regimes. In contrast to profiles of lightning NO_x mass computed using 2-D cloud-scale simulations and presented in Pickering et al. [1998], vertical profiles based on these 3-D simulations show the majority of lightning NO_x remains in the mid to upper troposphere near the altitudes where it originated. The Pickering et al. [1998] profiles place most NO_x in the upper troposphere and near the surface. Global and regional CTMs which have adopted C-shaped vertical profiles of lightning NO_x mass may be underestimating the amount of lightning NO_x in the mid- troposphere and overestimating the amount near the surface. Changes in the vertical placement of lightning NO_x in CTMs may significantly alter distributions of species such as O_3 and OH, although future modeling studies are needed to determine the magnitude of these changes.

Output from three different cloud-resolving models was used to drive the offline CSCTM. The 3-D GCE model output provided the most realistic transport of tracer species in the July 21 EULINOX and July 10 STERAO storms. The use of data assimilation in the ARPS model resulted in a varying cloud top height which negatively impacted both the transport of species to the upper levels of the storm and the distribution of lightning NO_x in the CSCTM. Using MM5 output to drive the CSCTM resulted in significant overrepresentation of both upward and downward transport in the model.

The CSCTM simulations of these four storms were also used to investigate the impact of lightning NO_x on O_3. In storms with the highest flash rates, lightning NO_x

results in decreased ozone production in the 24 hours following convection, while in storms with more moderate flash rates, lightning NO_x increases ozone production in the 24 hours following convection in the convective plume. Once the convective plume is diluted, lightning NO_x will likely result in increased ozone production in the outflow from storms with large flash rates. It is possible that storms with large flash rates may produce more ozone than storms with moderate flash rates when production over multiple days is considered.

The estimate of the annual global lightning NO_x source strength and the average vertical profiles of lightning NO_x mass in midlatitude continental and subtropical regimes following convection can be used to improve the parameterizations of lightning NO_x production currently employed in global CTMs. In addition, the parameterization of flash rates based on total ice mass calculated by convective parameterizations in GCMs may be possible in the future, though a much more thorough analysis is required. More studies of the relationship between ice content and flash rate are needed, particularly in tropical thunderstorms, to determine if a robust relationship between these parameters exists. In addition, observational and modeling studies of the dynamical evolution, convective transport, and lightning NO_x production in tropical storms are needed. Estimates of NO production per flash in tropical storms will reduce uncertainty in the global lightning NO_x source and, in turn, improve the representation of lightning NO_x in global models. Because the majority of lightning flashes occur in the tropics, it is imperative to determine if these flashes are significantly different than midlatitude and subtropical flashes in terms of the energy dissipated and NO production. If so, adjustments to the estimate of global source strength will be required.

Appendix A. Additional Chemical Reactions included in the CSCTM
(original reaction scheme listed in DeCaria, 2000)

R1 $H_2COO + NO \rightarrow HCHO + NO_2$

R2 $H_2COO + H_2O \rightarrow HCOOH + H_2O$

R3 $C_3H_6 + OH \rightarrow HOC_3H_6O_2$

R4 $HOC_3H_6O_2 + NO \rightarrow NO_2 + CH_3CHO + HCHO + HO_2$

R5 $C_3H_6 + O_3 \rightarrow 0.5HCHO + 0.075CH_3HCOO + 0.425CH_3HCOOX$

R6 $ISOP + OH \rightarrow ISOH$

R7 $ISOP + O_3 \rightarrow 0.67MACR + 0.26MVK + 0.3OH + 0.07PAR + 0.07OLE$

$0.07H_2COO + 0.8HCHO + 0.06HO_2 + 0.15CO_2 + 0.05CO$

R8 $ISOP + O(^3P) \rightarrow 0.22MACR + 0.63MVK + 0.08ISOH$

R9 $ISOP + NO_3 \rightarrow ISNT$

R10 $ISOH + NO \rightarrow 0.364MACR + 0.477MVK + 0.84HCHO + 0.08ISNI1 +$

$0.08ISNI2 + 0.886HO_2 + 0.84NO_2$

R11 $ISNT + NO \rightarrow 1.1NO_2 + 0.8HO_2 + 0.8ISNI1 + 0.1MACR + 0.15HCHO +$

$0.05MVK + 0.05DISN$

R12 $ISNI1 + OH \rightarrow ISNIR$

R13 $ISNIR + NO \rightarrow 0.05DISN + 0.05HO_2 + 1.9HO_2 + 0.95CH_3CHO +$

$0.95*CH_3COCH_3$

R14 $ISNI1 + O_3 \rightarrow 0.2O(^3P) + 0.08OH + 0.5HCHO + 0.5IALD1 + 0.5ISNI2 +$

$0.5NO_2$

R15 $ISOH + ISOH \rightarrow 0.6MACR + 0.6MVK + 1.2HCHO + 1.2HO_2$

R16 $ISOH + HO_2 \rightarrow IPRX$

R17 IPRX + OH → ISOH

R18 IPRX + O_3 → 0.7 HCHO

R19 MACR + O_3 → $0.8CH_3COCHO + 0.7HCHO + 0.2O(^3P) + 0.09H_2COO +$

$0.2CO + 0.275HO_2 + 0.215OH + 0.16CO_2 +$

$0.15CH_2{=}CHCCH_3OO$

R20 MVK + O_3 → $0.82CH_3COCHO + 0.8HCHO + 0.2O(^3P)$ + 0.11H2COO +

$0.05CO + 0.06HO_2 + 0.08OH + 0.04CH_3CHO +$

$0.07OOCHCCH_3CH_2$

R21 MVK + OH → 0.28MV1 + 0.72MV2

R22 $CH_2CCH_3CO_3 + NO_2$ → MPAN

R23 MPAN → $CH_2CCH_3CO_3 + NO_2$

R24 $CH_2CCH_3CO_3 + NO_2$ → $C_2H_4 + CH_3O_2 + NO_2 + CO_2$

Photolysis Reactions

P1 MVK + h*v* → $CH_3CO_3 + C_2H_4 + HO_2$

P2 MACR + h*v* → $C_2H_4 + HO_2 + CO + CH_3O_2$

P3 CH3COCHO + h*v* → $CH_3CO_3 + CO + HO_2$

Abbreviations

DISN – Dinitrate of isoprene

IALD1 – Hydroxy carbonyl alkene from isoprene

IPRX – Organic peroxide from isoprene

ISNI1 – Organic nitrate from isoprene

ISNI2 – Organic nitrate from isoprene

ISNIR – Alkyl peroxy radical from ISNI1 or ISNI2

ISNT – Isoprene-NO_3 adduct

ISOH - Alkyl radicals from OH + ISOP

ISOP – isoprene

MACR – Methacrolein

MPAN – Methylperoxyacetyl nitrate

MVK – Methyl vinyl ketone

MV1 – MVK OH adduct

MV2 – MVK OH adduct

OLE – Olefinic carbon bond

PAR – Paraffin carbon bond

References

Allen, D.J. and K.E. Pickering, Evaluation of lightning flash rate parameterizations for use in a global chemical-transport model, *J. Geophys. Res.*, 107(D23), 4711, doi:10.1029/2002JD002066, 2002.

Baker M. B., A. M. Blyth, H. J. Christian, J. Latham, K. L. Miller, and A. M. Gadian, Relationships between lightning activity and various thundercloud parameters: Satellite and modeling studies. *Atmos. Res*, *51*, 221–236, 1999.

Barth, M.C., S.-W. Kim, W.C. Skamarock, A.L. Stuart, K.E. Pickering, and L.E. Ott, Simulations of the redistribution of formaldehyde and peroxides in the July 10, 1996 STERAO deep convection storm, *Journal of Geophysical Research*, submitted, 2006.

Beirle, S., N. Spichtinger, A. Stohl, K. L. Cummins, T. Turner, D. Boccippio, O. R. Cooper, M. Wenig, M. Grzegorski, U. Platt, and T. Wagner, Estimating the NO_x produced by lightning from GOME and NLDN data: a case study in the Gulf of Mexico, *Atmos. Chem. Phys.* 6, 1075-1089, 2005.

Biazar, A.P., and R.T. McNider, Regional estimates of lightning production of nitrogen oxides, *J. Geophys. Res.*, *100,* 22,861-22,874, 1995.

Blyth, A.M., H.J. Christian, K. Driscoll, A.M. Gadian, and J. Latham, Determination of ice precipitation rates and thunderstorm anvil ice contents from satellite observations of lightning. *Atmos. Res.*, *59-60*, 217-229, 2001.

Boccippio, D.J., K.L. Cummins, H.J. Christian, and S.J. Goodman, Combined satellite- and surface-based estimation of the intracloud–cloud-to-ground lightning ratio over the continental United States**,** *Monthly Weather Review, 129*, 108–122, 2001.

Borucki, W.J. and W.L. Chameides, Lightning: Estimates Of The Rates Of Energy Dissipation And Nitrogen Fixation, *Rev. Geophys. and Space Phys., 22*, 363-372, 1984.

Bradshaw, J., D. Davis, G. Grodzinsky, S. Smyth, R. Newell, S. Sandholm, and S. Liu, Observed distributions of nitrogen oxides in the remote free troposphere from the NASA global tropospheric experiment programs, *Rev. of Geophys.*, *38*, 61-116, 2000.

Chameides, W.L.; D.H. Stedman, R.R. Dickerson, D.W. Rusch, and R.J. Cicerone, NO_x Production in Lightning, *J. Atmos. Sci.*, *34*, 143-149, 1977.

Chameides, W. L., The role of lightning in the chemistry of the atmosphere, In *The Earth's Electrical Environment,* National Academy Press, Washington, D.C., 70-77, 1986.

Christian, H.J., et al., Global frequency and distribution of lightning as observed from space by the Optical Transient Detector, *J. Geophys. Res., 108*(D1)*,* 4005, doi:10.1029/2002JD002916, 2003.

Cooper, O.R., et al., Large upper tropospheric ozone enhancements above mid-latitude North America during summer: In situ evidence from the IONS and MOZAIC ozone measurement network, *J. Geophys. Res.,* in press, 2006.

Cummins, K.L., M.J. Murphy, E.A. Bardo, W.L. Hiscox, R.B. Pyle, and A.E. Pifer, A Combined TOA/MDF Technology Upgrade of the U.S. National Lightning Detection Network, *J. Geophys. Res., 103*, 9035-9044, 1998.

DeCaria, A.J., Effects of convection and lightning on tropospheric chemistry studied with cloud, transport, and chemistry models, PhD dissertation, University of Maryland, College Park, 169 pp., 2000.

DeCaria, A.J., K.E. Pickering, G.L. Stenchikov, J.R. Scala, J.L. Stith, J.E. Dye, B.A. Ridley, and P. Laroche, A cloud-scale model study of lightning-generated NO_X in an individual thunderstorm during STERAO-A, *J. Geophys. Res.*, *105*, 11,601-11,616, 2000.

DeCaria, A.J., K.E. Pickering, G.L. Stenchikov, and L.E. Ott, Lightning-generated NO_X and its impact on tropospheric ozone production: A three-dimensional modeling study of a Stratospher-Troposphere Experiment: Radiation, Aerosols, and Ozone (STERAO-A) thunderstorm, *J. Geophys. Res., 110,* D14303, doi:10.1029/2004JD005556, 2005.

Dickerson, R.R., G. J. Huffman, W. T. Luke, L. J. Nunnermacker, K. E. Pickering, A. C. D. Leslie, C. G. Lindsey, W. G. N. Slinn, T. J. Kelly, A. C. Delany, J. P. Greenberg, P. R. Zimmerman, J. F. Boatman, J. D. Ray, and D. H. Stedman, Thunderstorms: An Important Mechanism in the Transport of Air Pollutants, *Science,* 235, 460-465, 1987.

Dotzek, N., H. Höller, and C. Théry, VHF-Interferometry and Radar Observation: Implications for Nitrogen Oxides Production, in *EULINOX – The European Lightning Nitrogen Oxides Experiment*, edited by H. Höller and U. Schumann, *Rep. DLR-FB 2000-28*, pp. 147-166, Deutches Zentrum für Luft- und Raumfahrt, Köln, 2000.

Dye, J. E., et al., An Overview of the STERAO--Deep Convection Experiment with Results for the 10 July Storm, *J. Geophys. Res.*, *105***,** 10,023-10,045, 2000.

Fehr, T., H. Höller, and H. Huntrieser, Model study on production and transport of lightning-produced NO_x in a EULINOX supercell storm, *J. Geophys. Res., 109*, D09102, doi:10.1029/2003JD003935, 2004.

Gallardo, L., and V. Cooray, Could cloud-to-cloud discharges be as effective as cloud-to-ground discharges in producing NO_X?, *Tellus*, *48B*, 641-651, 1996.

Höller, H., U. Finke, H. Huntrieser, M. Hagen, and C. Feigl, Lightning-Produced NOX (LINOX): Experimental design and case study results, *J. Geophys. Res., 104,* 13911-13922, 1999.

Höller, H., H. Huntrieser, C. Feigl, C. Théry, P. Laroche, U. Finke, and J. Seltmann, The Severe Storms of 21 July 1998 – Evolution and Implications for NO_X-Production, in *EULINOX – The European Lightning Nitrogen Oxides Experiment*, edited by H. Höller and U. Schumann, *Rep. DLR-FB 2000-28*, pp. 109-128, Deutches Zentrum für Luft- und Raumfahrt, Köln, 2000.

Holmes, C., M. Brook, P. Krehbiel, and R. McRory, On the power spectrum and mechanism of thunder, *J. Geophys. Res., 76,* 2106-2115, 1971.

Hudman, R.C., et al., Surface and lightning sources of nitrogen oxides in the United States: magnitudes, chemical evolution and outflow, *J. Geophys. Res.,* submitted, 2006.

Huntrieser, H., H. Schlager, C. Feigl, and H. Höller, Transport and production of NO_X in electrified thunderstorms: Survey of previous studies and new observations at mid-latitudes, *J. Geophys. Res.,103,* 28,247-28,264, 1998.

Huntrieser, H., et al., Airborne measurements of NO_x, tracer species, and small particles during the European Lightning Nitrogen Oxides Experiment, *J. Geophys. Res.,*107(D11), 4113, doi:10.1029/2000JD000209, 2002.

IPCC (Intergovernmental Panel on Climate Change), *Climate Change 2001: The Scientific Basis. Contribution of Working Group I to the Third Assessment Report of the IPCC*, Edited by J.T. Houghton et al. Cambridge: Cambridge University Press, 2001.

Johnson, R. H. and P. J. Hamilton, The relationship of surface pressure features to the precipitation and airflow structure of an intense midlatitude squall line. *Mon. Wea. Rev., 116*, 1444–1472, 1988.

Labrador, L. J., R. von Kuhlmann, and M. G. Lawrence, Strong sensitivity of the global mean OH concentration and the tropospheric oxidizing efficiency to the source of NO_X from lightning, *Geophys. Res. Lett.*, *31*(6), L06102, doi:10.1029/2003GL019,229, 2004.

Labrador, L. J., R. von Kuhlmann, and M. G. Lawrence, The effects of lightning-produced NO_x and its vertical distribution on atmospheric chemistry: sensitivity simulations with MATCH-MPIC, *Atmospheric Chemistry and Physics, 5*, 1815-1834, 2005.

Langford, A. O., R. W. Portmann, J. S. Daniel, H. L. Miller, and S. Solomon, Spectroscopic measurements of NO_2 in a Colorado thunderstorm: Determination of the mean production by cloud-to-ground lightning flashes, *J. Geophys. Res.*, *109*, D113404, doi:10.1029/2003JD004158, 2004.

Lawrence, M. G., W. L. Chameides, P. S. Kasibhatla, H. Levy II, and W. Moxim, Lightning and atmospheric chemistry: the rate of atmospheric NO production, In *Handbook of Atmospheric Electrodynamics,* Vol. 1, Bonn, Germany: CRC Press, 189-202, 1995.

Liu, S. C., Trainer, M., Feshenfeld, F. C., Parrish, D. D., Williams, E. J., Fahey, D. W., Hübler, G., and Murphy, P. C., Ozone production in the rural troposphere and the implications for regional and global ozone distributions, *J. Geophys. Res.,* 92, 4191–4207, 1987.

Lin, X., M. Trainer, and S. C. Liu, On the nonlinearity of the tropospheric ozone production. *J. Geophys. Res.,* 93**,** 15879–15888, 1988.

Lee D.S., I. Köhler, E. Grobler, F. Rohrer, R. Sausen, L. Gallardo-Klenner, J.G.J. Olivier, F. J. Dentener and A. F. Bouwman, Estimations of global NOx emissions and their uncertainties. *Atmospheric Environment, 31*, 12 1735-1749, 1997.

Levine, J.S., R.S. Rogowski, G.L. Gregory, W.E. Howell, and J. Fishman, Simultaneous measurements of NO_x, NO, and O_3 production in a laboratory discharge - Atmospheric implications, *Geophys. Res. Lett., 8*, 357-360, 1981.

Levy, H. II, W. J. Moxim, and Kasibhatla, A global three-dimensional time-dependent lightning source of tropospheric NO_x. *Journal of Geophysical Research,* 101(D17), 22,911-22,922, 1996.

Logan, J.A., An Analysis of Ozonesonde Data for the Troposphere: Recommendations for Testing 3-D Models, and Development of a Gridded Climatology for Tropospheric Ozone, *J. Geophys. Res., 104*, 16115-16149, 1999.

Lopez, J. P., et al., CO signatures in subtropical convective clouds and anvils during CRYSTAL-FACE: An analysis of convective transport and entrainment using observations and a cloud-resolving model, *J. Geophys. Res.*, 111, D09305, doi:10.1029/2005JD006104, 2006.

Luke, W. T., R. R. Dickerson, W. F. Ryan, K. E. Pickering, and L. J. Nunnermacker, Tropospheric chemistry over the lower Great Plains of the United States: 2. Trace gas profiles and distributions, *J. Geophys. Res.*, *97*, 20,647–20,670, 1992.

MacGorman, D. R., and W. D. Rust, *The Electrical Nature of Storms.* Oxford University Press, 422 pp, 1998.

Madronich S., Photodissociation in the atmosphere: 1. Actinic fluxes and the effects of ground reflections and clouds. *J. Geophys. Res.*, *92*, 9740–9752, 1987.

Marshall, T. C., and M. Stolzenburg, Voltages inside and just above thunderstorms, *Journal of Geophysical Research, D106,* 4757-4768, 2001.

Nielsen, K.E., R.A., Maddox, S.V.,Vasiloff, The Evolution of Cloud-to-Ground Lightning within a Portion of the 10–11 June 1985 Squall Line, *Monthly Weather Review, 122*, 1809-1817, 1994.

Ogawa, T. and M. Brook, The mechanism of the intracloud lightning discharge. *J. Geophys. Res.*, 69, 5141-5150, 1964.

Orville, R. E., G. R. Huffines, W. R. Burrows, R. L. Holle, and K. L. Cummins, The North American Lightning Detection Network (NALDN) - First Results: 1998-2000, *Mon. Wea. Rev., 130, 8*, 2098-2109, 2002.

Park, R. J., K. E. Pickering, D. J. Allen, G. L. Stenchikov, and M. S. Fox-Rabinovitz , Global simulation of tropospheric ozone using the University of Maryland Chemical Transport Model (UMD-CTM): 1. Model description and evaluation, *J. Geophys. Res.*, *109*, D09301, doi:10.1029/2003JD004266, 2004.

Petersen, W.A., and S.A. Rutledge, Regional Variability in Tropical Convection: Observations from TRMM. *J. Climate, 14*, 3566-3585, 2001.

Petersen, W. A., H. J. Christian, and S. A. Rutledge, TRMM observations of the global relationship between ice water content and lightning, *Geophys. Res. Lett., 32,* L14819, doi:10.1029/2005GL023236, 2005.

Pickering, K.E., R. R. Dickerson, G. J. Huffman, J. Boatman, and A. Schanot, J., Trace Gas Transport in the Vicinity of Frontal Convective Clouds, *J. Geophys. Res., 93*(1), 759-773, 1988.

Pickering, K. E., A. M. Thompson, R. R. Dickerson, B. S. Gockel, W. T. Luke, D. P. McNamara, J. P. Greenberg, and P. R. Zimmerman, Model Calculations of Tropospheric Ozone Production Potential Following Observed Convective Events, *J. Geophys. Res., 95*(9), 14,049-14062, 1990.

Pickering, K.E., Y. Wang, W.-K. Tao, C. Price, and J.-F. Müller, Vertical distributions of lightning NO_X for use in regional and global chemical transport models, *J. Geophys. Res.*, *103*, 31,203-31,216, 1998.

Price, C., and D. Rind, A simple lightning parameterization for calculating global lightning distributions, *J. Geophys. Res*., *97,* 9919-9933, 1992.

Price, C., and D. Rind, What determines the cloud-to-ground fraction in thunderstorms?, *Geophys. Res. Lett., 20,* 463-466, 1993.

Price, C., J. Penner, and M. Prather, NO_X from lightning 1. Global distribution based on lightning physics, *J. Geophys. Res.*, *102*, 5929-5941, 1997.

Ridley B.A., et al., Florida thunderstorms: A faucet of reactive nitrogen to the upper troposphere, *Journal of Geophysical Research*, 109, D17305, doi:10.1029/2004JD004769, 2004.

Ridley, B.A., K.E. Pickering, and J.E. Dye, Comments of the parameterization of lightning-produced NO in global chemistry-transport models, *Atmos. Environ., 39,* 6184-6187, 2005.

Rutledge, S. A., R. A. Houze Jr., M. I. Biggerstaff, and T. Matejka, The Oklahoma–Kansas mesoscale convective system of 10–11 June 1985: Precipitation structure and single-Doppler radar analysis. *Mon. Wea. Rev., 116*, 1409–1430, 1988.

Rutledge, S. A. and D. R. MacGorman, Cloud-to- ground lightning activity in the 10-11 June 1985 mesoscale convective system observed during the Oklahoma-Kansas PRE-STORM project, *Mon. Wea. Rev.*, *116*, 1393-1408, 1988.

Skamarock, W. C., et al., Numerical simulations of the July 10 Stratospheric-Tropospheric Experiment: Radiation, Aerosols, and Ozone/Deep Convection Experiment convective system: Kinematics and transport, *J. Geophys. Res.*, 105(D15), 19,973–19,990, 2000.

Skamarock, W. C., J. E. Dye, E. Defer, M. C. Barth, J. L. Stith, B. A. Ridley, K. Baumann, Observational- and modeling-based budget of lightning-produced NO_x in a continental thunderstorm, *J. Geophys. Res.* 108(D10), 4305, doi:10.1029/2002JD002163, 2003.

Stenchikov G., Pickering K., DeCaria A., Tao W. K., Scala J., Ott L., Bartels D., Matejka T., Simulation of the fine structure of the 12 July 1996 Stratosphere-Troposphere Experiment: Radiation, Aerosols and Ozone (STERAO-A) storm accounting for effects of terrain and interaction with mesoscale flow, *Jl Geophys. Res.*, 110, D14304, doi:10.1029/2004JD005582, 2005.

Stith, J., J. Dye, B. Ridley, P. Laroche, E. Defer, K. Baumann, G. Hübler, R. Zerr, and M. Venticinque, NO signatures from lightning flashes, *J. Geophys. Res.*, 104, 16,081-16,089, 1999.

Stockwell, D.Z., C. Giannakopoulos, P.-H. Plantevin, G.D. Carver, M.P. Chipperfield, K.S. Law, J.A. Pyle, D.E. Shallcross and K.-Y. Wang, Modelling NO_x from lightning and its impact on global chemical fields, *Atmos. Environ., 33*, 4477-4493, 1999.

Strahan, S.E., A.R. Douglass, J.E. Nielsen, and K.A. Boering, The CO_2 seasonal cycle as a tracer of transport. *J. Geophys. Res., 103,* 13729-13741, 1998.

Tao, W.-K., and J. Simpson, Goddard Cumulus Ensemble Model. Part I: Model description, *Terr., Atmos., Oceanic Sci.*, *4*, 35-72, 1993.

Tao, W.-K., et al., Microphysics, Radiation and Surface Processes in the Goddard Cumulus Ensemble (GCE) Model, submitted to *Meteorology and Atmospheric Physics*, 2001.

Tao, W.-K., et al., Regional-scale modeling at NASA Goddard Space Flight Center, *Research Signpost - Recent Res. Devel. Atmos. Sci.*, *2*, 1-52, 2003.

Théry, C., Evaluation of LPATS data using VHF interferomteric observations of lightning flashes during the EULINOX experiment, in *EULINOX – The European Lightning Nitrogen Oxides Experiment*, edited by H. Höller and U. Schumann, *Rep. DLR-FB 2000-28*, pp. 77-83, Deutches Zentrum für Luft- und Raumfahrt, Köln, 2000.

Théry, C., P. Laroche, and P. Blanchet, Lightning activity during EULINOX and estimations of NO_X production by flashes, in *EULINOX – The European Lightning Nitrogen Oxides Experiment*, edited by H. Höller and U. Schumann, *Rep. DLR-FB 2000-28*, pp. 129-145, Deutches Zentrum für Luft- und Raumfahrt, Köln, 2000.

Ushio, T., S. J. Heckman, D. J. Boccippio, and H. J. Christian, A survey of thunderstorm flash rates compared to cloud top height using TRMM satellite data, *J. Geophys. Res.,* 106, 24089-24095, 2001.

Wang, Y., W.-K. Tao, K.E. Pickering, A.M. Thompson, J.S. Kain, R.F. Adler, J. Simpson, P.R. Keehn, and G.S. Lai, Mesoscale model simulations of TRACE A and Preliminary Regional Experiment for Storm-scale Operational and Research Meteorology convective systems and associated tracer transport. *J. Geophys. Res.*, *101*, 24013-24027, 1996.

Wang Y., A. W. DeSilva, G. C. Goldenbaum, and R. R. Dickerson, Nitric Oxide Production by Simulated Lightning: Dependence on Current, Energy, and Pressure, *J. Geophys. Res.,* 103(15), 19,149-19,159, 1998.

Wang C. and R.G. Prinn, On the roles of deep convective clouds in tropospheric chemistry, *J. Geophys. Res*., 105, 22269-22297, 2000.

Xue, M., K. K. Droegemeier, and V. Wong, The Advanced Regional Prediction System (ARPS) - A multiscale non-hydrostatic atmospheric simulation and prediction tool. Part I: Model dynamics and verification, *Meteor. Atmos. Physics., 75,* 161-193, 2000.

Xue, M., K. K. Droegemeier, V. Wong, A. Shapiro, K. Brewster, F. Carr, D. Weber, Y. Liu, and D.-H. Wong, The Advanced Regional Prediction System (ARPS) - A multiscale non-hydrostatic atmospheric simulation and prediction tool. Part II: Model physics and applications, *Meteor. Atmos. Physics., 76,* 134-165, 2001.

Zhang, D.-L., K. Gao and D.B Parsons, Numerical simulation of an intense squall line during 10 - 11 June 1985 PRE-STORM. Part I: Model verification. *Monthly Weather Review*, *117*, 960-994, 1989.

Zhang , X., J.H. Helsdon, and R.D. Farley, Numerical modeling of lightning-produced NO_x using an explicit lightning scheme: 1. Two-dimensional simulation as a “proof of concept”, *J. Geophys. Res*. 108(D18), 4579, doi:10.1029/2002JD003224, 2003.